

LEVEL II

AFRPL-TR 78-80

ELECTROCHEMICAL TEST METHOD FOR EVALUATING
LONG-TERM PROPELLANT MATERIAL COMPATIBILITY

FINAL REPORT

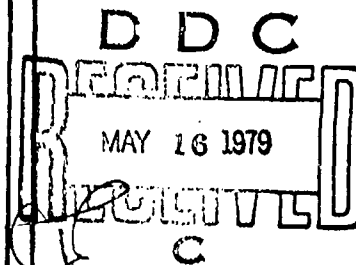
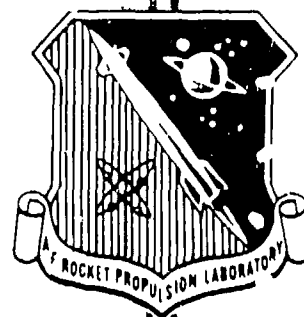
UNITED TECHNOLOGIES RESEARCH CENTER
EAST HARTFORD, CONNECTICUT 06108

AUTHOR: C.T. BROWN

DECEMBER 1978

*Approved for public release;
Distribution Unlimited.*

Prepared for:
AIR FORCE ROCKET PROPULSION LABORATORY
DIRECTOR OF SCIENCE AND TECHNOLOGY
AIR FORCE SYSTEMS COMMAND
EDWARDS AFB, CALIFORNIA 93523



AD A068626

DDC FILE COPY

NOTICES

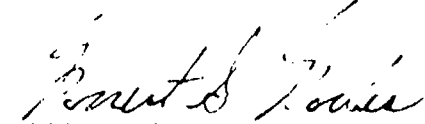
When U.S. Government drawings, specifications, or other data are used for any purpose other than a definitely related government procurement operation, the Government thereby incurs no responsibility nor any obligation whatsoever, and the fact that the Government may have formulated, furnished, or in any way supplied the said drawings, specifications or other data, is not to be regarded by implication or otherwise, or in any manner licensing the holder or any other person or corporation, or conveying any rights or permission to manufacture, use, or sell any patented invention that may in any way be related thereto.

FOREWORD

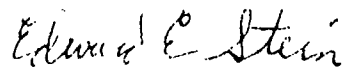
The work described herein was performed at United Technologies Research Center, East Hartford, Connecticut for the Air Force Rocket Propulsion Laboratory under Contract F04611-77-C-0020, initiated March 1, 1977 and ending November 30, 1978. Those who participated in the performance of this work were: Dr. C. T. Brown, Principal Investigator, Dr. L. J. Spadaccini, Dr. H. T. Couch, Chief, Chemical Technologies Section and Program Manager, Mr. D. G. McMahon, Ms. P. D. DeFelice, Mr. Scott T. Kehoe and Mr. Gene Lind.

The work was conducted under the technical management of Lt. William T. Leyden USAF and Mr. Forrest S. Forbes, Chief, Propellant Systems Section (AFRPL/LKCP).

This report has been reviewed by the Information Office/XCJ and is releasable to the National Technical Information Service (NTIS). At NTIS it will be available to the general public, including foreign nations. This report is unclassified and suitable for general public release.


FORREST S. FORBES, Chief
Propellant Section

FOR THE COMMANDER


EDWARD E. STEIN
Deputy Chief, Liquid Rocket Division

UNCLASSIFIED

SECURITY CLASSIFICATION OF THIS PAGE (When Data Entered)

19 REPORT DOCUMENTATION PAGE		READ INSTRUCTIONS BEFORE COMPLETING FORM	
1. REPORT NUMBER	2. GOVT ACCESSION NO.	3. RECIPIENT'S CATALOG NUMBER	
(18) AFRPL-TR-78-80		(7)	(34)
4. TITLE (and Subtitle)		5. TYPE OF REPORT & PERIOD COVERED	
(6) ELECTROCHEMICAL TEST METHOD FOR EVALUATING LONG-TERM PROPELLANT-MATERIAL COMPATIBILITY.		Final Report, March 1977 - November 1978	
7. AUTHOR(s)		8. CONTRACT OR GRANT NUMBER(s)	
(10) C. T. Brown		(15) F04611-77-C-0020	
9. PERFORMING ORGANIZATION NAME AND ADDRESS		10. PROGRAM ELEMENT, PROJECT, TASK AREA & WORK UNIT NUMBERS	
United Technologies Research Center Silver Lane East Hartford, CT 06108			
11. CONTROLLING OFFICE NAME AND ADDRESS		12. REPORT DATE	
Air Force Rocket Propulsion Laboratory Edwards AFB, California 93523		(11) December 1978	
14. MONITORING AGENCY NAME & ADDRESS (if different from Controlling Office)		13. NUMBER OF PAGES	
(12) 295p.		15. SECURITY CLASS. (of this report)	
		Unclassified	
		16a. DECLASSIFICATION/DOWNGRADING SCHEDULE	
16. DISTRIBUTION STATEMENT (of this Report)			
Approved for public release - Distribution unlimited.			
17. DISTRIBUTION STATEMENT (of the abstract entered in Block 20, if different from Report)			
18. SUPPLEMENTARY NOTES			
19. KEY WORDS (Continue on reverse side if necessary and identify by block number)			
Hydrazine, Monomethylhydrazine, Compatibility, Electrochemical Test Method			
20. ABSTRACT (Continue on reverse side if necessary and identify by block number)			
An electrochemical technique for evaluating the long-term compatibility of liquid propellants in various containment materials is described. The method requires that the liquid and containment material be electrical conductors, that the exchange current be measurable, and that the propellant decomposition mechanism be known. The time base is then altered by electrolysis of the system at some multiple of the natural decomposition rate. As a result, a			

DD FORM 1473

1 JAN 73

EDITION OF 1 NOV 68 IS OBSOLETE

S/N 0102-LF-014-6601

UNCLASSIFIED

SECURITY CLASSIFICATION OF THIS PAGE (When Data Entered)

409 252

1B

UNCLASSIFIED

SECURITY CLASSIFICATION OF THIS PAGE(When Data Entered)

simulated time scale is achieved in which the propellant decomposition rate can be predicted up to fifteen years while the actual time required for the tests is on the order of one to two months, depending on the particular metal tested.

The procedure for simulating long-term exposure of various metals to hydrazine and monomethylhydrazine, without changing the decomposition mechanism, is described and data comparisons elucidating the effects of metal type and configuration on propellant (i.e., hydrazine and monomethylhydrazine) decomposition are presented. The test program included detailed evaluations of alloys selected from five base-metal groups (Aluminum, Titanium, Iron, Cobalt, and Nickel) as well as the effects of bends, edges, crevices, bimetallic couples, metal stress, propellant impurities and metal pretreatment procedures. The data provided serve as a guide for the selection of materials and material configurations compatible with hydrazine and monomethylhydrazine. Also, the procedure for using the decomposition data to predict pressure rise in a propellant tank is presented. In addition, metal dissolution data are used to predict loss in tank wall strength, assuming uniform corrosion.

The results of experimental studies to evaluate the applicability of the electrical chemical test method to the determination of compatibility of selected materials in N_2O_4 are presented in a separate report (AFRPL-TR-78-72).

ACCESSION

HTP

DEC

1978

1978

1978

1978

1978

1978

1978

1978

1978

1978

1978

1978

1978

1978

1978

1978

1978

1978

1978

1978

1978

1978

1978

1978

1978

1978

1978

UNCLASSIFIED

SECURITY CLASSIFICATION OF THIS PAGE(When Data Entered)

SUMMARY

The objective of this program was to determine the long-term compatibility of hydrazine and monomethylhydrazine with selected metals by means of an electrochemical test method. The electrochemical test method is based on the fact that the reaction of an electrolyte (in this case either hydrazine or monomethylhydrazine) on a metal surface can be described in terms of electron transfer. The rate of this transfer is measured in terms of an equilibrium exchange current which can be translated into quantitative terms, i.e., the rate of metal dissolution and the rate of propellant decomposition, provided the reaction mechanism is known. Accordingly, to predict propellant/tank material long-term compatibility on a simulated time scale, the exchange current is determined by standard electrochemical techniques, and then the surface reactions are simulated on a quantitative basis by the imposition of an external potential.

The feasibility of determining material compatibility in the presence of monomethylhydrazine was carried out by comparing results from the electrochemical test method to existing real-time data. The mechanisms for hydrazine and monomethylhydrazine decomposition were obtained from the literature and translated into electrochemical terms. Good agreement was obtained between the electrochemical test prediction and available data for 304LSS, Ti6Al4V, and AAl100. Once the reaction mechanism and equilibrium exchange current is determined, the time scale for the tests can be condensed by passing a known current (electrolysis) through the electrode (metal) - electrolyte (hydrazine) interface. The ratio of this current density to the equilibrium current density is the simulation factor. After each predetermined interval of electrolysis has been completed, the results are analyzed and the process is repeated for the next time interval. The ultimate result is a decomposition rate - simulated time profile of the metal-propellant couple.

In addition to baseline compatibility tests, the present program was concerned with the experimental evaluation of the long-term compatibility of hydrazine and monomethylhydrazine with various metals and metal configurations normally found in propellant fuel systems. Some of the important special conditions found in these systems include: vapor-liquid interface, crevices, bimetallic junctions, bends, edges, metal stress and welds and brazes. The relative effects of each of these configurations were evaluated with respect to baseline tests where the metal was in the form of either a slug or a strip. The latter configuration was used for evaluation of the comparative rate of propellant degradation as a function of metal stress, bends, welds, and brazed joints. The effects of metal pretreatment and concentration level of various important propellant impurities on the comparative rate of propellant decomposition and extent of metal dissolution was determined.

Generally, the test results indicate that hydrazine decomposes approximately an order of magnitude faster than monomethylhydrazine, but that monomethylhydrazine results in higher metal dissolution rates. Both propellants tend to follow the same pattern in that the various aluminum or titanium alloys are most compatible as a containment material whereas the stainless steels, and nickel or cobalt base alloys are not recommended (on a comparative basis). The presence of excess water, (as a contaminate material) does not affect this relationship but small ppm concentrations of the chloride ion are very harmful to compatibility in the case of the aluminum alloys. Surprisingly, welds and brazes, and the state of metal stress or even plastic deformation had little effect on material compatibility. Even bimetallic couples failed to substantially increase propellant decomposition rate beyond the average of the two materials involved. Vapor-liquid interface appeared to have some effect, but the effect was not consistent from one alloy to the next. Finally, the effect of three different metal cleaning procedures on propellant compatibility was evaluated again with mixed results.

The compatibility data were used to predict the pressure rise in a typical spherical storage tank having one percent ullage volume and charged with either hydrazine or monomethylhydrazine propellant. The propellant ullage gas composition was corrected for evolved gas solubility (e.g., N_2 and NH_3 in N_2H_4 , and N_2 and CH_4 in MMH), and pressure rises were calculated for AA6061-T6, Ti6Al4V, and 304LSS tanks. After 15 years simulated time, the storage tank pressure rise due to hydrazine decomposition was approximately 3 to 5 atm. The pressure rise due to MMH decomposition could not be predicted due to uncertainty regarding the CH_4 solubility level; however, estimates are presented for the maximum possible pressure rise assuming zero CH_4 solubility.

Estimates of the reduction in tank wall thickness, assuming uniform corrosion indicated that in all cases the loss of strength due to metal dissolution was negligible.

TABLE OF CONTENTS

<u>Section</u>	<u>Page</u>
I. INTRODUCTION	1
II. ELECTROCHEMICAL THEORY AND EXPERIMENTAL TECHNIQUES	3
Electrochemical Theory	3
Experimental Techniques	8
III. LONG-TERM COMPATIBILITY DETERMINATIONS -- HYDRAZINE	12
Baseline Compatibility of Various Metal Alloys with Hydrazine	12
Effect of Special Metal Configurations	13
Effect of Metal Stress, Welds, and Brazes	16
Effect of Metal Pretreatment and Propellant Impurities	18
Extent of Metal Dissolution	19
IV. MONOMETHYLHYDRAZINE FEASIBILITY DEMONSTRATION	22
Data Comparison	22
Metal Dissolution	24
Conclusions	24
V. LONG-TERM COMPATIBILITY DETERMINATIONS - MONOMETHYLHYDRAZINE	26
Baseline Compatibility of Various Metal Alloys with Monomethylhydrazine	26
Effect of Special Metal Configurations	27
Effect of Metal Stress, Welds, and Brazes	29
Effect of Metal Pretreatment and Propellant Impurities	30
Extent of Metal Dissolution	32
VI. APPLICATION OF COMPATIBILITY DATA	33
Prediction of Storage Tank Pressure Rise	33
Prediction of Loss in Tank Wall Strength	35
VII. CONCLUSIONS AND RECOMMENDATIONS	37
REFERENCES	40
TABLES	42
FIGURES	101

TABLE OF CONTENTS (cont'd)

<u>Section</u>	<u>Page</u>
APPENDIX A EQUIPMENT AND TEST PROCEDURES	A-1
Experimental Test Cell	A-1
Instrumentation	A-2
Experimental Procedures	A-3
APPENDIX B EXTENT OF HYDRAZINE DECOMPOSITION	B-1
APPENDIX C EXTENT OF MONOMETHYLHYDRAZINE DECOMPOSITION	C-1
APPENDIX D METAL PRETREATMENT PROCEDURES	D-1
Cleaning Procedure A (Aluminum)	D-2
Cleaning Procedure A (300 Steel)	D-3
Cleaning Procedure A (400 Steel)	D-4
Cleaning Procedure A (Titanium)	D-5
Cleaning Procedure A (Nickel and Cobalt)	D-6
Cleaning Procedure B (Aluminum)	D-7
Cleaning Procedure B (Stainless Steel)	D-8
Cleaning Procedure B (Titanium)	D-9
Cleaning Procedure B (Nickel and Cobalt)	D-10
Cleaning Procedure C (Isopropyl Alcohol (IPA) and Detergent)	D-11

LIST OF TABLES

<u>Table</u>		<u>Page</u>
I	HYDRAZINE-MATERIAL COMPATIBILITY RATINGS	42
II	EFFECTS OF A VAPOR-LIQUID INTERFACE ON HYDRAZINE DECOMPOSITION	43
III	EFFECTS OF EDGES ON HYDRAZINE DECOMPOSITION	44
IV	EFFECTS OF CREVICES ON HYDRAZINE DECOMPOSITION	45
V	EFFECTS OF BIMETALLIC JUNCTIONS ON HYDRAZINE DECOMPOSITION	46
VI	EFFECTS OF METAL STRESS ON HYDRAZINE DECOMPOSITION	47
VII	EFFECTS OF BENDS ON HYDRAZINE DECOMPOSITION	48
VIII	EFFECTS OF WELDS, BRAZES ON HYDRAZINE DECOMPOSITION	49
LX	EFFECTS OF METAL PRETREATMENT ON HYDRAZINE DECOMPOSITION AT 15 YEARS SIMULATED TIME	50
X	EFFECTS OF IMPURITIES ON HYDRAZINE DECOMPOSITION	51
XI	METAL DISSOLUTION IN HYDRAZINE-BASELINE TESTS	52
XII	METAL DISSOLUTION IN HYDRAZINE-VAPOR-LIQUID TESTS	53
XIII	METAL DISSOLUTION IN HYDRAZINE-EDGE TESTS	54
XIV	METAL DISSOLUTION IN HYDRAZINE-CREVICE TESTS	55
XV	METAL DISSOLUTION IN HYDRAZINE-BIMETALLIC TESTS	56
XVI	METAL DISSOLUTION IN HYDRAZINE-STRESS AND NONSTRESS TESTS	57
XVII	METAL DISSOLUTION IN HYDRAZINE-BEND TESTS	58
XVIII	METAL DISSOLUTION IN HYDRAZINE-WELD AND BRAZE TESTS	59
XIX	SUMMARY OF METAL DISSOLUTION IN HYDRAZINE AT THE 1 ppm SIGNIFICANCE LEVEL	60
XX	MONOMETHYLHYDRAZINE COMPATIBILITY DATA-BASELINE	61
XXI	REAL TIME COMPATIBILITY DATA	62
XXII	EXTENT OF MONOMETHYLHYDRAZINE DECOMPOSITION ON PURE IRON, TITANIUM, AND ALUMINUM	63
XXIII	METAL DISSOLUTION IN MONOMETHYLHYDRAZINE	64
XXIV	HYDRAZINE-MONOMETHYLHYDRAZINE BASELINE DATA COMPARISON	65
XXV	MATERIAL-PROPELLANT COMPATIBILITY RATINGS (MONOMETHYLHYDRAZINE DECOMPOSITION)	66
XXVI	EFFECTS OF A VAPOR-LIQUID INTERFACE ON MONOMETHYLHYDRAZINE DECOMPOSITION	67
XXVII	EFFECTS OF EDGES ON MONOMETHYLHYDRAZINE DECOMPOSITION	68
XXVIII	EFFECTS OF CREVICE ON MONOMETHYLHYDRAZINE DECOMPOSITION	69
XXIX	EFFECTS OF BIMETALLIC JUNCTIONS ON MONOMETHYLHYDRAZINE DECOMPOSITION	70
XXX	EFFECTS OF METAL STRESS ON MONOMETHYLHYDRAZINE DECOMPOSITION	71
XXXI	EFFECTS OF BENDS ON MONOMETHYLHYDRAZINE DECOMPOSITION	72
XXXII	EFFECTS OF WELDS AND BRAZES ON MONOMETHYLHYDRAZINE DECOMPOSITION	73
XXXIII	EFFECTS OF METAL PRETREATMENT ON MONOMETHYLHYDRAZINE DECOMPOSITION AT 110 F AND 15 YEARS SIMULATED TIME	74
XXXIV	EFFECT OF WATER CONCENTRATION ON MONOMETHYLHYDRAZINE DECOMPOSITION	75

LIST OF TABLES (cont'd)

<u>Table</u>		<u>Page</u>
XXXV	EFFECT OF CHLORIDE CONCENTRATION ON MONOMETHYLHYDRAZINE DECOMPOSITION	76
XXXVI	METAL DISSOLUTION IN MONOMETHYLHYDRAZINE-BASELINE TESTS	77
XXXVII	METAL DISSOLUTION IN MONOMETHYLHYDRAZINE-VAPOR-LIQUID TESTS	78
XXXVIII	METAL DISSOLUTION IN MONOMETHYLHYDRAZINE-EDGE TESTS	79
XXXIX	METAL DISSOLUTION IN MONOMETHYLHYDRAZINE-CREVICE TESTS	80
XL	METAL DISSOLUTION IN MONOMETHYLHYDRAZINE-BIMETALLIC TESTS	81
XLI	METAL DISSOLUTION IN MONOMETHYLHYDRAZINE-NONSTRESS TESTS	82
XLII	METAL DISSOLUTION IN MONOMETHYLHYDRAZINE-STRESS TESTS	83
XLIII	METAL DISSOLUTION IN MONOMETHYLHYDRAZINE-BEND TESTS	84
XLIV	METAL DISSOLUTION IN MONOMETHYLHYDRAZINE-WELD AND BRAZE TESTS	85
XLV	METAL DISSOLUTION IN MONOMETHYLHYDRAZINE-METAL PRETREATMENT A	86
XLVI	METAL DISSOLUTION IN MONOMETHYLHYDRAZINE-METAL PRETREATMENT B	87
XLVII	METAL DISSOLUTION IN MONOMETHYLHYDRAZINE-METAL PRETREATMENT C	88
XLVIII	METAL DISSOLUTION IN MONOMETHYLHYDRAZINE-2.1% H ₂ O	89
XLIX	METAL DISSOLUTION IN MONOMETHYLHYDRAZINE-2.6% H ₂ O	90
L	METAL DISSOLUTION IN MONOMETHYLHYDRAZINE-3.1% H ₂ O	91
LI	METAL DISSOLUTION IN MONOMETHYLHYDRAZINE-CHLORIDE TESTS 50 F - 15 Years	92
LII	METAL DISSOLUTION IN MONOMETHYLHYDRAZINE-CHLORIDE TESTS 160 F - 15 Years	93
LIII	SUMMARY OF METAL DISSOLUTION IN MONOMETHYLHYDRAZINE AT THE 1 ppm SIGNIFICANCE LEVEL	94
LIV	STORAGE TANK DIMENSIONS AND PHYSICAL PROPERTIES OF PROPELLANTS	95
LV	PRESSURE REQUIRED TO DISSOLVE AMMONIA IN HYDRAZINE	96
LVI	CALCULATED PRESSURE RISE IN N ₂ H ₄ TANK (43C)	97
LVII	CALCULATED PRESSURE RISE IN MMH TANK (43C)	98
LVIII	METAL DISSOLUTION IN N ₂ H ₄ (BASELINE TESTS	99
LIX	METAL DISSOLUTION IN MMH (BASELINE TESTS)	100

APPENDIX A EQUIPMENT AND TEST PROCEDURES

A-1	LIST OF EQUIPMENT
-----	-------------------

LIST OF FIGURES

<u>Figure</u>		<u>Page</u>
1	TYPICAL EXPERIMENTAL CURRENT-VOLTAGE SCAN (PT-10% Ir) IN PROPELLANT GRADE HYDRAZINE	101
2	MATERIAL COMPATIBILITY TEST CELL	102
3	MATERIAL COMPATIBILITY TEST CELL (CROSS SECTION)	103
4	MATERIAL COMPATIBILITY TEST SPECIMENS-SLUG CONFIGURATIONS	104
5	MATERIAL COMPATIBILITY TEST SPECIMENS-STRIP CONFIGURATIONS	105
6(A)	EXTENT OF HYDRAZINE DECOMPOSITION (BASELINE TESTS)	106
6(B)	EXTENT OF HYDRAZINE DECOMPOSITION (BASELINE TESTS)	107
7	EXTENT OF HYDRAZINE DECOMPOSITION ON SELECTED METALS AT 110 F	108
8(A)	EXTENT OF HYDRAZINE DECOMPOSITION ON VAPOR-LIQUID, EDGE, AND CREVICE CONFIGURATIONS AT 110F (AA6061-T6, Ti6Al4V, and 304LSS)	109
8(B)	EXTENT OF HYDRAZINE DECOMPOSITION ON VAPOR-LIQUID, EDGE, AND CREVICE CONFIGURATIONS AT 110F (HAYNES 25 AND INCONEL X750)	110
9	EXTENT OF HYDRAZINE DECOMPOSITION ON BIMETALLIC JUNCTIONS AT 110 F	111
10(A)	EFFECT OF METAL STRESS AND BENDS ON HYDRAZINE DECOMPOSITION AT 110 F (AA6061-T6, Ti6Al4V AND 304LSS)	112
10(B)	EFFECT OF METAL STRESS AND BENDS ON HYDRAZINE DECOMPOSITION AT 110 F (HAYNES 25 AND INCONEL X750)	113
11	EXTENT OF HYDRAZINE DECOMPOSITION ON WELDS AND BRAZES AT 110 F	114
12	TEST MATRIX FOR EVALUATING CLEANING PROCEDURES FOR USE WITH HYDRAZINE	115
13	TEST MATRIX FOR EVALUATING EFFECTS OF IMPURITIES IN HYDRAZINE	116
14	COMPARISON OF UTRC AND JPL COMPATIBILITY DATA IN MONOMETHYLHYDRAZINE AT 110 F	117
15	COMPARISON OF UTRC AND SRI COMPATIBILITY DATA IN MONOMETHYLHYDRAZINE	118
16	EXTENT OF MONOMETHYLHYDRAZINE DECOMPOSITION ON SELECTED METALS AT 110 F	119
17(A)	EXTENT OF MONOMETHYLHYDRAZINE DECOMPOSITION (BASELINE TESTS)	120
17(B)	EXTENT OF MONOMETHYLHYDRAZINE DECOMPOSITION (BASELINE TESTS)	121
18(A)	EXTENT OF MONOMETHYLHYDRAZINE DECOMPOSITION ON VAPOR-LIQUID, EDGE, CREVICE CONFIGURATIONS AT 110 F (AA6061-T6, Ti6Al4V, AND HAYNES 25)	122
18(B)	EXTENT OF MONOMETHYLHYDRAZINE DECOMPOSITION ON VAPOR-LIQUID, EDGE, CREVICE CONFIGURATIONS AT 110 F (304LSS AND INCONEL X750)	123
19	EXTENT OF MONOMETHYLHYDRAZINE DECOMPOSITION ON BIMETALLIC JUNCTIONS AT 110 F	124
20(A)	EFFECT OF METAL STRESS AND BENDS ON MMH DECOMPOSITION AT 110 F (AA6061-T6, Ti6Al4V, AND 304LSS)	125
20(B)	EFFECT OF METAL STRESS AND BENDS ON MMH DECOMPOSITION AT 110 F (HAYNES 25 AND INCONEL X750)	126

LIST OF FIGURES (Cont'd)

<u>Figure</u>		<u>Page</u>
21	EXTENT OF MONOMETHYLHYDRAZINE DECOMPOSITION ON WELDS AND BRAZES AT 110 F	127
22	PRESSURE BUILD-UP IN FUEL STORAGE TANKS	128

APPENDIX A EQUIPMENT AND TEST PROCEDURES

A-1	MATERIAL COMPATIBILITY TEST CELL	A-6
A-2	MATERIAL COMPATIBILITY TEST CELL (CROSS SECTION)	A-7
A-3	THREADED TEFLON CAP (25 mm)	A-8
A-4	THREADED TEFLON CAP (15 mm)	A-9
A-5	ELECTRODE HOLDER	A-10
A-6	ELECTROCHEMICAL TESTING APPARATUS	A-11

APPENDIX B EXTENT OF HYDRAZINE DECOMPOSITION

B-1	EFFECT OF VAPOR-LIQUID INTERFACE ON HYDRAZINE DECOMPOSITION	B-2
B-2	EFFECT OF EDGES ON HYDRAZINE DECOMPOSITION	B-3
B-3	EFFECT OF CREVICES ON HYDRAZINE DECOMPOSITION	B-4
B-4	EFFECT OF BIMETALLIC JUNCTION ON HYDRAZINE DECOMPOSITION	B-5
B-5	EXTENT OF HYDRAZINE DECOMPOSITION-NONSTRESS TESTS	B-6
B-6	EFFECT OF METAL STRESS ON HYDRAZINE DECOMPOSITION	B-7
B-7	EFFECT OF BENDS ON HYDRAZINE DECOMPOSITION	B-8
B-8	EFFECT OF WELDS AND BRAZES ON HYDRAZINE DECOMPOSITION	B-9
B-9	EFFECT OF METAL PRETREATMENT (A) ON HYDRAZINE DECOMPOSITION	B-10
B-10	EFFECT OF METAL PRETREATMENT (B) ON HYDRAZINE DECOMPOSITION	B-11
B-11	EFFECT OF METAL PRETREATMENT (C) ON HYDRAZINE DECOMPOSITION	B-12
B-12	EFFECT OF METAL PRETREATMENT ON HYDRAZINE DECOMPOSITION	B-13
B-13	EFFECT OF H ₂ O IMPURITY ON HYDRAZINE DECOMPOSITION	B-14
B-14	EFFECT OF Cl ⁻ IMPURITY ON HYDRAZINE DECOMPOSITION	B-15
B-15	EFFECT OF CO ₂ IMPURITY ON HYDRAZINE DECOMPOSITION	B-16
B-16	EFFECT OF PROPELLANT IMPURITY ON HYDRAZINE DECOMPOSITION	B-17

APPENDIX C EXTENT OF MONOMETHYLHYDRAZINE DECOMPOSITION

C-1	EXTENT OF MONOMETHYLHYDRAZINE DECOMPOSITION (EFFECT OF VAPOR-LIQUID INTERFACE)	C-2
C-2	EXTENT OF MONOMETHYLHYDRAZINE DECOMPOSITION (EDGE EFFECT)	C-3
C-3	EXTENT OF MONOMETHYLHYDRAZINE DECOMPOSITION (CREVICE EFFECT)	C-4

LIST OF FIGURES (Cont'd)

<u>Figure</u>		<u>Page</u>
APPENDIX C (cont'd)		
C-4	EXTENT OF MONOMETHYLHYDRAZINE DECOMPOSITION (EFFECT OF BIMETALLIC JUNCTION)	C-5
C-5	EXTENT OF MONOMETHYLHYDRAZINE DECOMPOSITION (NONSTRESS TESTS)	C-6
C-6	EXTENT OF MONOMETHYLHYDRAZINE DECOMPOSITION (STRESS EFFECT)	C-7
C-7	EXTENT OF MONOMETHYLHYDRAZINE DECOMPOSITION (BEND EFFECT)	C-8
C-8	EXTENT OF MONOMETHYLHYDRAZINE DECOMPOSITION (WELD BRAZE EFFECT)	C-9
C-9	EXTENT OF MONOMETHYLHYDRAZINE DECOMPOSITION (EFFECT OF METAL PRETREATMENT A)	C-10
C-10	EXTENT OF MONOMETHYLHYDRAZINE DECOMPOSITION (EFFECT OF METAL PRETREATMENT B)	C-11
C-11	EXTENT OF MONOMETHYLHYDRAZINE DECOMPOSITION (EFFECT OF METAL PRETREATMENT C)	C-12
C-12	EXTENT OF MONOMETHYLHYDRAZINE DECOMPOSITION (EFFECT OF IMPURITIES-2.1% H ₂ O)	C-13
C-13	EXTENT OF MONOMETHYLHYDRAZINE DECOMPOSITION (EFFECT OF IMPURITIES-2.6% H ₂ O)	C-14
C-14	EXTENT OF MONOMETHYLHYDRAZINE DECOMPOSITION (EFFECT OF IMPURITIES-3.1% H ₂ O)	C-15

SECTION I

INTRODUCTION

The history of space missions for satellites illustrates the continuing requirement for successively longer missions and has now reached a point where the projected life-times may be of the order of fifteen (15) years. These missions place restrictions on the design of satellite propulsion system components beyond the limitations of real-time testing and evaluation. In the case of unmanned satellites, components which are in contact with the propellant cannot be examined, maintained or repaired.

In order to predict the performance of these materials and their compatibility with the propellant, it becomes necessary to employ testing techniques which are capable of accelerating the reactions between the material and the propellant without exposing the system to conditions far different from those that would be experienced in actual use.

In general, only two methods for compatibility testing have been previously employed; real-time tests over periods extending several years and accelerated testing by using temperature as an independent variable to increase the reaction rate between the material and the propellant. The former method is clearly inadequate, since the required time periods for performance are too large (up to fifteen years). The latter method is deficient, since the mechanism for the propellant decomposition is changed (excessive decomposition to ammonia in the case of hydrazine). Equally, the nature of the propellant/material surface interaction may also be changed.

An electrochemical technique developed at UTRC is capable of measuring decomposition and metal dissolution rates of electrically conducting propellants (and other liquids) on a metal surface. In particular, the object of the present investigation was to apply these techniques on an accelerated time scale to the determination of the long-term compatibility of the monopropellants hydrazine, N_2H_4 , and monomethylhydrazine, $CH_3N_2H_3$, with a variety of materials used in tank construction. In this study, the decomposition rate is proportional to an equilibrium exchange current which can be determined experimentally. Propellant decomposition and metal dissolution rates can then be quantified in terms of mass decomposed (or dissolved) per unit surface area per unit time, once the mechanism for the decomposition is determined. Having defined the mechanism, the surface reactions may be quantitatively accelerated by passing a current through the system (electrolysis) which is some multiple of the predetermined equilibrium exchange current. The ratio of the electrolysis current to the equilibrium exchange current is the time-base simulation factor.

This test method was used at UTRC in previous Air Force-sponsored compatibility studies conducted using propellant-grade hydrazine and was found to yield reliable data when compared to real-time test results.

The experimental program described herein was designed to extend the previous hydrazine studies to include the effects of special metal configurations commonly found in propellant feed systems. Metal slug configurations were used to evaluate the effects of a vapor-liquid interface, bimetallic couples, edges, and crevices. Metal strip configurations were used to evaluate the effects of bends, welds, brazes, and metal stress. In addition, the effects of metal pretreatment and propellant impurities on propellant/material compatibility were investigated. All test sequences were coincident with a maximum simulated time of fifteen years and results are compared to baseline tests performed using plain metal slugs and metal strips.

In addition, a feasibility study was made of the applicability of the electrochemical test technique for use with monomethylhydrazine by comparing the test results with real-time data using a decomposition mechanism that is consistent with that determined by other investigators. Once feasibility was established, by measurement of the exchange current and identification of the reaction mechanisms, a testing program was initiated which was identical to the one performed for hydrazine.

This report summarizes the test results in a form which permits evaluation of the relative effects of propellant-material configuration and material type on the long-term stability of both hydrazine and monomethylhydrazine. Included in this report are sections describing (1) the electrochemical theory and experimental techniques, (2) a demonstration of the feasibility of applying the technique to determine material compatibility with monomethylhydrazine, (3) the results of long-term compatibility testing of hydrazine and monomethylhydrazine with selected metals and metal configurations, (4) applications of the propellant decomposition and metal dissolution data to predict pressure rise and reduction of tank wall thickness, and (5) a summary of the conclusions and recommendations.

Experimental studies were also carried out to evaluate this applicability of an electrochemical test method for the measurement of compatibility of selected metals with nitrogen tetroxide (N_2O_4). This work was performed under the subject contract and the results were summarized in a separate report (Ref. 1). In this report, available real-time compatibility data for N_2O_4 are reviewed and the results of N_2O_4 compatibility testing, using the electrochemical test method, are discussed. Test results are presented for Ti6Al4V, 304LSS, AA6061-T6, Inconel X750 and Pt-10% Ir alloys. In addition, the decomposition mechanism for N_2O_4 - H_2O phase diagram are also discussed.

SECTION II

ELECTROCHEMICAL THEORY AND EXPERIMENTAL TECHNIQUES

Electrochemical Theory

The electrochemical test method is based on the fact that reactions taking place on a metal surface in contact with an electrolyte (in this case the propellant) can be described in terms of electron transfer across the metal-electrolyte interface. The following paragraphs describe the theory of the method.

The electrochemical test method has several advantages over other test methods when applied to the measurement of propellant decomposition and metal dissolution in the presence of a propellant. Both these processes can be described in terms of an oxidation-reduction mechanism which implies that electron transfer is taking place at the metal-propellant interface. Propellant decomposition and metal dissolution rates are proportional to the rate of electron transfer and are, therefore, directly proportional to current (i.e., electron) flow. It has been determined that the anodic process is controlled by electron transfer while the cathodic process is diffusion controlled (Ref. 2). This natural equilibrium exchange current flow can be upset by altering the potential energy barrier at the metal-propellant interface with an externally applied potential. The mechanism of the reaction is not changed since the entire process takes place at constant temperature. The rates are specific for processes taking place at the metal surface and, typically, decomposition on the container walls (glass) is a negligible contributor to measured results, unlike the case when gas evolution methods are used.

If by some external means, the metal potential is changed in such a manner as to favor an oxidation or reduction reaction, a net overall current will flow through the system. (A second current-carrying electrode is necessary for this process.) In addition a constant potential reference electrode is used. In this case an ordinary glass pH electrode preconditioned in hydrazine or monomethylhydrazine serves as the reference. All potential differences are measured and controlled between the test piece and the glass reference. The reference electrode does not carry current, but is used as a potential measuring and control device. The exact potential of the glass electrode is not known; however, the important parameter is the potential difference, which is measured and controlled independent of absolute potential values. Assuming the potential is changed so that the oxidation reaction is favored, i_{ox} will increase and i_{red} will decrease since

$$i_{ox} + i_{red} = i_{net} \quad (1)$$

The net current can be expressed as:

$$i_{\text{net}} = i_0 \left[\exp \frac{\alpha F}{RT} \eta + \exp \frac{(1-\alpha)F}{RT} \eta \right] \quad (2)$$

where i_0 = the exchange current density (amperes/cm²)

i = current (amperes)

η = overpotential (volts)

R = the gas constant (Joules/deg K/mole)

T = temperature (deg K)

F = the Faraday (96,488 amp-sec g mole equivalent)

α = transfer coefficient

At low overpotentials (near the equilibrium potential of the metal-solution interface) the exponentials in Eq. (2) can be expanded so that

$$i_{\text{net}} \approx i_0 \frac{F\eta}{RT} \quad (3)$$

Equation (3) is known as the Low Field Approximation of Eq. (2), (Ref. 3).

or

$$i_0 = \frac{RT}{F} \frac{di}{d\eta} \quad (4)$$

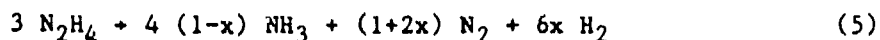
The exchange current density (i_0) is a measure of the natural reaction rate at the metal solution interface, and is proportional to the current-voltage slope ($di/d\eta$) near the equilibrium potential. A typical current-voltage curve is shown in Fig. 1. The linear portion of the plot is within a ± 50 mv range. At higher overpotentials Eqs. (3) and (4) no longer apply.

In order to translate the measured exchange current density values into quantitative rates of propellant decomposition, it is necessary to know the mechanism for the electrochemical reaction of the propellant on a metal surface.

Details of the reaction mechanism for the decomposition of hydrazine (N_2H_4) and monomethylhydrazine ($\text{CH}_3\text{N}_2\text{H}_3$) are discussed below.

Hydrazine Decomposition

The overall process for the decomposition of hydrazine can be expressed as:



where x represents the fraction of ammonia decomposed. If x is zero, i.e., no ammonia decomposition, the overall reaction is:

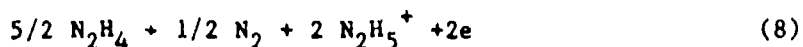


The overall process is really composed of two processes; the oxidation of some of the nitrogen present in hydrazine to nitrogen gas, and the reduction of the remaining hydrazine-bound nitrogen to ammonia. Any oxidation-reduction process (in this case auto oxidation-reduction) involves the formal transfer of electrons from one species to another. In the presence of a metal, the transfer of electrons is accomplished across the metal-liquid interface.

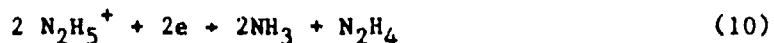
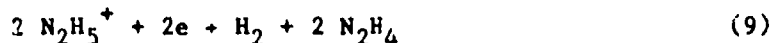
In the presence of small amounts of water (about 0.3 to 0.5 percent in propellant-grade hydrazine) a hydrolysis reaction takes place according to:



The N_2H_5^+ (hydrazonium) ion is analogous to the hydrated hydrogen ion in water (H_3O^+) and provides the basis for the electrochemical reactions taking place during hydrazine decomposition. It has been established (Ref. 4) that the overall anodic reaction is:

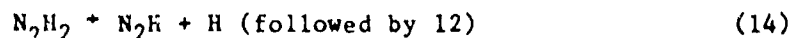
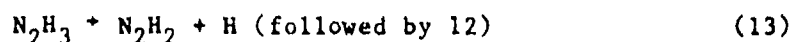


which is followed by either of the cathodic reactions;



The cathodic reaction path appears to be dependent on the metal present. In the presence of platinum, the cathodic reaction proceeds exclusively according to Eq. 9. In many other cases it is a combination of Eqs. 9 and 10. Thus one half of the decomposition reaction is expressed by Eq. 8, and the other half by Eqs. 9 and 10 or a combination of the two.

Examination of the mechanism for hydrazine decomposition, based on published work for hydrazine in aqueous solutions (Ref. 5) and work performed at UTRC (Ref. 4), indicates that the rate-determining step occurs at very low overpotentials (< 100 mv) and is not dependent on gas formation. Although gas formation rates control the process at high overpotentials (> 1.5 volts), the process of interest in this case is the low overpotential region, since it approximates the equilibrium situation. Equations describing the anodic decomposition (oxidation) process for hydrazine are shown in Eqs. 11 through 16. Step 12 is rate controlling, and is repeated four times.



Relative to this reaction sequence, studies concluded at UTRC (Ref. 4) show that the hydrazonium ion (N_2H_5^+) is one of the products of the anodic reaction. This reaction mechanism results in a current-voltage relationship which is linear in the low overpotential region, thereby indicating both activation (electron transfer) control and the absence of rate controlling influence of either diffusion or gas formation effects.

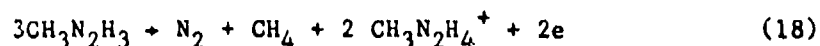
An inspection of reactions 11 through 16 indicates that four electrons are transferred for each mole of hydrazine decomposed. This corresponds to four Faradays ($385,952$ amp-sec/mole or 1.21×10^4 amp-sec/gram). This factor, when combined with i_0 in amperes/cm² of surface area, can be used to calculate the rate of hydrazine decomposition in terms of mass/unit area/unit time. Thus, the decomposition rate, in terms of mg N_2H_4 decomposed/cm²/year, is:

$$\begin{aligned} \text{Decomposition rate} &= \frac{i_o (\text{amp/cm}^2)}{1.21 \times 10^1 \text{ amp-sec/mg}} \times 3.1536 \times 10^7 \text{ sec/year} \quad (17) \\ &= 2.61 \times 10^6 i_o \text{ mg/cm}^2 \text{ year.} \end{aligned}$$

Monomethylhydrazine Decomposition

The mechanism for the decomposition of MMH on a metal surface has been studied by several investigators. Axworthy (Ref. 6) investigated the thermal decomposition of liquid MMH at 200C and found the major products of decomposition to be ammonia, monomethylamine, azomethane, nitrogen and methane. Hydrogen was found only in trace amounts, especially at lower temperatures. Investigators at JPL (Ref. 7) have studied MMH decomposition at 43C on Ti6Al4V, 304L SS and 303SS and found approximately equivalent amounts of methane and nitrogen in the volatile products. The volatile products formed in the higher temperature work of Axworthy (loc. cit.) also contained approximately equal amounts of nitrogen and methane. In view of this 1:1 mole ratio of methane to nitrogen, it is possible to write an anodic electrochemical reaction for MMH that is analogous to that written previously for hydrazine.

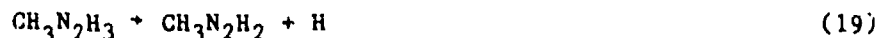
i.e.:



In this case, two electrons are transferred per mole of MMH decomposed. Since the studies noted above were either not performed in the presence of metals or were run at temperatures exceeding 200C, it is probable that more extensive molecular rearrangements could be achieved than in lower temperature compatibility studies. The fact that the JPL work (loc. cit.) indicates the presence of methane and nitrogen at 43C suggests that these products are preferred at the operating temperature used in the present compatibility program.

A detailed mechanism for MMH decomposition was postulated by Ross, et al., (Ref. 8). In this study, the dehydrogenation of MMH to form the radical

(CH₃N-NH) was postulated, which ultimately disproportionates to form CH₄ and N₂. This reaction sequence involves the transfer of two electrons, as;



and finally the rearrangement reaction of the radical:



In this sequence it can be seen that the overall reaction is the same as Reaction (18). As indicated in Reaction (22), the radical CH₃N-NH can undergo rearrangement (Ref. 8) to form equal amounts of CH₄ and N₂ (Ref. 7).

The formation of ammonia and methylamine are explained in terms of the cyclic oxidation-reduction of metal ions in homogeneous solution. However, because the reactions occur in solution and not on the metal surface; there is no effect on the exchange current density. Consequently, only the anodic reaction is required to evaluate the decomposition rate of MMH in contact with a metal surface. As seen earlier, the anodic reaction involves the transfer of two electrons per molecule MMH decomposed, (Reaction 18). This corresponds to two Faradays (i.e., 192,976 amp-sec/mole or 4190 amp-sec/gram). Thus, the rate of MMH decomposition, in terms of mg/cm²/year, is:

$$\begin{aligned} \text{Decomposition rate} &= \frac{i_o \text{ (amp/cm}^2\text{)}}{4.190 \text{ amp-sec/mg}} \times 3.1536 \times 10^7 \text{ sec/year} \quad (23) \\ &= 7.53 \times 10^6 i_o \text{ mg/cm}^2 \text{ yr} \end{aligned}$$

Experimental Techniques

According to the theory outlined earlier, the experiments require specialized electronic test equipment suitable for polarizing the metal and recording

the associated current density as a function of applied voltage. The present section describes the geometry of the test specimens and the experimental test cell; the equipment required for the tests and the test procedure are described in Appendix A.

The metals used in the compatibility testing program were purchased as either flat plates or bars. Two basic test specimens were used in this study: (a) Disk type - reference baseline compatibility, and edge, crevice, bimetallic contact, and vapor-liquid interface effects; (b) Strip type - comparative effect of bends (plastic and elastic deformations) and welded or brazed junctions. Disk type test specimens were machined from the stock material to form cylinders 0.8-cm in diameter and approximately 0.5-cm thick. They were then press fit into Teflon holders so that the exposed surface area of the test piece was 0.5 cm^2 . The holders are illustrated in Figs. 2 and 3. Figure 2 is a photograph of a completely assembled test cell. Figure 3 is a drawing of a cross section of the test cell, showing the position of the test piece (D) near the bottom of the Teflon holder (C). Prior to the insertion of the test piece, a test piece lead wire (F) is inserted in a 0.32-cm-dia. hole which terminates flush with the bottom surface of the test piece hole. The bottom portion of the lead wire is flattened and contact is made when the test piece is force fit into place. In instances where the test piece holders had been used several times, it was necessary to wrap Teflon tape around the test specimen prior to insertion in order to ensure a leak-tight fit. The test piece lead wire was sealed at the top of the test piece holder using a silicone rubber adhesive. This procedure was found to be necessary to prevent liquid from coming into contact with any metal other than the front surface of the test piece. As an additional precaution, the test piece lead wires were always the same material as the test piece itself, in order to avoid any potential difference due to a bimetallic contact.

Once the test piece and holder assembly was completed, the test pieces were ground using 120, 180, and 240 grit silicon carbide paper in successive steps so that a progressively smoother surface was obtained. An acceptable surface was achieved when the test specimen was judged free of scratches or grooves and had a uniform appearance. Once grinding was completed, each test piece was degreased using isopropyl alcohol followed by a deionized water rinse. This procedure was followed by detergent cleaning using liquid detergent in deionized water at 180 F for five minutes. The test specimen was then double rinsed with clean deionized water. All the above sample preparation procedures are identical to those specified in the NASA-JPL long-term compatibility test program (Ref. 9).

The 0.5 cm^2 slug-type test specimens were used for baseline testing and, in a slightly modified form, for the evaluation of the effects of a

vapor-liquid interface, edges, crevices, and bimetallic junctions. In the case of the vapor-liquid interface, the surface area of the slug test piece was increased to 1.0 cm^2 . However, only one-half of the test piece was immersed in the liquid so that an estimated liquid/metal contact area of 0.5 cm^2 was maintained. The slug-type test pieces are illustrated in Fig. 4. The edge test piece is thicker than the standard baseline slugs so that a circumferential edge is exposed. The total exposed surface area is 0.75 cm^2 . The crevice test piece is recessed in the Teflon holder and a Teflon ring is inserted to form the crevice. The exposed surface area is 0.25 cm^2 . The bimetallic test pieces were formed by press fitting a tapered slug specimen into a metal ring specimen. The tapered configuration forms a seal against crevice formation between the two metals. The bimetallic pieces were sized so that each metal had a surface area of 0.5 cm^2 . The compatibility data for each metal configuration were normalized with respect to surface area and compared to the baseline data. The effect of each configuration on propellant decomposition was evaluated in terms of the baseline-to-configuration ratio.

Evaluations of the effects of bends, metal stress, welds and brazes were carried out using metal strips. The special test piece holders for these tests are illustrated in Fig. 5. In each case a special glass holder was used which was of the same design as those used by JPL (Ref. 9), with the exception that a test leadwire of the same metal as the test piece was inserted through the top of the glass holder and was press fit against the top of the metal strip. The nonstress specimens were approximately 2.54-cm long by 0.64-cm wide. The total surface area, counting both sides, was approximately 3.22 cm^2 . The nonstress test pieces were used as a separate baseline reference for all metal strip tests, since the drastic change in geometry precludes reliable direct comparisons between slug and metal strip compatibility data. The stress test pieces were cut to lengths which, when inserted in the standard holder, resulted in stressing the material to approximately 50 percent of its yield strength. Therefore, each test sample was cut to a predetermined length so that the required deflection could be obtained. The actual deflection was measured after the test sample was inserted in the holder and stress was calculated using the equation:

$$\sigma = \frac{6YE d}{l^2} \quad (24)$$

where σ is the stress, Y is the deflection, E is the modulus of elasticity for each metal, d is the thickness of the metal, and l is the length of the test piece. Because of the difficulty in precisely setting the deflection required for each metal, the percentage of yield strength actually obtained was 50 for Inconel X750, 40 for Haynes 25 and Ti6Al4V, and 70 for 304L SS and AA6061-T6.

AFRPL-TR-78-80

Both the weld and braze test pieces were formed by two metal strips which were welded or brazed longitudinally; the resulting total surface area was approximately 6.45 cm^2 . As was the case for the other nonstress specimens, care was taken that no metal stress was induced when the samples were mounted in the glass holders.

SECTION III

LONG TERM COMPATIBILITY DETERMINATIONS -- HYDRAZINE

Detailed results obtained with hydrazine in long-term compatibility testing are discussed in this section of the report. In addition to determining the extent of hydrazine decomposition on a variety of metals, the effect of various special metal configurations on propellant decomposition rate were also evaluated. These configurations included: vapor-liquid interface, edges, crevices, bimetallic junctions, metal stress, bends, welds, and brazes. The effects of propellant impurities and metal cleaning procedures were also evaluated. In each case, simple slug-type test pieces, described previously, were used as a base line for evaluating the effects of other more complex slug-type configurations (i.e., vapor-liquid interface, edges, crevices, and bimetallic junctions). Metal-strip configurations in a nonstress condition were used as a base line for evaluating the effects of metal stress, bends (plastic strain), welds, and brazes on propellant compatibility. In addition, the effects of propellant impurities were evaluated as a function of metal type, impurity, and impurity concentration. The effect of metal pretreatments were characterized according to metal type and temperature. The extent of metal dissolution was determined at the fifteen (15) year simulated time level, and the potential for adverse effect on propellant performance discussed.

Baseline Compatibility of Various
Metal Alloys with Hydrazine

Twelve different alloys were selected for the compatibility testing. Slug type test specimens were fabricated and tested in hydrazine at 110 F. Figure 6 depicts the measured extent of propellant (N_2H_4) decomposition with time which resulted. The data at fifteen years simulated time are also presented in the bar chart of Fig. 7. From these data it can be seen that all four aluminum alloys tested as well as Ti6Al4V and 17-4PHSS have a small effect on hydrazine decomposition (i.e., $< 2 \text{ mg/cm}^2$), while 430SS and 304L SS have a moderate effect (i.e., 2 to 5 mg/cm^2). The remainder of the metals tested (Haynes 25, Inconel X750, Hastelloy B, and Pt-10%Ir) have a marked effect (i.e., $> 5 \text{ mg/cm}^2$). The latter materials are not considered to be practical for applications requiring long-term exposure to hydrazine. The material/hydrazine compatibility ratings in terms of cumulative mg/cm^2 decomposed at fifteen (15) years are summarized in Table I. Detailed results are presented in Appendix B (Figs. B-1 to B-16). As a result of the baseline testing, one alloy from each base-metal group was selected for further evaluation. These alloys include AA6061-T6 (Aluminum), Ti6Al4V (Titanium), 304L SS (Iron), Haynes 25 (Cobalt), and Inconel X750 (Nickel). These five metals were evaluated in terms of the special metal configurations noted above as well as for the effects of impurities and cleaning or passivation procedures.

Effect of Special Metal Configurations

Some of the structural configurations which might conceivably influence propellant-material compatibility are metal edges, crevices, bimetallic junctions, and special conditions at the vapor-liquid interface. A comparison of hydrazine/alloy compatibility under these circumstances as measured with modified slug-type base specimens is discussed in this section.

Vapor-Liquid Interface

Generally, a vapor-liquid interface did not appear to affect the ranking of the materials with respect to compatibility with hydrazine. In other words, the aluminum alloy AA6061-T6 was the most inert (or most compatible) of the five materials tested, followed by titanium, Ti6Al4V, 304L SS, Haynes 25 (cobalt), and Inconel X750 (nickel) in that order. Further, in the case of the most compatible materials, aluminum and titanium, the presence of an interface did not appreciably affect the results. This is shown in Table II and also in Figs. 8(a). However, as is apparent from both the figures (Figs. 8(a) and 8(b)) and the table, in the case of 304L SS, Haynes 25, and Inconel X750 propellant degradation occurred much more rapidly where an interface was involved than in base hydrazine. This effect, which presently appears to be significant, (i.e., being observed beyond the cumulative ± 20 percent uncertainty limits anticipated for these tests), should be checked against other data because it would otherwise put 304L SS along with Haynes 25 and Inconel X750 into the "not recommended" category as a candidate material for the manufacture of hydrazine tanks. A complete summary of data obtained during these tests appears in Fig. B-1.

In comparing these data with the baseline data it should be noted that equivalent metal surface areas were exposed to hydrazine in both the vapor-liquid interface tests and the baseline tests. At fifteen years simulated time, the amount of hydrazine decomposed as a result of a vapor-liquid interface was approximately twice that for all liquid exposure for Inconel X750, three times for Haynes 25, and four times for 304L SS. In the case of Ti6Al4V, the difference between the vapor-liquid interface and all liquid exposure was small, although the presence of the vapor-liquid interface did result in a slight increase in the amount of hydrazine decomposed. The AA6061-T6 test results indicate that partial immersion resulted in decreasing the rate of hydrazine decomposition. This unexpected result could perhaps be due to preferential passivation at the vapor-liquid interface. However, post-test examination of the metal specimen revealed that it had become pitted below the liquid level and, therefore, proportionately more of the electrical current measured may have been related to metal dissolution rather than hydrazine decomposition. There was no evidence of preferential attack at the vapor-liquid interface, but in this regard, there was no change in the appearance of the surfaces of the Ti6Al4V, 304L SS, and Haynes 25 test pieces either. However, there was evidence of preferential metal attack at the vapor-liquid interface for Inconel X750.

Effects of Edges

The effect of edges on hydrazine compatibility generally follows the same pattern as was noted for vapor-liquid interfaces. This was shown previously in Figs. 8(a) and 8(b). A complete summary of results of tests to determine the effect of edges on hydrazine decomposition appears in Fig. B-2. The edge test specimens, described previously, were standard metal slugs except that the slug thickness was increased so that the test piece protruded from the Teflon holder. The total surface area was 0.774 cm^2 as compared to 0.50 cm^2 for the standard slugs; however, all decomposition data was normalized with respect to the surface area of the test specimens. Comparison of the edge test data for up to 15 year simulated exposure times are presented in Table III. The effect of the edge is important only in the case of 304L SS and Ti6Al4V, where the decomposition rate is significantly higher than the baseline data. For AA6061-T6 and Inconel X750 the edge-to-baseline ratios were at the 70 to 80 percent level, which is within experimental error. It is concluded that there is very little edge effect in these two cases; in the first instance because of the usually low activity on aluminum alloys in general, and in the second instance because the high decomposition rates on Inconel X750 have a tendency to mask changes in decomposition rate.

Effect of Crevices

The result of the crevice tests are summarized in Table IV. A complete summary of data taken is shown in Fig. B-3. A crevice was created by placing a teflon ring over a slug test piece which was recessed (approx. 0.25 cm) in the Teflon holder, thereby creating a narrow annular space in which a thin film of hydrazine could be trapped, i.e., between the teflon and the test piece. The Teflon ring restricted the movement of decomposition products away from the metal-solution interface. The open surface area of the test piece was 0.25 cm^2 . In a gaseous system, crevices represent a point of preferential attack, largely because of slow replenishment of oxygen; however, this did not appear to be the case for hydrazine.

The crevice data is compared to the corresponding baseline data in Table IV. As stated above, for the baseline configuration, the metals tested can be ranked in the following order for increasing activity in hydrazine: Ti6Al4V < AA6061-T6 < 304L SS < Haynes 25 < Inconel X750. The results of the crevice test at 15 years simulated exposure time indicate a change in the rankings as follows: Inconel X750 < Ti6Al4V < 304L SS < AA6061-T6 < Haynes 25. The change in order reflects the high rate of preferential decomposition occurring in the AA6061-T6 crevice (approximately six times greater than the baseline data) and the surprisingly low hydrazine decomposition levels measured for Inconel X750. In the latter case, the extent of decomposition

was reduced relative to the baseline by a factor of almost 200. Obviously, the Inconel X750 was highly passivated; however, it does not appear that this effect can be attributed solely to the crevice condition. For the remaining three metals, hydrazine decomposition was increased by the presence of a crevice, but the effect was less severe, approximately a factor of two for 304L SS and Ti6Al4V and even less for Haynes 25. In general, the presence of a crevice condition has an adverse effect on AA6061-T6 and the crevice condition should be avoided when this metal is used in hydrazine tank fabrication.

Bimetallic Junctions

An evaluation of the relative compatibility of hydrazine with bimetallic junctions of 304L SS with AA6061-T6, Ti6Al4V, 17-4PHSS, and Inconel X750 was made using the press-fitted slug samples discussed earlier. Also evaluated was the effect of the Haynes 25/Inconel X750 couple. A comparison of some of the results obtained with that of the individual alloys is shown in Fig. 9. A complete set is presented in Fig. B-4. The total amount of hydrazine decomposed for simulated times of one, five, nine, and fifteen years are summarized in Table V where the baseline data for the individual metals used in each bimetallic couple are included for comparison. The decomposition of hydrazine on the 304L SS/17-4PHSS and the 304L SS/Ti6Al4V couples is similar to the 304L SS baseline data. For the 304L SS/AA6061-T6 couple, the extent of hydrazine decomposition is similar to AA6061-T6. In the case of the 304L SS/Inconel X750 couple, the amount of hydrazine decomposed is greater than that for 304L SS and less than that for Inconel X750. Although the amount of hydrazine decomposed on the Haynes 25/Inconel X750 couple is slightly less than that observed for either of the single metals involved, the absolute values obtained are nearly equal to those obtained using Haynes 25 and the differences are within experimental error. The data for the Haynes 25/Inconel X750 bimetallic couple is not shown in Fig. 9 since the test had been terminated after nine years due to cell breakage. In general, the extent of hydrazine decomposition more nearly approximated that of Haynes 25. Thus, with the exception of 304L SS/AA6061-T6, the presence of a bimetallic couple increases the extent of hydrazine decomposition.

Summary of Slug Configuration Tests

The 15 year hydrazine decomposition results discussed above have been arranged according to metal type and were summarized graphically in Figs. 8(a) and 8(b). The experimental error was estimated on the basis of the results of repeated baseline tests performed on Ti6Al4V and amounted to ± 20 percent of the cumulative decomposition (mg/cm^2) at 15 years simulated time. As shown in Fig. 8, the presence of a vapor-liquid interface significantly accelerates the rate of hydrazine decomposition on 304LSS, Haynes 25, and Inconel X750 and, for these metals, this configuration produced the greatest change as compared to the baseline. In the case of 304L SS, there was also a significant

increase in hydrazine decomposition due to the presence of an edge and a crevice. The extent of hydrazine decomposition on AA6061-T6 was affected only by the crevice; however, the effect was very pronounced. The only metal which was unaffected, or at most, minimally affected, by metal configuration was Ti6Al4V.

Effect of Metal Stress, Welds, and Brazes

The influence of metal stress, welds, and brazes on baseline hydrazine/material compatibility was evaluated using the metal strip pieces discussed previously (Section II). Two stressed type configurations were tested; (1) a configuration where the piece was restrained in a flexed state so that the elastic stress was approximately 50 percent of yield, and (2) a bent configuration where plastic deformation was incurred. The welded and brazed samples consisted of an unflexed strip which was welded (or brazed) along the major axis. As mentioned previously, all strip compatibility results obtained were referenced to compatibility measured with unstressed strip samples having the same total surface area.

Effect of Metal Stress

In each of the stressed metal/hydrazine compatibility tests, test piece length was adjusted to a value which, when installed in the rigid holder, would result in a surface stress which was approximately 50 percent of yield strength. However, due to experimental inaccuracies, the measured deflections indicated that the percentages of the yield stress actually obtained were 50 percent for Inconel X750, 40 percent for Haynes 25 and Ti6Al4V, and 70 percent for 304L SS and AA6061-T6. The results of the stressed and non-stressed material compatibility tests are presented in Figs. B-5 and B-6. A summary comparison of data for those two configurations is presented in Table VI. It is apparent that the effects of metal stress are minimal in the case of 304L SS, Ti6Al4V and Haynes 25. There appears to be a passivating effect for AA6061-T6 and a marked increase in hydrazine decomposition for Inconel X750. The latter result indicates that this metal should be avoided in the stress condition.

Effect of Bends

The results of the bend tests are presented in Fig. B-7 and summarized in Table VII. The test results obtained for 1.0, 5.0, 9.0 and 15 years simulated time are compared to the nonstress tests, since in each case the test piece geometry is the same with the exception of a right angle bend. These test pieces are illustrated in Section II, Fig. 5 and are identical to

those used for the stress tests. The results shown in Table VII indicate that the rate of hydrazine decomposition is increased with plastic deformation in the case of Ti6Al4V, Inconel X750, and Haynes 25. For these materials the extent of hydrazine decomposition was about twice that of the nonstress condition. The 304L SS tests indicate very little difference between the bend and nonstress conditions. Although slightly lower values for the extent of hydrazine decomposition were achieved for the 304L SS bend condition compared to the nonstress 304L SS condition, the results are within the estimated ± 20 percent experimental error. The results obtained for AA6061-T6 are unusual in that the bend tests indicate much lower hydrazine decomposition values than the nonstress test. In this particular case it appears that the test piece was passivated to a much greater extent than any previous AA6061-T6 test, regardless of the test configuration; however, it appears more logical to attribute this result to an inadequate experimental deviation than to the state of strain. In general, it appears that metal stress (or plastic deformation) contributes to higher than normal hydrazine decomposition rates with the alloys Ti6Al4V, Haynes 25 and Inconel X750, whereas little or no effect was observed with the alloys 304L SS and AA6061-T6.

Effect of Welds and Brazes

The results of the weld and braze tests are summarized in Fig. B-8. Comparison of the data with that for the nonstress tests is summarized in Table VIII. In each case two metal strips approximately 0.64-cm wide by 2.5-cm long were welded or brazed longitudinally so that the total surface area was twice that of the baseline (nonstress) test piece. Two brazing materials were evaluated; Permabraz 130, a gold(82%)-nickel(18%) alloy, and Palmiro #7, a gold(70%)-nickel(22%)-palladium(8%) alloy. In addition, electron beam welding and tungsten-inert gas (TIG) welding was employed. The two brazing alloys were evaluated for joining of Inconel X750 to 304L SS and TIG welding was evaluated for joining Inconel X750 to Haynes 25 and Ti6Al4V to Ti6Al4V. Electron beam welding was evaluated for joining 304L SS to 304L SS. The results of these tests indicate that the gold-nickel brazes had no significant adverse effect on hydrazine decomposition. In the case of Palmiro #7 braze, the extent of hydrazine decomposition was approximately the same as the nonstress condition for Inconel X750 and slightly greater than was observed for 304L SS in the nonstressed condition. The same type of behavior was noted when Permabraz-130 was used to join these two metals; however, the extent of hydrazine decomposition was generally lower than for Palmiro #7 and within experimental error. The TIG welding of Ti6Al4V to Ti6Al4V and the electron beam welding of 304L SS to 304L SS indicated a slight reduction in N_2H_4 decomposition relative to that for the nonstressed samples as time in test increases. In both cases, the weld-to-nonstress decomposition ratio is at a maximum at one year and is reduced to unity (within experimental error) by the time the 15 year point is reached. Although none of the welds and brazes tested indicated a marked increase in hydrazine decomposition, welding techniques appear to have less of an effect on hydrazine decomposition than the brazing alloys.

Summary of Metal Strip Results

The results of the metal strip configuration tests are arranged according to metal type and summarized graphically in Figs. 10(a), 10(b), and 11. As noted previously, the only adverse effects in terms of increased hydrazine decomposition were due to metal stress, in the case of Inconel X750, and, to a much lesser degree, metal bends, in the case of Ti6Al4V, Haynes 25, and Inconel X750. This is shown in Figs. 10(a) and 10(b). The only ueld and braze configuration which resulted in increased hydrazine decomposition was Palmiro #7 Braze (70% Au, 22% Ni, 8% Pd) of Inconel X750 to 304L SS. These data appear in Fig. 11. The remainder of the welding techniques evaluated had no significant effect on hydrazine decomposition.

Effect of Metal Pretreatment and Propellant Impurities

The effects of metal pretreatment and propellant impurities on the extent of hydrazine decomposition were evaluated over a matrix of conditions statistically designed to elucidate possible differences in the effects of temperature and impurity concentration on hydrazine/material compatibility as a result of variations in the cleaning procedure. The test matrix shown in Fig. 12 was designed to highlight these differences while minimizing the number of required experiments.

The metal pretreatment procedures evaluated in these studies are described in detail in Appendix D. The A and B procedures differ only in that the A procedures, except for aluminum, contain an acid passivation step usually employing HNO_3 while the B procedures contain a pickling step, usually employing HF. The C procedure is a simple detergent clean followed by an isopropyl alcohol (IPA) degreasing step. The latter procedure was used for the baseline and metal configuration tests performed using hydrazine.

The results of the tests to evaluate the effect of metal pretreatments as a function of metal type and hydrazine temperature are summarized in Figs. B-9 through B-12. The test matrix used for the data analysis is shown in Fig. 12. A summary of the fifteen year data, shown in Table IX, can be used as a guide showing certain obvious trends. Metal pretreatment C (IPA and detergent) always resulted in the highest level of hydrazine decomposition when the test temperature was 160F (cf., AAl100, 304L SS and Haynes 25). The hydrazine decomposition for this combination of cleaning procedure and temperature is at least an order of magnitude greater than the other test results for these three metals. For the remaining metals (including 304LSS) the results indicate a regular increase in the extent of decomposition as a function of increasing propellant temperature. This result indicates that the temperature has a much greater effect on hydrazine decomposition than the relative effects of metal pretreatment A or B. There are only three cases in which

the temperature effects are such that a possible preference can be chosen for metal pretreatment procedures. These are: Procedure B for AA1100, and 17-4PHSS and Procedure A for AA5086. In each of these cases, the lowest extent of hydrazine decomposition was obtained at either 110 F or 160 F. In all other cases temperature effects predominate so that no clear cut choice can be made for the selection of metal pretreatment procedures.

The results of impurity tests conducted using hydrazine containing trace concentrations of H_2O , Cl^- , and CO_2 are presented in Figs. B-13 through B-16. The matrix of test conditions is illustrated in Fig. 13. A statistically designed test matrix (Graeco-Latin Cube) could not be used because of passivation effects encountered with aluminum alloy and Ti6Al4V in hydrazine containing carbon dioxide as an impurity. The tests were terminated because they resulted in current levels below the limit of detection of the instrumentation, i.e., < 0.005 microamp. These test results are summarized in Table X, where the extent of hydrazine decomposition at the end of each test is listed along with the baseline data at the corresponding times. In some cases, the tests were inadvertently terminated at 11, 13 or 17 years. However, this data is so close to the normal 15 year test period that the results can be extrapolated or interpolated with a reasonable degree of accuracy. The same approach was applied to Ti6Al4V in the presence of 150 ppm CO_2 since the hydrazine decomposition rate was essentially linear in the simulated time period of 4.0 to 6.5 years. Linear extrapolation of the titanium data to 15 years simulated time results in a final decomposition level of 0.753 mg/cm^2 .

The data was examined using statistical techniques to evaluate the relative effect of the metal, impurity and impurity level on the extent of hydrazine decomposition. The four tests which were terminated prematurely by passivation all involved CO_2 . Therefore, evaluation of the effects of all three impurities (i.e., H_2O , Cl^- , and CO_2) was restricted to the five remaining metals. The compatibility of all nine metals was evaluated in hydrazine containing water and chloride. The results of the statistical analysis indicate that the differences in metals are the primary factor affecting the differences in decomposition rates, and not the impurities or the impurity levels. However, the difference between water and chloride is statistically significant. In this case one percent water had a greater effect on accelerating hydrazine decomposition than did 10 ppm of the chloride ion. The CO_2 results were not statistically significant and, therefore, the effect of dissolved CO_2 on hydrazine decomposition could not be evaluated.

Extent of Metal Dissolution

The total amount of dissolved metals present in hydrazine at the end of each fifteen year simulated time test was determined by emission and atomic adsorption spectroscopy. The total dissolved metals are based on the hydrazine

volume noted in Tables XI through XVIII. This volume was 80 to 90 ml, except for the vapor-liquid tests where the volume was reduced to approximately 50 ml so that only half of each test piece was exposed to hydrazine. Thus, approximately 80 to 90 micrograms of metal in solution corresponds to a 1 ppm (by weight) metal concentration. (Concentrations above 1 ppm (by weight) for a given metal over the 15 year simulated test period are considered significant.) Keeping the microgram-ppm relationship in mind, it is possible to draw some conclusions about metal dissolution in hydrazine.

a) Dissolved aluminum was high for the baseline tests (Table XI) for AA2219, AA508 430SS, Ti6Al4V, and Inconel X750. The dissolved metal concentrations are 2.9 ppm, 19.9 ppm, 7.9 ppm, and 11.9 ppm for the alloys in the order noted above. Iron dissolution was high for AA6061-T6, 430SS, and 17-4PHSS, amounting to 1.6 and 3.9 and 1.1 ppm, respectively. The nickel concentration for the Inconel X750 baseline test was also significant at the 1.9 ppm level.

b) The trend toward high iron concentrations was also noted for the vapor-liquid, edge and bend tests (Tables XII, XIII, and XVII). The iron concentration was 2.9 ppm for 304L SS and 1.6 ppm for Haynes 25 for the vapor-liquid tests and 1.2 ppm for the Ti6Al4V bend test, and 1.9 ppm for the AA6061-T6 edge test. In addition, the nickel concentration was high in both the bend and edge tests for Inconel X750, increasing to 4.6 and 3.6 ppm, respectively.

c) High concentrations of iron and nickel were also noted for the Inconel X750 tests in the stress condition (Table XVI) and were 2.6 and 12.0 ppm, respectively. The only significant metal dissolution levels for the nonstress tests were 2 ppm iron for AA6061-T6 and 1 ppm iron for Ti6Al4V. The only significant concentration of dissolved metal detected for the crevice tests was 1 ppm aluminum for AA6061-T6 (Table XIV).

d) The trend toward preferential iron dissolution was also noted for the bimetallic and weld and braze tests (Tables XV and XVIII). The 304L SS to Inconel X750 gold-nickel braze, the 304L SS to 304L SS electron beam weld and the Ti6Al4V to Ti6Al4V TIG weld all resulted in iron concentrations in excess of 1 ppm. A 2 ppm iron concentration was also noted for the 304L SS to 17-4PHSS bimetallic junction, while the Haynes 25-Inconel X750 bimetallic junction resulted in a 12 ppm nickel concentration.

When the large number of samples tested are considered in light of the total number of elements present in each metal, it is found that relatively few situations existed where the metal concentrations exceeded the defined significance level of 1 ppm in 15 years simulated time. These elements and their concentrations are summarized in Table XIX. The metals and alloys have been rated based on the extent of metal dissolution according to the following criteria: compatible < 2 ppm; probably compatible 2 to 5 ppm; doubtful compatibility 5 to 10 ppm; and not compatible > 10 ppm. Thus, Inconel X750

is not considered to be compatible in terms of metal dissolution in the baseline, stress and bimetallic conditions (in conjunction with Haynes 25 in the latter case). In addition, AA5086 is not compatible in the baseline condition. The remainder of the materials all fall into the compatible and probably compatible categories. The highest amount of dissolved metal found was 1791 micrograms Al for the AA5086 baseline test. This value translates to 19.9 ppm Al after a fifteen year exposure. There is no aluminum limit specified in the hydrazine mil spec (MIL-P-26536C); however, for iron the limit is 20 ppm. The highest iron content found in this test sequence was 312 micrograms, or 4 ppm, which is well below the specified value. In view of the above results, it appears that hydrazine decomposition rates are the predominant factor to be considered in terms of metal propellant compatibility, and metal dissolution is not a significant problem.

SECTION IV

MONOMETHYLHYDRAZINE FEASIBILITY DEMONSTRATION

Feasibility studies to demonstrate measurability of the exchange current, establish a plausible surface reaction mechanism and compare results to real time compatibility test data were carried out to demonstrate the applicability of the electrochemical test method for the measurement of compatibility of selected metals with propellant grade monomethylhydrazine (MMH). Available real-time compatibility data for MMH was reviewed. Their comparison to the simulated time results of this study is discussed in this section. This review included comparison of both MMH decomposition and metal dissolution as functions of time and other pertinent operating parameters.

The experimental techniques were identical to those used for hydrazine as outlined in Appendix A. However, it was necessary to first determine the MMH decomposition mechanism in order to translate the exchange current density (i_0) data into quantitative terms. This mechanism and the resulting equation for converting i_0 to MMH decomposition rates were discussed earlier in Section II.

The results of the monomethylhydrazine feasibility studies on Ti6Al4V, 304L SS and AA1100 using the standard baseline slug configuration, are summarized in Table XX. The data indicate that the total amount of MMH decomposed per unit surface area decreased in the order Ti6Al4V > 304L SS > AA1100 for exposure times longer than one year. For shorter exposure time, the order was 304L SS > Ti6Al4V > AA1100 due to an initially lower rate of MMH decomposition on Ti6Al4V. The results of the analyses for metal content at the end of each test are summarized in Table XXIII in terms of total metal dissolution (μg) and residual solute concentration (ppmw) levels. Except for dissolved iron which is present as a contaminant in MMH (0.1-2 ppm), and dissolved aluminum, in the case of the Ti6Al4V tests, metal dissolution was minimal. Since the tests were only extended to a 4.0 to 6.5 year simulated times, the significance level for each element was estimated to be 0.33 ppmw according to the criteria described in Section III.

Data Comparison

The present data were compared to existing real time test data for both MMH decomposition and metal dissolution. Quantitative data for AA1100, 304L SS and Ti6Al4V at the specified test conditions were used whenever possible; however, in most cases the data available in the literature were either semi-quantitative or the test conditions (particularly temperature and metal alloy compositions) were substantially different from those specified in the present

study. Thus some of the comparisons are semiquantitative or qualitative because of differences in temperature, the physical state of the metal and, in one case in the alloy itself.

Monomethylhydrazine Decomposition

A recent survey of the MMH literature was compiled by Toth, et al. (Ref. 7) and an earlier survey was compiled by Uney, et al. (Ref. 10). The only quantitative data found for MMH at test conditions similar to those discussed herein were those of Toth (Ref. 9) for Ti6Al4V and 304L SS at 110 F and of Ross (Ref. 8) for pure aluminum, iron and titanium at 112 F. In the latter case, propellant (MMH) decomposition rates measured with pure aluminum were identical to those measured in this study for AAl100. In addition, Rosenberg (Ref. 11) reported data on Ti6Al4V at 158 F. The data of Refs. 9 and 11 are summarized in Table XXI; data from Ref. 8 are summarized in Table XXII. Tables XXI and XXII also contain a tabulation of the corresponding data obtained in the present investigation at 110 F. The data comparison is discussed below, in terms of the variations in test conditions and alloying constituents for each of the three investigations.

A comparison of results obtained by Toth, et al. (Ref. 9) for Ti6Al4V and 304L SS in MMH with results obtained from the present study is shown in Fig. 14. The Ti6Al4V used in the work of Toth (loc. cit.) was a bimetal standard which was tested in conjunction with 303 SS, and the 304L SS was a stressed slug. MMH decomposition was calculated from the data of Ref. 9, using the volume of gas produced at STP and the mole percentage of nitrogen. In Fig. 14, it should be noted that the estimated error in the UTRC data is ± 20 percent of the absolute value, while the error for the gas evolution method is estimated to be ± 25 percent of the absolute value. The latter estimate has been used previously at AFRPL to evaluate material compatibility data.

The present data for Ti6Al4V indicate higher MMH decomposition rates for the alloy alone than was obtained by JPL (Ref. 9) for a bimetallic couple containing the alloy as one component (see Fig. 14). In this regard, in the case of N_2H_4 compatibility, it was found that the 304L SS/Ti6Al4V bimetallic couple induces propellant decomposition rates which are similar to the 304L SS baseline results and are not very different from the individual values. Since hydrazine and MMH are expected to behave similarly in this respect, i.e., two alloys (304L SS and Ti6Al4V) usually have about the same degree of compatibility, there should be a minimal effect on the MMH decomposition rate due to the bimetallic configuration. Based upon these considerations the JPL data shown in Fig. 14 should be roughly comparable to the pure Ti6Al4V data shown for comparison. Thus, although a difference is noted between the JPL and UTRC data, it is not substantial when the respective error bands are taken into consideration.

The work by Ross, et al. (Ref. 8) included MMH compatibility data on pure aluminum, titanium, and iron. Although these metals are not equivalents of the alloys tested in the present work, the data are in essential agreement for general compatibility comparisons. The data obtained at 50 C (122 F) on 3.27 cm² samples exposed to 1 ml (870 mg) of MMH for 0.92 years, are compared to the present data in Table XXII and Fig. 15. Interestingly the data for Ti, Al and Fe are very similar to the present data.

Rosenberg (Ref. 11) tested Ti6Al4V in MMH at 70 C (158 F) for 107 days (0.293 yrs). The surface area of the test piece was 2.5 cm². The gas evolution was 1.25 cc of N₂ and corresponds to a total decomposition of 1.038 mg/cm² of metal surface, compared to the smaller UTPC value of 0.10 mg/cm² at 110 F for the same time period (see Table XXI). The disparity in temperature may account for the differences in the decomposition rates, but without a better knowledge of the reaction kinetics and their variation with temperature a quantitative comparison cannot be justified.

Metal Dissolution

In addition to the MMH decomposition data, the extent of metal dissolution in MMH was measured for Ti6Al4V and 304L SS (Table XXIII). The results were compared to data obtained by Toth (Ref. 9) and Green (Ref. 12). Toth found 9.5 ppm metal in MMH exposed to 304L SS and 6.5 ppm metal in MMH exposed to Ti6Al4V after 3.75 years real time for a 20 gram MMH sample; a total of 190 µg dissolved metal for 304L SS and 130 µg dissolved metal for Ti6Al4V, as compared to 77 µg and 182 µg for these two metals in the present study.

The results obtained by Green (Ref. 12) indicated no metal dissolution after 60 days exposure to MMH at 110 F in the case of Ti6Al4V and only 0.6 µg dissolved nickel for 304L SS. If these results are extrapolated on a linear basis to the 3.75 yr data, the result would be 13 µg nickel as compared to 3.0 µg nickel measured in the present study.

Conclusions

Since the data available in the literature were obtained for test conditions which varied considerably, it appeared most appropriate to rate the metals tested in terms of the extent of both propellant decomposition on the metal surface and metal dissolution. In terms of MMH decomposition, the metals tested rank in the order of decreasing compatibility: AAl100, 304L SS, and Ti6Al4V, for exposure times of 6.5, 5.0, and 4.0 years, respectively. However, if the fact that a rapid increase in MMH decomposition was noted on Ti6Al4V after 0.75 yrs is taken into consideration, then the extent of MMH decomposition

at 0.75 yrs is 0.071 mg/cm^2 for AA1100, 0.270 mg/cm^2 for Ti6Al4V, and 0.601 mg/cm^2 for 304L SS, confirming the ranking of Uney (Ref. 10). The ratings in terms of increasing metal dissolution are AA1100, 304L SS, and Ti6Al4V, and it appears that iron and aluminum are preferentially dissolved.

The UTRC MMH simulated compatibility data have been found to be in good agreement with real time data generated by other workers. Generally the UTRC data are either close to real-time results or can be reconciled in terms of differences in operating parameters. On a semiquantitative basis, metal compatibility ratings are identical to ratings found in the literature for AA1100, Ti6Al4V, and 304L SS. Therefore, it is concluded that reliable long-term MMH-metal compatibility data can be obtained using the electrochemical test method.

SECTION V

LONG-TERM COMPATIBILITY DETERMINATIONS - MONOMETHYLHYDRAZINE

Long term compatibility testing in monomethylhydrazine was carried out in the same manner as the hydrazine testing discussed in Section III except that the investigation of metal pretreatment and impurity effects was modified since it was determined in the course of hydrazine testing that metal and temperature effects were predominant and, thus, masked the effects of metal pretreatment and impurities. All special metal configurations were evaluated in terms of baseline to metal configuration ratios using both slug and metal strip test specimens, as was done with N_2H_4 .

Baseline Compatibility of Various Metal Alloys
with Monomethylhydrazine

The results of the baseline testing of twelve different metal alloys using slug-type test specimens exposed to monomethylhydrazine at 110 F are summarized in Table XXIV as a function of simulated time. Also shown in the table is the average ratio of MMH to hydrazine decomposition rate previously measured with the same metal. The data at fifteen years simulated time are also presented in Fig. 16. As can be seen from the figure, within the ± 20 percent experimental error, the four aluminum alloys tested are identical in terms of cumulative MMH decomposition at fifteen years simulated time, with values of less than 1.0 mg/cm^2 . Ti6Al4V has a somewhat larger effect on MMH decomposition, but may still be considered to have excellent compatibility with MMH. Haynes 25, 304L SS, 430SS, Inconel X750 and 17-4PHSS all appear to have a nearly equal effect on MMH decomposition and are probably compatible. Only Pt-10% Ir and Hastelloy B are considered to be incompatible with MMH. In general the extent of decomposition of MMH is lower than that for hydrazine (Fig. 6); except for Ti6Al4V which exhibits essentially equal compatibility with either propellant. It is noteworthy that the four most active metals in terms of hydrazine decomposition, i.e., Haynes 25, Inconel X750, Hastelloy B and Pt-10% Ir, indicate a much lower effect on MMH decomposition. In the case of Pt-10% Ir, the MMH decomposition at fifteen years simulated time is only eleven percent of that for hydrazine. A complete set of data taken with the twelve metal alloys is presented in Figs. 17(a) and 17(b), and the compatibility ratings are summarized in Table XXV.

The baseline test results were used in a comparative evaluation of the effects of a vapor-liquid interface, edges, crevices and bimetallic junctions as well as metal pretreatments and propellant impurities. These tests were performed with both slug type and metal strip test specimens using AA6061-T6, 304L SS, Ti6Al4V, Haynes 25, and Inconel X750.

Effect of Special Metal Configurations

The effect of special metal configurations, including the vapor-liquid interface, edges, crevices, and bimetallic junctions, was determined using the metal slug type test specimens. A complete data set of results obtained with MMH is found in Appendix C, Figs. C-1 through C-4.

Effect of Vapor-Liquid Interface

The results of the vapor-liquid interface tests are presented in Figs. 18(a) and 18(b). These data were compared to the baseline results in order to evaluate the comparative effect of the vapor-liquid interface on the decomposition rate of MMH. As shown in Table XXVI and Figs. 18(a) and 18(b), there was a positive effect (i.e., accelerated MMH decomposition) with four of the five metals tested. Only Haynes 25 yielded lower decomposition rates at the vapor-liquid interface. At the fifteen year simulated time period, the metals tested can be ranked in the following order with respect to the effect of a vapor-liquid interface: Inconel X750 > 304L SS > Ti6Al4V > AA6061-T6 > Haynes 25. However, only Inconel X750 and 304L SS show a serious effect due to the presence of a vapor-liquid interface when the results are measured in terms of the absolute values of MMH decomposition. In the case of these metals this deficiency is deemed sufficiently serious to disqualify them as candidates for tanks to be used for the long term storage of hydrazine.

Effect of Edges

Results obtained from the edge tests are compared to results from the baseline slug specimens in Table XXVII and Figs. 18(a) and 18(b). The edge test specimens are similar to the standard metal slugs except that they have a circumferential edge which is also exposed to the MMH. Consequently, the surface area of the edge test specimen is 0.77 cm^2 ; whereas, the surface area of the standard slug is 0.5 cm^2 . A significant increase in MMH decomposition due to the presence of edges was observed only for Ti6Al4V. As shown in Figs. 18(a) and 18(b), at the end of fifteen years simulated time differences observed with the other alloys do not appear to be beyond the respective uncertainty limits. A complete summary of the compatibility results obtained with the edge specimens appears in Fig. C-2.

Effect of Crevices

The results of the crevice test data are also compared to the slug baseline data in Fig. 18(a) and 18(b). Table XXVIII highlights this comparison, where a significant acceleration ratio (i.e., crevice decomposition rate-to-baseline) was found only in the case of the aluminum alloy, AA6061-T6. A complete data set is provided in Fig. C-3. Crevices were created by placing

a Teflon ring over a slug test piece which was recessed (approximately 0.25 cm) in the teflon holder, thereby creating a narrow annular space where a thin film of MMH could be trapped between the teflon and the test piece. The teflon ring restricts the movement of decomposition products away from the metal-solution interface, thereby accentuating any possible autocatalytic enhancement of MMH by reaction products if it should occur. The open surface area of the test piece is 0.25 cm^2 . The positive effect noted with AA6061-T6 (i.e., increased rate of MMH decomposition), due to preferential crevice attack, indicates some autocatalytic effect of decomposition products which was not indicated in the case of the other materials tested. As seen from Table XXVIII the average crevice-to-baseline ratios for these metals were 1.35 for Inconel X750, 0.60 for Ti6Al4V, 0.54 for 304L SS and 0.50 for Haynes 25.

Bimetallic Junctions

The results of the bimetallic junction tests are summarized in Table XXIX and Fig. 19. When the results are compared to the single metal values (baseline slug), the values of MMH decomposition for the combinations of 304L SS with the aluminum, titanium, and steel couples, (i.e., 304L SS/AA6061-T6, 304L SS/Ti6Al4V, and 304L SS/17-4PH), appear to roughly correspond to the average of the two metals involved. The MMH decomposition rate observed for the 304L SS/Inconel X750 couple was higher than either of the single metals, but not so far beyond the anticipated uncertainty limits that this could not be attributed to experimental error. Surprisingly, the Haynes 25/Inconel X750 couple had a lesser effect on MMH decomposition than either of the single metals, as shown by Fig. 19. This result was also observed in the case of hydrazine, so possibly the effect is real. At present, there is no satisfactory explanation for this behavior. In summary, the effect of the bimetallic couples on propellant compatibility appear to correspond to at least one of the metals involved and; therefore, no synergistic effects have been observed except, possibly, for the passivation effect of the Haynes 25/Inconel X750 couple. A complete data set for the bimetallic junction tests is presented in Fig. C-4.

Summary of Slug Configuration Tests

The results of the metal slug configuration tests were summarized graphically in Figs. 18 and 19 in terms of the relative effects of a vapor-liquid interface, edges, crevices, and bimetallic couples on the extent of monomethylhydrazine decomposition at fifteen years simulated time. The error bands shown in the figures reflect the estimated experimental error in the measurements (i.e., $\pm 20\%$) of cumulative decomposition at fifteen years simulated time.

Of the five metals tested, the presence of a vapor-liquid interface had a pronounced effect on MMH decomposition only for 304L SS and Inconel

X750. Edge effects present a compatibility problem in the case of Ti6Al4V, while the crevice effects were sufficiently small that, if present, they were not discernable beyond the experimental uncertainties.

Effect of Metal Stress, Welds and Brazes

Effect of Stress

The extent of MMH decomposition was evaluated as a function of metal stress using metal strip specimens set in specially designed glass holders which are described in more detail in Appendix A. The desired level of metal stress was fifty percent of yield strength in each test case; however, due to experimental inaccuracies, the actual stress levels obtained ranged from 40 to 70 percent of the yield strength. The results of the stress vs. nonstress tests are summarized in Table XXX and Figs. 20(a) and 20(b). As is apparent from the tables and figures there was very little effect of stress, with the possible exception of Inconel X750 where the average increase in MMH decomposition over fifteen years simulated time was approximately one and one-half times the nonstress results (c.f., Figs. C-5 and C-6). However, even in this case it is not clear that the measured effect is significant, (i.e., beyond the experimental uncertainties involved). Otherwise, the results of the AA6061-T6, 304L SS, Ti6Al4V and Haynes 25 tests do not indicate any effect of stress on MMH/alloy compatibility.

Effect of Bends

To evaluate the effect of bends on MMH decomposition, the results of the bend tests are compared to the nonstress test results in terms of bend-to-nonstress ratio. Although use of this ratio does not eliminate the influence of test piece surface area, it does emphasize the effect of the bend. These data are also presented in Fig. 20(a) and 20(b) and are summarized in Table XXXI. As shown in Fig. 20, except for Haynes 25, the data at fifteen years simulated time do not indicate an experimentally significant effect of metal strain on propellant (MMH)/material compatibility. A complete data set concerning the bend tests with MMH is compiled in Fig. C-7.

Effect of Welds and Brazes

The results of the weld and braze tests are summarized in Table XXXII and Fig. 21, where they are compared to the single metal nonstress results. All weld and braze configurations consist of metal strip specimens joined longitudinally and mounted in the holders described previously in conjunction with the stressed and nonstressed material compatibility studies. The sample lengths

are identical to the metal strips used for the nonstress tests and the widths due to metal joining, are double the nonstress width. The results for Electron Beam welding of 304L SS to 304L SS and Tungsten-Inert Gas (TIG) welding of Ti6Al4V to Ti6Al4V both suggest a small increase in MMH decomposition rate as evidenced by weld-to-nonstress ratios of 1.25 and 1.50, respectively; however, these conclusions are tentative, and are not supported by clearcut differences beyond the estimated uncertainty limits. The results for TIG welding of Inconel X750 to Haynes 25 indicates that the welded piece takes on the character of the Haynes 25, which is the less active of the two metals in terms of MMH decomposition. In the case of the brazing alloys used to join 304L SS and Inconel X750, the results of the tests indicate that the extent of MMH decomposition is approximately intermediate between that observed individually for the respective metals, (i.e., 304L SS and Inconel X750) with no significant difference with braze material. Thus, the effect of the braze on compatibility is not significant, and the resulting MMH decomposition rate is a compromise between that obtained with the two metals. Detailed test results obtained with the brazed and welded test specimens are found in Fig. C-8.

Summary of Metal Strip Results

The results of the metal strip configuration tests are summarized graphically in Figs. 20 and 21. As noted previously, the only statistically significant adverse effect noted with the stress and bend configurations was observed in the case of the bend with Haynes 25 (Fig. 20(b)). In all other cases, the effects of metal stress or plastic strain (bends) were insignificant within the experimental error limits.

Similarly, there was no effect on material compatibility from the weld and braze effects tested (c.f., Fig. 21). The only surprise resulting from these tests was with the TIG weld of Haynes 25/Inconel X750 which yielded an MMH decomposition level that was much lower than for Inconel X750 alone and approximately equal to the Haynes 25 base line.

Effect of Metal Pretreatment and Propellant Impurities

The effects of metal pretreatment and propellant impurities on MMH decomposition were evaluated using a simpler format than the statistically determined test matrix used for the hydrazine studies. In the latter case, the metal and temperature effects were so predominant that the true effects of metal pretreatment or impurities could not be determined.

Comparative Effect of Cleaning Procedures

The same three cleaning procedures outlined in Appendix D were used for the same five metals used in previous comparison tests; however, all tests were

performed at 110 F. These procedures include: passivation as the primary step for Procedure A, and acid pickling as the primary step for Procedure B. Procedure C is a simple degrease-detergent clean.

A summary of the results at fifteen years simulated time is shown in Table XXXIII. Metal pretreatment procedure B, was found to be superior (i.e., it resulted in the lowest MMH decomposition) for AA6061-T6 and 304L SS, while pretreatment procedure A was found superior for Ti6Al4V. Procedure C is best for Inconel X750, whereas in the case of Haynes 25, all three pretreatment procedures give essentially equivalent results. Since metal pretreatment procedure C (a simple IPA-detergent process) is the least complex, it should be chosen in those cases where complex pickling or passivation procedures do not appear to have any advantage. A complete data set for the evaluation of cleaning procedures is presented in Figs. C-9 through C-11.

Effect of Water Contamination

The results of the MMH impurity tests are summarized for the case of water contamination in Table XXXIV and for chloride contamination in Table XXXV. In the case of water, the tests were performed in MMH to which an additional 1.0, 1.5 and 2.0 percent distilled water was added to the 1.1 percent water found in the stock MMH used for these studies,* (the maximum water concentration specified in MIL-P-27404A is 1.5 percent). Therefore, the total water content ratios were 2.1, 2.6 and 3.1 percent, as shown in Table XXXIV, all of which are considerably higher than the normal MMH water concentration.

As can be seen from Table XXXIV, it is apparent that, over the range of concentrations tested, the observed effect of water on MMH was not systematic, and except for possibly the aluminum alloy (AA6061-T6) and Haynes 25, MMH decomposition appeared minimal and essentially independent of water concentration. In the case of Haynes 25 compatibility with MMH containing H₂O appeared to have a passivating effect. A complete data set concerning the effect of water contamination on MMH compatibility is found in Figs. C-12 through C-14.

Chloride Ion Contamination

The results of compatibility tests as a function of temperature and the chloride ion concentration as an impurity are summarized in Table XXXV. Generally these data were considerably more systematic than was observed in the case of water contamination. It is apparent that the combined chloride-temperature effects are statistically insignificant for 304L SS and Ti6Al4V.

*The water concentration level was verified by gas chromatography.

In the latter case both chloride and temperature levels are at the highest anticipated field values, so the absence of any observable effect on MMH compatibility may be accepted with confidence. In the case of Inconel X750, the effect of low temperature appears to predominate and masks any systematic effect of chloride as a contaminant. However, a large increase in MMH decomposition was obtained for the case of AA6061-T6 at 10 ppm concentration of the chloride ion and 160 F, where the extent of decomposition was ten to forty times greater than the baseline data. This appears sufficiently great that it can be inferred that the chloride ion is quite damaging to MMH compatibility with aluminum. This conclusion is consistent with other data concerning aluminum corrosion.

Extent of Metal Dissolution

The total dissolved metals in MMH at the end of each fifteen year simulated time test were determined by emission and adsorption spectroscopy. The total dissolved metals for each of the test series are tabulated in Tables XXXVI through LII for each of the metal configurations, metal pretreatments, and impurity tests. Table LIII is a summary of the metal dissolution data at the 1 ppm significance level. As was done in the case of hydrazine, in Table LIII material compatibility was evaluated in terms of metal dissolution according to the following criteria: compatible < 2 ppm; probable compatibility 2 ppm to 5 ppm; doubtful compatibility 5 ppm to 10 ppm; not compatible > 10 ppm.

There are four metal configurations that exceeded the 10 ppm level. These are, in decreasing order of metal dissolution, Haynes 25 - Crevice, Haynes 25/Inconel X750-Bimetallic couple, Hastalloy B - Baseline, 304L SS - Edge.

When the results of the impurity and metal pretreatment tests are evaluated in terms of metal dissolution, there are also four situations in which the 10 ppm impurity level is exceeded. Those are, in decreasing order of metal dissolution, Inconel X750 - H₂O, 304L SS - H₂O, Inconel X750 - Metal Pretreatment A, and 304L SS - Metal Pretreatment A.

In general, the extent of metal dissolution that resulted from exposure to MMH was much greater than for exposure to propellant grade N₂H₄. Thus, the relative effects of propellant decomposition and metal dissolution are opposite for the two propellants, e.g., with hydrazine propellant decomposition rates are generally higher than is observed with MMH, but the metal dissolution rates are generally less than those observed with MMH.

SECTION VI

APPLICATION OF COMPATIBILITY DATA

Prediction of Storage Tank Pressure Rise

An important application of long-term propellant decomposition data is involved in the prediction of storage tank pressure rise due to the evolution of gaseous products with increasing time. The baseline decomposition data on AA6061-T6, Ti6Al4V and 304LSS for both hydrazine and monomethylhydrazine (MMH) have been used to illustrate this data translation. Examples are based on a spherical tank, twenty inches in diameter with an ullage volume of one percent. In order to completely describe the system, it is necessary to know the mass of the propellant and the metal surface area exposed to the liquid, since the decomposition data is expressed in terms of mass decomposed per unit surface area per unit time. It is also necessary to know the molar composition of the evolved gases and their solubilities in the propellant in question. In addition, the vapor pressure of the propellant must be taken into consideration.

The tank dimensions and the physical properties of both propellants at a temperature of 43 C (110 F), are summarized in Table LIV.

Hydrazine Storage

As discussed in the preceeding sections of this report, the decomposition of hydrazine results in the formation of ammonia and nitrogen in a four to one molar ratio. Although some hydrogen might be formed as a consequence of ammonia decomposition, it was not considered in the present analysis because typically appreciable ammonia decomposition is not obtained except at higher temperatures involving heterogeneous reaction on active metal catalysts such as platinum (Ref. 6).

The solubility of ammonia in hydrazine was investigated by Chang, et al. (Ref. 13) and was reported to obey Henry's Law. The relationship between mole fraction NH_3 dissolved in hydrazine and its partial pressure in the gas phase is given by;

$$X_{\text{NH}_3} = K P_{\text{NH}_3} \quad (25)$$

where P_{NH_3} is the partial pressure of NH_3 in the gas phase, and the Henry's Law constant of proportionality, $K = 0.05283$ for $0 \leq P_{\text{NH}_3} < 7.571$ atm at 40 C (Ref. 9). To simplify the computations, the assumption was made

that all the NH_3 was dissolved and then Eq. 25 was used to calculate the partial pressure of NH_3 vapor. With only one percent ullage volume the incurred error from this assumption is negligible. The results of these calculations are summarized in Table LV. The calculated NH_3 partial pressure is the maximum vapor pressure which can exist consistent with the total NH_3 constraint. It can be seen that the highest of these pressures (8.2×10^{-3} atm) is still lower than the vapor pressure of N_2H_4 (5.0×10^{-2} atm) and therefore, the total pressure rise in the tank is determined primarily by the partial pressures of nitrogen and hydrazine.

The solubility of nitrogen in hydrazine has also been determined by Chang, et al. (Ref. 14). The equilibrium constant (K_{N_2}) for nitrogen solubility is given by;

$$C_{\text{N}_2} \text{ (ppm in liquid)} = K_{\text{N}_2} P_{\text{N}_2} \quad (26)$$

where P_{N_2} is the nitrogen partial pressure in atmospheres, C_{N_2} is the parts per million by weight of dissolved N_2 in the liquid phase. For the temperature of interest (110 F or 43 C) Chang determined that K_{N_2} is 7.9303.

If all NH_3 were assumed to be dissolved in the hydrazine (a negligible incurred error) the total pressure in the tank is given by;

$$P_T = P_{\text{N}_2} + P_{\text{N}_2\text{H}_4} \quad (27)$$

where P_{N_2} is the partial pressure of N_2 and $P_{\text{N}_2\text{H}_4}$ is the vapor pressure of hydrazine. Combining Eqs. 26 and 27 an equation for the total pressure in the tank is derived in terms of total N_2 production resulting from hydrazine decomposition, i.e.;

$$P_T = 22.0 n_{\text{N}_2, \text{TOT}} + 0.0505 \quad (28)$$

where $n_{\text{N}_2, \text{TOT}}$ is the total production of nitrogen in gram moles, and the constant of proportionality includes the solubility equilibrium constants, tank volume and fill ratio, and various unit conversion constants.

The results of the pressure rise calculations assuming complete ammonia solubility are summarized in Table LVI and the first half of Fig. 22. Thus, as shown by the figure for hydrazine storage, after 15 years exposure time, a pressure of 70 psia (4.8 atm) is predicted for 304LSS, 30 psia (2.0 atm) for Ti6Al4V and 48 psia (3.3 atm) for AA6061-T6 tanks.

Monomethylhydrazine Storage

The decomposition of monomethylhydrazine (MMH) results in the formation of equimolar amounts of methane and nitrogen for three moles of MMH decomposed. (See. Section II). The total pressure is given by:

$$P_T = P_{N_2} + P_{CH_4} + P_{MMH} \quad (29)$$

The solubility of nitrogen in MMH has also been measured by Chang, et. al. (loc cit) and is given by;

$$C_{N_2} \text{ (ppm in liquid)} = K_{N_2} P_{N_2} \quad (30)$$

where the solubility constant, K_{N_2} for nitrogen dissolution in MMH is 62.2 at 110 F.

However, the solubility constant for methane in MMH is not known and therefore, two expressions were derived to calculate the storage tank pressure rise from MMH decomposition. In one case it was assumed that the methane is completely soluble in MMH and in the second case the methane is completely insoluble, thereby representing the two extremes of tank pressure rise. If CH_4 is insoluble, then the expression for total pressure in the tank in terms of the N_2 and CH_4 production can be derived by combining equations 29 and 30 to give;

$$P_T = 4.812 n_{N_2, \text{TOT}} + 37.8 n_{CH_4, \text{TOT}} + 0.162 \quad (31)$$

where as before n represents total production in gram moles, and pressure is in atmospheres. When CH_4 is assumed to be completely soluble, then the total pressure in the tank is reduced, and is determined only by the partial pressure of N_2 and the vapor pressure of MMH, i.e.:

$$P_T = 4.812 n_{N_2, \text{TOT}} + 0.162 \quad (32)$$

Equations 31 and 32 were used to calculate the storage tank pressure rise due to MMH decomposition (i.e., evolution of methane and nitrogen) and the results are summarized in Table LVII and the second half of Fig. 22. After 15 years exposure to 304LSS, a maximum pressure rise (zero present CH_4 solubility) of 124 psia (8.4 atm) and a minimum pressure rise (100 percent CH_4 solubility) of 16 psia (1.1 atm) are predicted. The maximum pressure rise predicted for exposure to Ti6Al4V is 48 psia and for exposure to AA6061-T6, only 26 psia.

Prediction of Loss in Tank Wall Strength

The metal dissolution data obtained at the end of each test after fifteen years simulated time was used to calculate the reduction in wall thickness, and therefore, loss of structural strength of a typical propellant tank. The loss of metal was assumed to be uniform so that a penetration depth could be calculated. Since there was no evidence of pitting in any of the experiments, even with the aluminum alloys, the assumption of uniform corrosion may be appropriate.

The total dissolved metal measured for each of the baseline tests was used as the basis for the calculations. The results of the metal analyses are summarized in Tables XI and XXXVI for hydrazine and monomethylhydrazine, respectively. The reduction in tank wall thickness (penetration) was calculated according to the following equation.

$$\text{penetration (cm)} = \frac{\text{mass of metal in solution (grams)}}{\text{metal density (g/cm}^3\text{) x exposed surface area (cm}^2\text{)}} \quad (33)$$

The results of the calculations are summarized in Tables LVIII and LIX for hydrazine and monomethylhydrazine, respectively. The maximum reduction in tank wall thickness was 0.551 mil for AA5086 exposed to hydrazine. Typical tank wall thicknesses, for the three metals of major interest, are 10 to 15 mils for Ti6Al4V, 30 to 45 mils for AA6061-T6 and 5 to 10 mils for 304L SS. Therefore, from the penetration data, the average reduction in wall thickness for a typical hydrazine tank is approximately 0.16 percent for AA6061-T6, 1.1 percent for Ti6Al4V, and 0.05 percent for 304L SS.

Similarly, for exposure to MMH, the percentage reduction in wall thickness for AA6061-T6 is 0.04, for Ti6Al4V is 0.05 and for 304L SS is 0.19. Thus, it appears that metal dissolution does not present a significant problem with respect to loss in tank wall strength.

SECTION VII

CONCLUSIONS AND RECOMMENDATIONS

The investigations under this program demonstrated the viability of a new electrochemical test method for evaluating the long term compatibility of liquids in various containment materials. To utilize this method it is necessary only that the liquid and containment material under investigation be electrical conductors, and that the exchange current be measurable. With no external applied potential, the net exchange current is zero, consisting of parallel cells of anodic and cathodic current flow. With an applied external potential both exchange current contributors are perturbed according to well known electrochemical relationships; the current flow in the preferred direction increasing exponentially with applied voltage, whereas the counter current flow is similarly suppressed. Accurate measurement of the net current flow under these polarized conditions as a function of applied voltage defines a relationship from which the basic (zero applied voltage) exchange current density can be determined. This transfer of electrons associated with the exchange current is responsible for all interface reactions; metal dissolution and, in the case of the propellants hydrazine and monomethylhydrazine considered in this study, electrolyte decomposition. The successful demonstration in the present program that these reactions could be accelerated, without change in mechanism, in proportion to the ratio of electrolytic current flow relative to exchange current density is the most important conclusion of this program. Therefore, once the reaction mechanism attending the transfer of electrons under normal (zero applied potential) conditions can be established, the ability to predict long term compatibility on an accelerated time scale is guaranteed.

However, there were several shortcomings inherent in the scope of the present program. Principally, these were associated with a lack of understanding of the various phenomena associated with variations in the exchange current density. Accordingly, some unusual phenomena were recorded, such as the "passivation of certain materials with plastic deformation (bends)". At present these phenomena are attributed to either experimental uncertainty, or to different and uncategorized variations in electrode surface structure beyond that controlled by the precautions employed in this investigation. Thus, in the interest of identifying the comparative compatibility of the propellants (hydrazine and monomethylhydrazine) with a variety of different metal alloys as a function of temperature and metal condition; i.e., state of stress, plastic deformation, crevices, bimetallic couples, as well as weld and braze effects, there were few data where a direct comparison of results could be made to characterize experimental variances. Further work in this area is most

desirable if the present test procedure is to be upgraded to a standard method for the quantitative evaluation of long-term compatibility between various electrolyte materials and metals.

From the present study it can be asserted that generally hydrazine decomposes approximately an order of magnitude faster than monomethylhydrazine, but that monomethylhydrazine results in higher metal dissolution rates. Both propellants tend to follow the same pattern in that the various aluminum or titanium alloys are most compatible whereas the stainless steels, and nickel or cobalt base alloys are not recommended (on a comparative basis). The presence of excess water, (as a contaminant material) does not affect this relationship but small ppm concentrations of the chloride ion are very harmful to compatibility in the case of the aluminum alloys. Surprisingly, welds and brazes, and the state of metal stress or even plastic deformation had little effect on material compatibility. Even bimetallic couples failed to substantially increase propellant decomposition rate beyond the average of the two materials involved. Vapor-liquid interfaces appeared to have some effect, but the effect was not consistent from one alloy to the next. Finally the effect of three different metal cleaning procedures on propellant compatibility was evaluated again with mixed results.

It has been shown that propellant decomposition data can be used to predict propellant tank pressure rise, provided the solubilities of the decomposition gases in the particular propellant are known. It is also possible to predict loss in tank wall thickness by use of metal dissolution data. On the basis of the hydrazine decomposition results, it is recommended that contaminant materials be limited to aluminum alloys, Ti6Al4V and 17-4PHSS. In addition, crevices should be avoided when aluminum alloys are used. The results of the monomethylhydrazine decomposition evaluations indicate that only the aluminum alloys and Ti6Al4V are compatible; however, the edge configuration should be avoided when using Ti6Al4V.

The results of the experimental program described herein suggest a number of problem areas that deserve further attention. The present program was designed to apply the electrochemical test method to special metal configurations for hydrazine and to determine the applicability of the test method to monomethylhydrazine. Both of these goals were met and the experimental program was successfully extended to include special metal configuration tests in monomethylhydrazine. However, in many cases apparent "passivation" effects were encountered in which the apparent extent of propellant decomposition was reduced. Generally these anomalies were not resolved in terms of whether they were real or were occasioned by variations in alloy composition or experimental procedure, and the sample-to-sample variations which might be used to establish uncertainty limits in the application of these techniques to predicting long term propellant/material compatibility in practical circumstances is as yet undetermined.

Finally, the results of the nitrogen tetroxide feasibility study (Ref. 13) suggest that at very low water concentrations (less than one percent) N_2O_4 does not react on metal surfaces in any measurable amounts. Even when water is deliberately added to the system, it is necessary to achieve water contents equivalent to High Density Acid (HDA) type systems (N_2O_4 - HNO_3) in order to achieve measurable decomposition rates. Neither the single-phase region, below about two percent water concentration, nor the two-phase region, up to about 10 percent water concentration, was sufficiently conductive for electrochemical measurements, even in systems where the electrode spacing was on the order of 2 to 4 mm. It is not known whether this was an instrument limitation or intrinsic limitation of the test method.

Comparison of the data obtained in this study, with information available in the literature, indicates that the lack of any appreciable metal attack in the presence of propellant grade N_2O_4 is typical of N_2O_4 -metal systems with a low water content.

Thus, real-time results coupled with the results of the present feasibility study indicate that drastic contamination of N_2O_4 is necessary before any appreciable corrosion and/or propellant decomposition takes place. In the present study none of the test pieces were corroded or even tarnished by the contaminated N_2O_4 . However, it should be noted that as soon as the water content of N_2O_4 is sufficiently high to cause the formation of two phases, the acid rich phase will result in HDA type nitric acid corrosion in localized zones (i.e., crevices, etc.). Electrochemical measurements were made in this region and relatively high decomposition rates were noted.

It is suggested that future investigations of N_2O_4 -material compatibility emphasize detailed studies of the high-acid side of the two-phase region. These studies should include consideration of the localization of the high density phase at crevice positions, such as valve seats and swage type fittings.

REFERENCES

1. Brown, C. T.: Feasibility Studies of an Electrochemical Test Method for Nitrogen Tetroxide Compatibility Testing. AFRPL-TR-78-72, August, 1978.
2. Brown, C. T.: Electrochemistry of Hydrazine-Hydrazine Azide Mixtures. Presented at the International Conference on "The Properties of Hydrazine and Its Potential Applications as an Energy Source," Poitiers, France, October 1974.
3. Mansfield, F.: The Polarization Resistance Technique for Measuring Corrosion Currents. Advances in Corrosion Science and Technology. (1975), Rockwell International Science Center, Thousand Oaks, California.
4. Brown, C. T.: Determination of Long-Term Compatibility of Hydrazine with Selected Materials of Construction. Final Report, AFRPL-TR-76-21, United Technologies Research Center, East Hartford, Connecticut, May 1976.
5. Conway, B. E., N. Mainic, D. Gilroy, and E. Rudd: Oxide Involvement in Some Anodic Oxidation Reactors. Journal of the Electrochemical Society, Vol. 113, No. 11, pp. 1144-1158, November 1966.
6. Axworthy, A., et al.: Kinetics of Thermal Decomposition of Liquid MMH. Rocketdyne Division, Rockwell International, Canoga Park, California, Presented at 11th Liquid Propulsion Symposium, Miami Beach, Florida, September 16-18, 1969.
7. Toth, L. R., et al.: Survey - Monomethylhydrazine Propellant/Material Compatibility, AFRPL-TR-77-35. Jet Propulsion Laboratory, Pasadena, California, July 1977.
8. Ross, D. S. et al.: Study of the Basic Kinetics of Decomposition of MMH and MHF and the Effects of Impurities on Their Stability. AFRPL-TR-71-114, Stanford Research Institute, Menlo Park, California, September 1971.
9. Toth, L. R., et al.: Propellant/Material Compatibility Program and Results. Technical Memorandum 33-779, Jet Propulsion Laboratory, Pasadena, California, August 1976.
10. Uney, P. E., et al.: Materials Compatibility with Space Storable Propellants - Design Guidebook. MCR-72-26 (NAS7-100) Martin Marietta Corporation, Denver, Colorado, March 1972.

REFERENCES (Cont'd)

11. Rosenberg, S. D., et al.: Evaluation of High Energy Materials as Liquid Propellants. Report AGC-3344, Aerojet General Corporation, Azusa, California, January 1967.
12. Green, R. L., et al.: Advanced Techniques for Determining Long-Term Compatibility of Materials with Propellants. Final Report D180-14839-2 (NAS7-789), Boeing Company, Seattle, Washington, December 1973.
13. Chang, E. T., et al.: Solubilities of NH_3 , CO , CO_2 , and SF_6 in Liquid Propellants. SAMSO-TR-71-17. November 1970.
14. Chang, E. T., et al.: Solubilities of Gases in Simple and Complex Propellants, J. of Spacecraft and Rockets, Volume 6, No. 10, October 1969.

TABLE I
HYDRAZINE-MATERIAL COMPATIBILITY RATINGS
(15 Year Baseline Tests)
(110 F)

Category	Decomposition Rate Range mg/cm ²	Metals Included in Each Category
Compatible	< 2.0	AA1100, AA5086 AA6061-T6, AA2219 17-4PH3S, Ti6Al4V
Probable Compatibility	2.0 to 5.0	430SS, 304L SS
Doubtful Compatibility	5.0 to 10.0	HAYNES 25
Not Compatible	> 10.0	HASTELLOY B, PT-10% IR, INCONEL X750

TABLE II
EFFECTS OF A VAPOR-LIQUID INTERFACE
ON HYDRAZINE DECOMPOSITION
110 F

Metal	Time (yrs)	Vapor-Liquid Decomposition (mg/cm ²)	Baseline Decomposition (mg/cm ²)	Vapor-Liquid to Baseline Ratio
AA6061-T6	1.0	0.03	0.14	0.22
	5.0	0.20	0.82	0.24
	9.0	0.40	1.12	0.36
	15.0	0.89	1.85	0.48
304LSS	1.0	0.57	0.50	1.13
	5.0	4.12	1.33	3.10
	9.0	7.09	1.85	3.83
	15.0	10.90	2.70	4.03
Ti6Al4V	1.0	0.10	0.07	1.44
	5.0	0.49	0.42	1.18
	9.0	0.98	0.76	1.28
	15.0	2.28	1.26	1.81
INCONEL X750	1.0	1.27	1.06	1.20
	5.0	7.57	5.58	1.35
	9.0	16.34	9.44	1.73
	15.0	34.30	15.20	2.25
HAYNES 25	1.0	0.48	0.73	0.66
	5.0	6.11	3.36	1.81
	9.0	16.10	5.70	2.82
	15.0	27.00	8.92	3.30

TABLE III
EFFECTS OF EDGES ON HYDRAZINE DECOMPOSITION
110 F

Metal	Time (yrs)	Edge Decomposition (mg/cm ²)	Baseline Decomposition (mg/cm ²)	Edge to Baseline Ratio
AA6061-T6	1.0	0.19	0.14	1.35
	3.5	0.39	0.58	0.67
	11.0	0.87	1.33	0.66
	15.0	1.08	1.85	0.58
304L SS	1.0	0.41	0.50	0.83
	5.0	1.86	1.33	1.40
	9.0	3.07	1.85	1.66
	15.0	6.92	2.70	2.56
Ti6Al4V	1.0	.06	0.07	0.97
	5.0	1.12	0.42	2.69
	9.0	1.48	0.76	1.94
	15.0	1.88	1.26	1.49
INCONEL X750	1.0	0.52	1.06	0.49
	5.0	4.20	5.58	0.75
	9.0	7.41	9.44	0.78
	15.0	11.8	15.20	0.77
HAYNES 25	1.0	0.16	0.72	0.22
	5.0	0.66	3.36	0.19
	9.0	1.45	5.70	0.25
	15.0	2.00	8.92	0.22

TABLE IV
EFFECTS OF CREVICES ON HYDRAZINE DECOMPOSITION
110 F

Metal	Time (yrs)	Baseline Decomposition (mg/cm ²)	Crevice Decomposition (mg/cm ²)	Crevice to Baseline Ratio
AA6061-T6	1.0	0.14	0.92	6.41
	5.0	0.82	3.75	4.58
	9.0	1.12	6.73	6.01
	15.0	1.85	10.50	5.68
304L SS	1.0	0.50	1.11	2.20
	5.0	1.33	2.87	2.16
	9.0	1.85	4.50	2.43
	15.0	2.70	7.40	2.74
T16A14V	1.0	0.07	0.13	1.83
	5.0	0.42	0.70	1.69
	9.0	0.76	1.37	1.80
	15.0	1.26	2.53	2.01
INCONEL X750	1.0	1.06	0.02	0.02
	5.0	5.58	0.09	0.01
	9.0	9.44	0.18	0.02
	15.0	15.20	0.31	0.02
HAYNES 25	1.0	0.73	0.75	1.04
	5.0	3.36	2.40	0.71
	9.0	5.70	7.05	1.23
	15.0	8.92	11.7	1.31

TABLE V
EFFECTS OF BIMETALLIC JUNCTIONS
ON HYDRAZINE DECOMPOSITION

110 F

Time (yrs)	Bimetallic Couple 304L SS/17-4PH	Single Metals	
		304L SS	17-4PH
1.0	0.50	0.50	0.134
5.0	1.69	1.33	0.476
9.0	2.45	1.85	0.762
15.0	3.43	2.70	0.989

Time (yrs)	Bimetallic Couple 304L SS/AA6061-T6	Single Metals	
		304LSS	AA6061-T6
1.0	0.194	0.50	0.144
5.0	0.757	1.33	0.818
9.0	1.05	1.85	1.12
15.0	1.81	2.70	1.85

Time (yrs)	Bimetallic Couple 304L SS/INCONEL X750	Single Metals	
		HAYNES 25	INCONEL X750
1.0	0.559	0.72	1.06
5.0	2.92	3.36	5.58
9.0	5.19	5.70	9.44
15.0	-	8.92	15.20

Time (yrs)	Bimetallic Couple 304L SS/Ti6Al4V	Single Metals	
		304LSS	Ti6Al4V
1.0	0.482	0.50	0.071
5.0	1.15	1.33	0.416
9.0	1.70	1.85	0.762
15.0	2.50	2.70	1.26

Time (yrs)	Bimetallic Couple 304L SS/INCONEL X750	Single Metals	
		304LSS	INCONEL X750
1.0	0.878	0.50	1.06
5.0	3.72	1.33	5.58
9.0	5.30	1.85	9.44
15.0	7.30	2.70	15.2

TABLE VI
EFFECTS OF METAL STRESS ON
HYDRAZINE DECOMPOSITION
110 F

Metal	Time (yrs)	Stress Decomposition (mg/cm ²)	Nonstress Decomposition (mg/cm ²)	Stress to Nonstress Ratio
AA6061-T6	1.0	0.01	0.0	1.00
	5.0	0.01	0.04	0.25
	9.0	0.02	0.06	0.33
	15.0	0.03	0.10	0.30
304L SS	1.0	0.16	0.10	1.67
	5.0	0.61	1.02	0.60
	9.0	1.06	1.69	0.62
	15.0	1.69	2.35	0.71
Ti6Al4V	1.0	0.031	0.02	1.82
	5.0	0.11	0.11	0.98
	9.0	0.21	0.20	1.05
	15.0	0.36	0.35	1.04
INCONEL X750	1.0	0.41	0.18	2.20
	5.0	3.49	1.05	3.32
	9.0	6.24	2.68	2.32
	15.0	14.00	3.85	3.97
HAYNES 25	1.0	0.14	0.17	0.83
	5.0	0.82	0.86	0.94
	9.0	1.55	1.72	0.90
	15.0	2.75	3.05	0.90

TABLE VII
EFFECTS OF BENDS ON HYDRAZINE DECOMPOSITION
110 F

Metal	Time (yrs)	Bend Decomposition (mg/cm ²)	Nonstress Decomposition (mg/cm ²)	Bend to Nonstress Ratio
AA6061-T6	1.0	0.002	0.0	0.250
	5.0	0.005	0.04	0.116
	9.0	0.007	0.06	0.111
	15.0	0.008	0.10	0.073
304L SS	1.0	0.06	0.10	0.594
	5.0	0.77	1.02	0.756
	9.0	1.54	1.69	0.911
	15.0	2.04	2.35	0.868
Ti6Al4V	1.0	0.05	0.02	2.50
	5.0	0.24	0.11	2.18
	9.0	0.39	0.20	1.86
	15.0	0.68	0.35	1.94
INCONEL X750	1.0	0.27	0.19	1.42
	5.0	1.96	1.05	1.87
	9.0	3.69	2.68	1.38
	15.0	6.51	3.85	1.69
HAYNES 25	1.0	0.29	0.17	1.72
	5.0	2.12	0.871	2.43
	9.0	4.22	1.72	2.45
	15.0	6.46	3.05	2.12

TABLE VIII
EFFECTS OF WELDS AND BRAZES ON
HYDRAZINE DECOMPOSITION
110 F

Weld or Braze	Materials	Time (yrs)	Hydrazine Decomposition (mg/cm ²)			Weld or Braze to Nonstress Ratio	
			Weld or Braze	(Nonstress) Metal #1	Metal #2	Metal #1	Metal #2
Perma- Braze -130	INCONEL X750/ 304L SS	1.0	0.16	0.18	0.10	0.86	1.62
		5.0	0.91	1.05	1.02	0.86	0.89
		9.0	1.80	2.68	1.69	0.67	1.07
		15.0	3.14	3.85	2.35	0.81	1.34
Palniro #7 Braze	INCONEL X750/ 304L SS	1.0	0.15	0.18	0.10	0.80	1.51
		5.0	1.19	1.05	1.02	1.13	1.17
		9.0	2.42	2.68	1.69	0.90	1.43
		15.0	4.71	3.85	2.35	1.22	2.00
TIG Weld	INCONEL X750/ HAYNES 25	1.0	0.15	0.18	0.17	0.82	0.90
		5.0	0.94	1.05	0.86	0.90	1.09
		9.0	1.88	2.68	1.72	0.70	1.09
		15.0	3.13	3.85	3.05	0.81	1.03
TIG Weld	Ti6Al4V/ Ti6Al4V	1.0	0.04	0.02	0.02	2.41	-
		5.0	0.12	0.11	0.11	1.08	-
		9.0	0.21	0.20	0.20	1.01	-
		15.0	0.32	0.35	0.35	0.92	-
Electron Beam Weld	304L SS/ 304L SS	1.0	0.11	0.10	0.10	1.16	-
		5.0	0.65	1.02	1.02	0.64	-
		9.0	1.12	1.69	1.69	0.66	-
		15.0	1.68	2.35	2.35	0.75	-

TABLE IX

EFFECTS OF METAL PRETREATMENT ON HYDRAZINE
DECOMPOSITION AT 15 YEARS SIMULATED TIME

Metal	Metal Pretreatment	Temp (*F)	Cumulative Decomposition mg/cm ²
AA1100	A	50	.245
	B	110	.078
	C	160	2.60
AA6061-T6	A	110	.39
	B	160	1.07
	C	50	.37
AA5086	A	160	1.07
	B	50	.29
	C	110	.88
17-4 PH SS	A	110	4.04
	B	160	2.53
	C	50	5.19
430 SS	A	160	5.49
	B	50	1.73
	C	110	4.74
304L SS	A	50	.65
	B	110	.84
	C	160	15.70
Ti6Al4V	A	160	2.57
	B	50	0.27
	C	110	1.26
HAYNES 25	A	50	.67
	B	110	2.47
	C	160	20.50
INCONEL X750	A	110	18.40
	B	160	44.10
	C	50	6.71

TABLE X
EFFECTS OF IMPURITIES ON
HYDRAZINE DECOMPOSITION
110 F

Metal	Impurity	Final Time (Years)	Decomposition (mg/cm ²)	
			Impurities	Baseline
AA2219	1.5% H ₂ O	13	0.08**	0.25
	30 ppm Cl ⁻	15	0.05	0.28
	50 ppm CO ₂	4.25*	0.22	0.09
AA6061-T6	1.0% H ₂ O	15	0.28	1.85
	20 ppm Cl ⁻	17	0.14**	2.07
	150 ppm CO ₂	1.50*	0.01	0.18
AA1100	2.0% H ₂ O	15	0.66	1.37
	20 ppm Cl ⁻	11	0.15**	1.04
	50 ppm CO ₂	2.00*	0.18	0.24
Ti6Al4V	1.5% H ₂ O	15	0.48	1.26
	10 ppm Cl ⁻	15	0.67	1.26
	150 ppm CO ₂	6.5*	0.75**	0.54
304L SS	2.0% H ₂ O	15	6.25	2.70
	10 ppm Cl ⁻	15	2.51	2.70
	100 ppm CO ₂	15	3.32	2.70
430 SS	2.0% H ₂ O	15	5.64	4.74
	10 ppm Cl ⁻	15	2.23	4.74
	100 ppm CO ₂	15	4.37	4.74
17-4 PH SS	1.0% H ₂ O	15	2.37	0.99 (13 yrs)
	30 ppm Cl ⁻	15	3.67	0.99
	100 ppm CO ₂	15	5.57	0.99
HAYNES 25	1.5% H ₂ O	15	4.45	8.92
	30 ppm Cl ⁻	13	1.83**	7.80
	50 ppm CO ₂	15	5.42	8.92
INCONEL X750	1.0% H ₂ O	15	11.8	15.2
	20 ppm Cl ⁻	15	24.1	15.2
	150 ppm CO ₂	15	28.6	15.2

* Test terminated due to passivation effects

** Extrapolated or interpolated data

TABLE XI
METAL DISSOLUTION IN HYDRAZINE -BASELINE TESTS

110 F - 15 Years

μg METAL IN SOLUTION

Metal	Co	Fe	Al	Mg	Cr	Ni	Ti	Cu	Mn	V	Volume of Hydrazine (cc)
AA1100	-	-	25.6	-	1.60	-	-	-	-	-	80
AA6061-T6	4.0	128.0	44.8	-	28.8	8.0	-	-	0.80	-	80
AA2219	-	52.5	217.5	-	6.0	6.0	-	3.0	0.90	-	75
AA5086	-	45.0	1791.0	-	-	-	45.0	3.6	-	-	90
304L SS	-	36.0	-	-	7.2	-	-	-	-	-	90
430 SS	-	312.0	632.0	16.0	64.0	12.8	12.8	9.6	-	-	80
17-4 PH SS	-	99.0	-	18.0	-	7.20	-	10.8	-	-	90
Ti6Al4V	-	56.0	632.0	9.6	-	16.0	28.8	3.2	-	0.64	80
INCONEL X750	-	45.0	1071.0	-	3.6	171.0	32.4	-	-	-	90
HASTELLOY B	-	36.0	-	-	3.6	10.8	-	-	-	-	90
HAYNES 25	720.0	3.6	-	-	-	7.2	-	-	-	-	90

TABLE XII
METAL DISSOLUTION IN HYDRAZINE-VAPOR LIQUID TESTS
160 F - 15 Years

Metal	μg METAL IN SOLUTION							Vol. of Hydrazine (cc)
	Al	Cr	Fe	Ni	Cu	Mn	Ti	
AA6061-T6	-	.312	12.5	-	14.0	-	-	52
304L SS	-	41.0	165.0	25.6	6.27	12.5	-	57
Ti6Al4V	4.77	-	16.4	6.36	-	-	3.18	53
INCONEL X750	10.0	18.0	-	2.00	10.0	-	-	50
HAYNES 25	10.4	8.32	83.2	2.08	31.2	2.08	-	52

TABLE XIII
METAL DISSOLUTION IN HYDRAZINE - EDGE TESTS

110 F - 15 Years

Metal	μg Metal in Solution							Volume of Hydrazine (cc)
	Al	Cr	Fe	Ni	Cu	Mn	Ti	
AA6061-T6	-	0.64	152.0	-	28.8	-	-	80
304L SS	-	2.4	29.6	6.4	2.4	0.8	-	80
Ti6Al4V	2.4	-	36.0	8.0	-	-	2.4	80
INCONEL X750	2.4	13.6	37.6	288.0	-	-	4.0	80
HAYNES 25	-	0.4	-	-	-	0.4	-	80

TABLE XIV
METAL DISSOLUTION IN HYDRAZINE - CREVICE TESTS

110 F - 15 Years

Metal	μg Metal in Solution								Volume of Hydrazine (cc)
	Cr	Fe	Ti	Al	Ni	Cu	Mn	Co	
AA6061-T6	4.0	20.0	-	80.0	-	0.4	-	-	80
304L SS	2.0	13.6	-	-	0.8	0.4	1.52	-	80
Ti6Al4V	-	16.8	7.2	1.2	4.0	-	-	-	80
INCONEL X750	39.2	12.0	1.28	4.0	27.2	-	-	-	80
HAYNES 25	3.2	-	-	-	8.0	-	3.2	32.0	80

TABLE XV
METAL DISSOLUTION - HYDRAZINE - BIMETALLIC TESTS
110 F - 15 Years

Metal	μg METAL IN SOLUTION								Volume of Hydrazine (cc)
	Co	Fe	Al	Mn	Mg	Cr	Ni	Ti	Cu
304L SS -	-	18.0	18.0	-	10.8	14.4	1.8	3.6	18.0
AA6061-T6	-	18.0	-	-	-	-	-	-	-
304L SS -	-	18.0	-	-	-	-	-	-	-
Ti6Al4V	10.8	184.5	-	10.8	-	9.9	39.6	-	15.3
304L SS -	1.7	-	-	-	-	13.6	25.5	-	17.0
17-4 PH SS	-	-	-	-	-	-	-	-	-
304L SS -	18.0	36.0	18.0	5.4	28.8	50.4	1053.0	3.6	54.0
INCONEL X750	-	-	-	-	-	-	-	-	-
HAYNES 25 -	-	-	-	-	-	-	-	-	-
INCONEL X750	-	-	-	-	-	-	-	-	-

TABLE XVI

METAL DISSOLUTION IN HYDRAZINE - STRESS AND NONSTRESS TESTS

110 F - 15 Years

Test	Metal	μg Metal in Solution							V	Volume of Hydrazine (cc)
		Al	Cr	Fe	Ni	Cu	Mn	Ti		
Stress	AA6061-T6	-	0.88	39.2	-	2.4	-	-	-	80
Stress	304L SS	-	1.6	32.0	46.4	11.2	0.8	-	-	80
Stress	Ti6Al4V	2.55	-	23.8	11.9	-	-	1.7	0.42	85
Stress	INCONEL X750	71.2	17.6	208.0	960.0	-	-	1.60	-	80
Stress	HAYNES 25	-	0.96	-	6.4	-	-	-	-	80
Nonstress	AA6061-T6	-	0.8	176.0	-	4.0	-	-	-	80
Nonstress	304L SS	-	1.6	15.2	12.0	28.0	1.6	-	-	80
Nonstress	Ti6Al4V	1.20	-	88.0	8.0	-	-	0.80	0.40	80
Nonstress	INCONEL X750	1.2	4.0	28.0	8.0	-	-	1.60	-	80
Nonstress	HAYNES 25	-	1.36	-	9.60	-	0.4	-	-	80

TABLE XVII
METAL DISSOLUTION IN HYDRAZINE - BEND TESTS

110 F - 15 Years

Metal	μg Metal in Solution							Volume of Hydrazine (cc)
	Al	V	Fe	Ni	Ti	Cr	Mn	
AA6061-T6	-	-	33.6	-	-	0.64	-	80
304L SS	-	-	29.6	12.0	-	2.4	8.0	80
Ti6Al4V	1.2	0.32	96.0	6.4	0.4	-	-	80
INCONEL X750	0.8	-	30.4	368.0	5.6	3.2	-	80
HAYNES 25	-	-	-	-	-	2.56	0.40	80

TABLE XVIII
METAL DISSOLUTION IN HYDRAZINE - WELD AND BRAZE TESTS

110 F - 15 Years

Test	Metal	μg Metal in Solution							V	Volume of Hydrazine (cc)
		Cr	Fe	Ti	Al	Ni	Cu	Mn		
Braze Palniro Braze #7	INCONEL X750 - 304L SS	7.2	10.4	3.2	1.2	0.8	2.8	5.6	-	80
Braze Au-Ni PermaBraze	INCONEL X750 - 304L SS	6.4	104.0	1.6	1.2	32.8	25.6	1.6	-	80
Weld TIG	INCONEL X750 - HAYNES 25	3.2	60.0	8.0	3.2	37.6	-	4.0	-	80
Weld Electron Beam	304L SS - 304L SS	4.0	128.0	-	-	8.0	12.8	1.6	-	80
Weld TIG	Ti6Al4V - Ti6Al4V	-	88.0	8.0	2.4	9.6	-	-	0.48	80

TABLE XIX
SUMMARY OF METAL DISSOLUTION IN HYDRAZINE
AT THE 1 ppm SIGNIFICANCE LEVEL

Configuration	Metal	Elements	Dissolved Metal (mg/cm ²)
Baseline	AA6061-T6	Fe	0.26
	AA2219	Fe, Al	0.44
	AA5086	Al	3.58
	430 SS	Fe	1.26, 0.62
	17-4 PH SS	Fe	1.26
	INCONEL X750	Al, Ni	2.14, 0.34
	HAYNES 25	Co	1.44
Vapor-Liquid	304L SS	Fe	0.33
	HAYNES 25	Fe	0.17
Bend	Ti6Al4V	Fe	0.19
	INCONEL X750	Ni	0.74
Edge	AA6061-T6	Fe	0.30
	INCONEL X750	Ni	0.60
Stress	INCONEL X750	Fe, Ni	0.42, 1.92
Non-Stress	AA6061-T6	Fe	0.35
	Ti6Al4V	Fe	0.18
Crevice	AA6061-T6	Al	0.16
Au-Ni Permabraz	304L SS-INCONEL X750	Fe	0.21
Electron Beam Weld	304L SS-304L SS	Fe	0.26
TIG Weld	Ti6Al4V-Ti6Al4V	Fe	0.18
Bimetallic Junction	304SS-17-4 PH SS	Fe	0.37
Bimetallic Junction	HAYNES 25-INCONEL X750	Ni	2.11

TABLE XX

MONOMETHYLHYDRAZINE COMPATIBILITY DATA - BASELINE
110 F

Metal	Simulated Time (Years)	i_o ($\mu\text{a}/\text{cm}^2$)	$\text{mg}/\text{cm}^2/\text{yr}$	Extent of Decomposition	
				mg/cm^2 Incremental	mg/cm^2 Cumulative
304L SS	0	0.062	4.666×10^{-1}	-	-
	0.25	0.160	1.20×10^0	0.30	0.30
	0.50	0.087	6.55×10^{-1}	0.16	0.46
	0.75	0.073	5.49×10^{-1}	0.14	0.60
	1.50	0.061	4.59×10^{-1}	0.42	1.02
	3.00	0.071	5.34×10^{-1}	0.80	1.82
	5.00	0.070	5.26×10^{-1}	1.05	2.87
Ti6Al4V	0	0.087	6.55×10^{-1}	-	-
	0.25	0.046	3.46×10^{-1}	0.09	0.09
	0.50	0.050	3.76×10^{-1}	0.09	0.18
	0.75	0.048	3.61×10^{-1}	0.09	0.27
	1.50	0.110	8.28×10^{-1}	0.62	0.89
	2.00	0.140	1.05×10^0	1.57	2.47
	4.00	0.280	2.11×10^0	4.22	6.69
AA1100	0	0.046	3.46×10^{-1}	-	-
	0.25	0.017	1.28×10^{-1}	0.03	0.03
	0.50	0.012	9.03×10^{-2}	0.02	0.05
	0.75	0.009	6.77×10^{-2}	0.02	0.07
	2.15	0.0638	4.80×10^{-1}	0.36	0.43
	3.50	0.035	2.63×10^{-1}	0.39	0.82
	6.50	0.044	3.31×10^{-1}	0.99	1.82

TABLE XVI
PEAL TIME COMPATIBILITY DATA
(Monomethylhydrazine)

Source	Metal	Surface Area (cm ²)	Temperature of	Amount of MMH Decomposed		Time of Exposure (years)	Cumulative mg/cm ²		
				moles	μg		Aerojet	JPL	UTRC
JPL (Ref. 9)	Ti6Al4V (Bimetallic)	8.93	110	5.03 x 10 ⁻⁴	23.2	3.75	--	2.60 ± 0.7	4.4 ± 0.8
JPL (Ref. 9)	304SS (Stress)	8.93	110	3.50 x 10 ⁻⁴	16.1	0.41	--	1.80 ± 0.5 * 0.67 ± 0.2	0.4 ± 0.08
Aerojet (Ref. 11)	Ti6Al4V	2.5	158	5.58 x 10 ⁻⁵	2.57	0.293	1.03 ± 0.5	--	0.10 ± 0.02

62

UTRC Data ± 20 percent

JPL Data ± 25 percent

Aerojet Data ± 50 percent

*Data corrected for stress condition.

TABLE XXII

EXTENT OF MONOMETHYLHYDRAZINE DECOMPOSITION

ON PURE IRON, TITANIUM AND ALUMINUM
(Ref. 8)

Metal	Percent Decomposition	SHI*			UTRC	
		mg decomposed	mg/cm ²	mg/cm ² /yr	mg/cm ²	mg/cm ² /yr
Al	.089	0.774	0.24 \pm 0.05	0.26	0.20 \pm .04	0.10
Ti	.080	0.696	0.21 \pm 0.05	0.23	0.38 \pm .08	0.47
Fe	0.21	1.83	0.56 \pm 0.12	0.61	0.70 \pm 0.14	0.55

* Data at 0.92 yr

UTRC Data \pm 20 percentSRI Data \pm 20 percent

TABLE XXIII
METAL DISSOLUTION IN MONOMETHYLHYDRAZINE

<u>Metal</u>	Simulated Time (Yrs)	Dissolved Metals (ppm)					
		<u>Al</u>	<u>Fe</u>	<u>Cr</u>	<u>Ni</u>	<u>Ti</u>	<u>V</u>
AA1100	6.50	0.04	0.4	-	-	-	-
304L SS	5.00	-	0.8	0.12	0.04	-	-
Ti6Al4V	4.00	1.2	1.0	-	0.04	0.04	0.04

<u>Metal</u>	<u>µg Metal in Solution*</u>					
	<u>Al</u>	<u>Fe</u>	<u>Ni</u>	<u>Cr</u>	<u>Ti</u>	<u>V</u>
AA1100	3.20	32.0	-	-	-	-
304L SS	-	64.0	3.20	9.60	-	-
Ti6Al4V	96.0	80.0	-	-	3.20	3.20

*Based on a cell volume of 80 cc

TABLE XXIV

HYDRAZINE-MONOMETHYLHYDRAZINE
BASELINE DATA COMPARISON

110 F

Metal	Time (yrs)	N ₂ H ₄		Metal	Time (yrs)	N ₂ H ₄		MMH Decomposition (mg/cm ²)	MMH/N ₂ H ₄ Ratio
		Decomposition (mg/cm ²)	Ratio			Decomposition (mg/cm ²)	Ratio		
AA1100	1.0	.07		430 SS	1.0	.48		.45	
	5.0	.52			5.0	1.83		1.49	
	9.0	.86			9.0	3.23		2.52	
	15.0	1.370	.411		15.0	4.74		3.85	.812
AA6061-T6	1.0	.144		Ti6Al4V	1.0	.07		.14	
	5.0	.818			5.0	.42		.48	
	9.0	1.12			9.0	.76		.90	
	15.0	1.85	.364		15.0	1.26		1.31	1.03
AA5086	1.0	.029		Haynes 25	1.0	.792		.17	
	5.0	.485			5.0	3.36		.87	
	9.0	.636			9.0	5.70		1.72	
	15.0	.877	.473		15.0	8.92		3.05	.342
AA2219	1.0	.028		Inconel X750	1.0	1.06		.34	
	5.0	.094			5.0	5.58		1.29	
	9.0	.197			9.0	9.44		2.46	
	15.0	.281	2.15		15.0	15.20		3.94	.259
304L SS	1.0	.50		Hastelloy B	1.0	3.93		1.16	
	5.0	1.33			5.0	20.30		6.69	
	9.0	1.85			9.0	38.20		12.50	
	15.0	2.70	1.31		15.0	69.00		21.10	.305
17-4PH SS	1.0	.134		PT-10% IR	1.0	2.39		.69	
	5.0	.476			5.0	18.60		2.91	
	9.0	.762			9.0	3.92		5.33	
	15.0	.989	4.70		15.0	82.60		9.36	.113

TABLE XXV

MATERIAL-PROPELLANT COMPATIBILITY RATINGS
(MONOMETHYLHYDRAZINE DECOMPOSITION)
(15 Year Baseline Tests)
(110 F)

Category	Decomposition Rate Range mg/cm ²	Metals Included in Each Category
Compatible	< 2.0	AA5086, AA1100, AA2219, AA6061-T6, Ti6Al4V
Probable Compatibility	2.0 to 5.0	HAYNES 25, 304LSS 430SS, INCONEL X750 17-4PHSS
Doubtful Compatibility	5.0 to 10.0	PT-10Z IR
Not Compatible	> 10.0	HASTELLOY B

TABLE XXVI

EFFECTS OF A VAPOR-LIQUID
INTERFACE ON MONOMETHYLHYDRAZINE DECOMPOSITION
110 F

Metal	Time (yrs)	Vapor-Liquid Decomposition (mg/cm ²)	Baseline Liquid Decomposition (mg/cm ²)	Vapor-Liquid to Baseline Ratio
AA6061-T6	1.0	.27	.03	8.37
	5.0	.68	.16	4.13
	9.0	1.09	.39	2.79
	15.0	1.86	.67	2.76
304L SS	1.0	.69	.27	2.48
	5.0	3.20	1.00	3.21
	9.0	5.38	1.95	2.76
	15.0	9.86	3.53	2.79
Ti6Al4V	1.0	.37	.14	2.68
	5.0	1.02	.48	2.11
	9.0	1.51	.90	1.68
	15.0	2.35	1.31	1.79
HAYNES 25	1.0	.13	.17	.77
	5.0	.53	.87	.61
	9.0	.91	1.72	.53
	15.0	1.40	3.05	.46
INCONEL X 750	1.0	.56	.34	1.63
	5.0	5.57	1.29	4.32
	9.0	9.65	2.46	3.92
	15.0	16.04	3.94	4.07

TABLE XXVII

EFFECTS OF EDGES
ON MONOMETHYLHYDRAZINE DECOMPOSITION
110F

Metal	Time (yrs)	Base-Line (mg/cm ²)	Edge (mg/cm ²)	Edge to Baseline Ratio
AA6061-T6	1.0	0.03	0.08	2.62
	5.0	0.16	0.43	2.61
	9.0	0.39	0.59	1.50
	15.0	0.67	1.00	1.48
304L SS	1.0	0.27	0.38	1.37
	5.0	1.00	1.20	1.20
	9.0	1.95	1.83	0.94
	15.0	3.53	2.65	0.75
Ti6Al4V	1.0	0.14	0.35	2.49
	5.0	0.48	1.98	4.09
	9.0	0.90	4.27	4.74
	15.0	1.31	7.59	5.79
INCONEL X750	1.0	0.34	0.68	1.98
	5.0	1.29	1.85	1.43
	9.0	2.46	3.54	1.44
	15.0	3.94	5.74	1.46
HAYNES 25	1.0	0.17	0.08	0.46
	5.0	0.87	0.25	0.28
	9.0	1.72	0.61	0.36
	15.0	3.05	2.65	0.87

TABLE XXVIII

EFFECTS OF A CREVICE
ON MONOMETHYLHYDRAZINE DECOMPOSITION
110 F

Metal	Time (years)	Baseline (mg/cm ²)	Crevice (mg/cm ²)	Crevice to Baseline Ratio
AA6061-T6	1.0	0.03	0.10	3.28
	5.0	0.16	0.56	3.39
	9.0	0.39	0.97	2.47
	15.0	0.67	1.66	2.47
304L SS	1.0	0.27	0.17	0.63
	5.0	1.00	0.66	0.66
	9.0	1.95	1.08	0.55
	15.0	3.53	1.92	0.54
Ti6Al4V	1.0	0.14	0.06	0.42
	5.0	0.48	0.25	0.52
	9.0	0.90	0.49	0.540
	15.0	1.31	1.22	0.93
INCONEL X750	1.0	0.34	0.65	1.90
	5.0	1.29	1.81	1.40
	9.0	2.46	2.68	1.09
	15.0	3.94	4.02	1.02
HAYNES 25	1.0	0.17	0.09	0.51
	5.0	0.87	0.46	0.52
	9.0	1.72	0.83	0.48
	15.0	3.05	1.42	0.47

TABLE XXIX
EFFECTS OF BIMETALLIC JUNCTIONS
ON MONOMETHYLHYDRAZINE DECOMPOSITION
110 F

Time (yrs)	Bimetallic Couple		Single Metals		Time (yrs)	Bimetallic Couple		Single Metals	
	304L SS	AA6061-T6	304L SS	AA6061-T6		304L SS	Ti6Al4V	304L SS	Ti6Al4V
1.0	.20		.27	.03	1.0	.20		.27	.40
5.0	.68		1.00	.16	5.0	.90		1.00	.48
9.0	1.46		1.95	.39	9.0	1.57		1.95	.90
15.0	2.28		3.53	.67	15.0	2.73		3.53	1.31
304L SS AA6061-T6					304L SS INCONEL X750				
1.0	.20		.27	.27	1.0	.80		.27	.34
5.0	.88		1.00	1.54	5.0	2.60		1.00	1.29
9.0	1.50		1.95	2.99	9.0	3.82		1.95	2.46
15.0	2.40		3.53	4.65	15.0	5.42		3.53	3.94
HAYNES 25 INCONEL X750					HAYNES 25 INCONEL X750				
1.0	.147		.17	.34					
5.0	.625		.87	1.29					
9.0	1.16		1.72	2.46					
15.0	1.86		3.05	5.94					

TABLE XXX
EFFECTS OF METAL STRESS
ON MONOMETHYLHYDRAZINE DECOMPOSITION
110 F

Metal	Time (yrs)	Nonstress (mg/cm ²)	Stress (mg/cm ²)	Stress to Nonstress Ratio
AA6061-T6	1.0	0.01	0.02	1.25
	5.0	0.04	0.04	1.22
	9.0	0.06	0.06	1.03
	15.0	0.08	0.08	1.06
304L SS	1.0	0.12	0.07	0.59
	5.0	0.37	0.43	1.16
	9.0	0.65	0.64	0.97
	15.0	1.03	0.84	0.82
Ti6Al4V	1.0	0.05	0.04	0.96
	5.0	0.15	0.14	0.95
	9.0	0.27	0.24	0.90
	15.0	0.42	0.40	0.95
INCONEL X750	1.0	0.17	0.11	0.64
	5.0	0.72	1.10	1.53
	9.0	1.17	2.80	2.39
	15.0	3.68	4.89	1.33
HAYNES 25	1.0	0.08	0.10	1.22
	5.0	0.38	0.43	1.14
	9.0	0.67	0.76	1.13
	15.0	1.13	1.33	1.18

TABLE XXXI

EFFECTS OF BENDS ON MONOMETHYLHYDRAZINE DECOMPOSITION
110 F

Metal	Time (yrs)	Nonstress (mg/cm ²)	Bends (mg/cm ²)	Bend to Nonstress Ratio
AA6061-T6	1.0	0.01	0.03	2.42
	5.0	0.04	0.07	1.89
	9.0	0.06	0.08	1.40
	15.0	0.08	0.10	1.17
304L SS	1.0	0.12	0.10	0.91
	5.0	0.37	0.26	0.70
	9.0	0.65	0.45	0.68
	15.0	1.03	0.74	0.72
Ti6Al4V	1.0	0.05	0.05	1.13
	5.0	0.15	0.20	1.32
	9.0	0.27	0.36	1.36
	15.0	0.42	0.56	1.34
INCONEL X750	1.0	0.17	0.14	0.81
	5.0	0.72	0.84	1.17
	9.0	1.17	1.63	0.95
	15.0	3.68	2.72	0.74
HAYNES 25	1.0	0.08	0.14	1.74
	5.0	0.38	0.82	2.16
	9.0	0.67	1.52	2.28
	15.0	1.13	2.63	2.33

TABLE XXXII
EFFECTS OF WELDS AND BRAZES ON
MONOMETHYLHYDRAZINE DECOMPOSITION
110 F

Weld or Braz	Materials #1 / #2	Time (Years)	Monomethylhydrazine Decomposition (mg/cm ²)				Weld or Braze to	
			Weld or Braze	Metal #1	Nonstress Metal #1	Metal #2	Metal #1	Nonstress Metal #2
Electron Beam Weld	304L SS/304L SS	1.0	0.14	0.12	-	-	1.24	-
		5.0	0.39	0.37	-	-	1.04	-
		9.0	0.74	0.65	-	-	1.13	-
		15.0	1.64	1.03	-	-	1.59	-
Palmiro #7 Braze	304L SS/INCONEL X750	1.0	0.11	0.12	0.17	0.66	1.00	0.66
		5.0	0.60	0.37	0.72	0.83	1.61	0.83
		9.0	1.28	0.65	1.71	0.75	1.96	0.75
		15.0	2.09	1.03	3.68	0.57	2.03	0.57
AuNi Braze	304L SS/INCONEL X750	1.0	0.08	0.12	0.17	0.44	0.65	0.44
		5.0	0.44	0.37	0.72	0.62	1.19	0.62
		9.0	0.94	0.65	1.71	0.55	1.44	0.55
		15.0	1.76	1.03	3.68	0.48	1.71	0.48
TIG Weld	Ti6Al4V/Ti6Al4V	1.0	0.07	0.05	-	-	1.54	-
		5.0	0.22	0.15	-	-	1.51	-
		9.0	0.36	0.27	-	-	1.35	-
		15.0	0.63	0.42	-	-	1.51	-
TIG Weld	INCONEL X750/ HAYNES 25	1.0	0.08	0.17	0.08	1.02	0.49	1.02
		5.0	0.35	0.72	0.38	0.92	0.49	0.92
		9.0	0.68	1.71	0.67	1.00	0.40	1.00
		15.0	1.25	3.68	1.13	1.11	0.34	1.11

TABLE XXXIII

EFFECTS OF METAL PRETREATMENT ON MONOMETHYLHYDRAZINE
DECOMPOSITION AT 110 F AND 15 YEARS SIMULATED TIME

Metal	Metal Pretreatment	Cumulative Decomposition mg/cm ²
AA6061-T6 (Al)	A	0.684
	B	0.361
	C	0.860
304LSS (Fe)	A	3.36
	B	1.80
	C	2.38
Ti6Al4V (Ti)	A	0.846
	B	1.33
	C	1.05
INCONEL X750 (Ni)	A	4.05
	B	2.82
	C	2.16
HAYNES 25 (Co)	A	1.35
	B	1.35
	C	1.52

TABLE XXXIV
EFFECT OF WATER CONCENTRATION ON
MONOMETHYLHYDRAZINE DECOMPOSITION AT 110 F
AND 15 YEARS SIMULATED TIME

Metal	%H ₂ O	Impurity/Baseline Ratio	Cumulative Decomposition mg/cm ²
AA6061-T6	2.1	0.91	0.614
	2.6	1.69	1.14
	3.1	1.52	1.02
304LSS	2.1	0.61	2.14
	2.6	0.91	3.22
	3.1	0.81	2.87
Ti6Al4V	2.1	1.74	2.28
	2.6	1.63	2.14
	3.1	0.79	1.04
INCONEL X750	2.1	0.59	2.34
	2.6	2.10	8.27*
	3.1	0.77	3.03
RAYNES 25	2.1	0.28	0.840
	2.6	0.21	0.630
	3.1	1.11	0.374

* Accelerated MMH Decomposition
Due to Sample Contamination

TABLE XXXV

EFFECT OF CHLORIDE CONCENTRATION ON
MONOMETHYLHYDRAZINE DECOMPOSITION

Metal	Temp (°F)	Chloride ($\mu\text{g}/\text{gram}$)	Time (Yr)	mg/cm^2 (cumulative)	mg/cm^2 Baseline (110 F)	Impurity to Baseline Ratio
AA6061-T6	160	10	1	1.29	0.03	40.3
			5	3.15	0.16	19.1
			9	4.78	0.39	12.2
			15	6.83	0.67	10.2
304LSS	50	10	1	0.21	0.27	0.78
			5	1.04	1.00	1.04
			9	1.84	1.95	0.94
			15	3.37	3.53	0.95
Ti6Al4V	160	30	1	0.16	0.14	1.12
			5	0.51	0.48	1.05
			9	0.98	0.90	1.09
			15	1.39	1.31	1.06
INCONEL X750	50	30	1	0.12	0.34	0.36
			5	0.76	1.29	0.59
			9	1.17	2.46	0.48
			15	2.08	3.94	0.53

TABLE XXXVI
METAL DISSOLUTION IN MONOMETHYLHYDRAZINE - BASELINE TESTS

110 F - 15 Years

Density of MMH = 0.87 g/cc

Metal	μg METAL IN SOLUTION										Vol. of MMH (cc)
	Co	Fe	Al	Mg	Cr	Ni	Ti	Cu	Mn	V	
AA1100	-	-	-	-	-	-	-	-	-	-	80
AA6061-T6	-	18.1	-	4.2	-	-	-	34.8	-	-	80
AA2219	-	23.7	-	-	-	2.92	-	30.0	2.09	-	80
AA5086	-	25.8	-	-	-	-	-	140.6	-	-	80
304L SS	96.7	18.8	-	-	-	1.25	-	29.9	2.09	-	80
430SS	-	27.1	-	-	-	2.44	-	-	2.78	-	80
17-4PHSS	-	23.7	-	7.66	-	4.59	-	18.8	-	-	80
Ti6Al4V	-	32.7	-	-	-	4.32	-	-	-	-	80
INCONEL X750	-	21.6	-	-	-	5.08	-	1.11	-	-	80
HASTELLOY B	-	50.8	-	-	-	1204.1	-	-	-	-	80
HAYNES B	320.2	-	-	-	-	8.35	-	-	-	-	80
PT-10ZIR	-	-	-	-	-	-	-	-	-	-	80

TABLE XXXVII

METAL DISSOLUTION IN MONOMETHYLHYDRAZINE - VAPOR-LIQUID TESTS

110 F - 15 years

Density of MMH = 0.87 g/cc

Metal	μ g METAL IN SOLUTION										Vol. of MMH (cc)
	Co	Fe	Al	Mg	Cr	Ni	Ti	Cu	Mn	V	
AA6061-T6	-	19.7	-	1.88	-	-	-	22.6	-	-	54
304L SS	-	27.0	-	-	-	1.83	-	20.9	3.48	-	50
Ti6Al4V	-	16.5	-	-	-	2.91	-	-	-	-	54
INCONEL X750	-	16.5	-	-	.479	6.96	-	-	-	-	50
HAYNES 25	16.1	12.2	-	-	-	1.74	-	-	-	-	50

TABLE XXXVIII
METAL DISSOLUTION IN MONOMETHYLHYDRAZINE- EDGE TESTS

110 F - 15 Years

Density of MMH = 0.87 g/cc

Metal	μg METAL IN SOLUTION										Vol. of MMH (cc)
	Co	Fe	Al	Mg	Cr	Ni	Ti	Cu	Mn	V	
AA6061-T6	-	11.8	-	2.4	-	-	34.1	59.2	-	-	80
304L SS	939.6	3.48	-	-	-	1.74	-	105.8	-	-	80
Ti6Al4V	-	19.5	-	-	-	2.51	-	-	-	-	80
INCONEL X750	-	34.1	-	-	.90	5.50	62.6	-	-	-	80
HAYNES 25	160.1	11.8	-	-	-	2.02	-	-	-	-	80

TABLE XXXIX

METAL DISSOLUTION IN MONOMETHYLHYDRAZINE - CREVICE TESTS

110 F - 15 Years

Density of MMH = 0.87 g/cc

Metal	μg METAL IN SOLUTION										Vol. of MMH (cc)
	Co	Fe	Al	Mg	Cr	Ni	Ti	Cu	Mn	V	
AA6061-T6	-	11.8	-	2.44	-	-	-	34.1	-	-	80
304L SS	-	-	-	-	-	-	-	-	-	-	80
Ti6Al4V	-	-	6.96	-	76.6	-	-	-	2.58	55.7	80
INCONEL X750	-	18.8	2.09	-	.348	66.8	-	-	-	-	80
HAYNES 25	1948.8	-	-	-	-	-	-	-	-	-	80

TABLE XL

METAL DISSOLUTION IN MONOMETHYLHYDRAZINE - BIMETALLIC TESTS

110 F - 15 Years

Density of MMH = 0.87 g/cc

Metal	μg METAL IN SOLUTION										Vol. of MMH (cc)
	Co	Fe	Al	Mg	Cr	Ni	Ti	Cu	Mn	V	
304L SS											
AA6061-T6	.90	50.8	-	2.09	1.11	5.29	-	27.8	3.48	-	80
304L SS											
17-4PH SS	389.7	23.0	-	6.96	-	12.5	-	27.1	2.78	-	80
304L SS											
Ti6Al4V	-	48.7	-	-	-	7.66	306.2	92.6	2.78	-	80
304L SS											
INCONEL X750	2.23	34.1	-	-	-	4.80	55.7	59.2	4.87	-	80
HAYNES 25											
INCONEL X750	4.59	16.7	-	-	.70	1705.2	-	-	-	-	80

TABLE XLI
METAL DISSOLUTION IN MONOMETHYLHYDRAZINE- NONSTRESS TESTS

110 F - 15 Years

Density of MMH = 0.87 g/cc

Metal	μ g METAL IN SOLUTION										Vol. of MMH (cc)
	Co	Fe	Al	Mg	Cr	Ni	Ti	Cu	Mn	V	
AA6061-T6	-	-	34.8	-	271.4	-	-	8.35	-	-	80
304L SS	-	20.9	-	-	9.74	-	-	8.35	-	-	80
Ti6Al4V	-	243.6	14.0	-	-	-	-	-	-	-	80
INCONEL X750	-	-	8.35	-	-	-	-	-	-	-	80
HAYNES 25	-	-	-	-	48.7	-	-	-	-	-	80

TABLE XLII
METAL DISSOLUTION IN MONOMETHYLHYDRAZINE - STRESS TESTS

110 F - 15 Years

Density of MMH = 0.87 g/cc

Metal	μg METAL IN SOLUTION										Vol. of MMH (cc)
	Co	Fe	Al	Mg	Cr	Ni	Ti	Cu	Mn	V	
AA6061-T6	-	-	27.8	-	-	-	-	-	-	-	80
304L SS	-	20.9	-	-	-	-	-	2.78	-	-	80
Ti6Al4V	-	243.6	14.0	-	-	-	-	-	-	-	80
INCONEL X750	-	-	13.9	-	-	-	-	-	-	-	80
HAYNES 25	55.7	-	-	-	-	-	-	-	-	-	80

TABLE XLIII

METAL DISSOLUTION IN MONOMETHYLHYDRAZINE - BEND TESTS

110 F - 15 Years

Density of MMH = 0.87 g/cc

Metal	μg METAL IN SOLUTION										Vol. of MMH (cc)
	Co	Fe	Al	Mg	Cr	Ni	Ti	Cu	Mn	V	
AA6061-T6	-	-	55.7	-	-	-	-	22.3	-	-	80
304L SS	-	23.7	-	-	.626	20.9	-	14.0	.626	-	80
Ti6Al4V	-	18.1	1.39	-	-	2.78	1.11	-	-	1.11	80
INCONEL X750	-	23.9	2.09	-	.557	10.4	-	-	-	-	80
HAYNES 25	47.3	20.9	-	-	-	1.39	-	11.8	-	-	80

TABLE XLIV

METAL DISSOLUTION IN MONOMETHYLHYDRAZINE - WELD AND BRAZE TESTS

110 F - 15 Years

Density of MMH = 0.87 g/cc

Metal	Co	Fe	Al	Mg	μ g METAL IN SOLUTION					Au	Vol. of MMH (cc)
					Cr	Ni	Ti	Cu	Mn		
304L SS INCONEL X750											
Palniro Braze	-	25.1	-	-	3.62	6.96	10.4	27.8	1.18	11.8	80
304L SS INCONEL X750											
Au-Ni Braze	-	22.3	27.8	-	3.62	4.87	-	10.4	1.81	12.5	80
Ti6Al4V-Ti6Al4V											
TIG	-	38.3	-	-	-	-	5.57	-	-	-	80
304L SS 304L SS											
E-Beam Weld	77.3	23.0	-	-	1.11	3.48	-	14.0	.696	-	80
HAYNES-INCONEL X750											
TIG	-	-	14.0	-	5.57	-	-	-	-	-	80

TABLE XLV
METAL DISSOLUTION IN MONOMETHYLHYDRAZINE - METAL PRETREATMENT A

110 F - 15 Years

Density of MMH = 0.87 g/cc

Metal	μg METAL IN SOLUTION							Vol. of MMH (cc)
	Co	Fe	Al	Mg	Cr	Ni	Ti	
AA6061-T6	-	-	-	97.4	-	-	-	80
304L SS	-	1252.8	-	-	480.2	139.2	-	80
Ti6Al4V	-	-	-	-	-	-	20.9	80
INCONEL X750	-	2394.2	-	-	480.2	362.0	-	80
HAYNES 25	-	-	-	-	-	-	-	80

TABLE XLVI
METAL DISSOLUTION IN MONOMETHYLHYDRAZINE - METAL PRETREATMENT B

110 F - 15 Years

Density of MMH = 0.87 g/cc

Metal	μ g METAL IN SOLUTION										Vol. of MMH (cc)
	Co	Fe	Al	Mg	Cr	Ni	Ti	Cu	Mn	V	
AA6061-T6	-	-	83.5	53.6	570.7	-	-	16.7	-	-	80
304L SS	-	181.0	-	-	11.8	16.7	-	9.74	6.26	-	80
Ti6Al4V	-	-	22.3	-	-	-	-	-	-	-	80
INCONEL X750	-	-	5.57	-	-	-	20.9	-	-	-	80
HAYNES 25	-	-	-	-	-	-	-	-	-	-	80

TABLE XLVII
METAL DISSOLUTION IN MONOMETHYLHYDRAZINE - METAL PRETREATMENT C

110 F - 15 Years

Density of MMH = 0.87 g/cc

Metal	μg METAL IN SOLUTION										Vol. of MMH (cc)
	Co	Fe	Al	Mg	Cr	Ni	Ti	Cu	Mn	V	
AA6061-T6	-	-	-	76.6	-	-	-	-	-	-	80
304L SS	-	640.0	-	-	153.1	83.5	-	9.74	32.0	-	80
Ti6Al4V	-	-	14.0	-	-	-	2.09	-	-	-	80
INCONEL X750	-	-	33.4	-	57.8	299.3	-	-	-	-	80
HAYNES 25	-	-	-	-	-	-	-	-	-	-	80

TABLE XLVIII

METAL DISSOLUTION IN MONOMETHYLHYDRAZINE - 2.1% H₂O

110 F - 15 Years

Density of MMH = 0.87 g/cc

Metal	μ g METAL IN SOLUTION										Vol. of MMH (cc)
	Co	Fe	Al	Mg	Cr	Ni	Ti	Cu	Mn	V	
AA6061-T6	-	-	27.8	-	39.0	-	-	22.3	-	-	80
304L SS	-	62.6	-	-	4.18	-	-	2.78	-	-	80
Ti6Al4V	-	243.6	27.8	-	-	-	2.78	-	-	-	80
INCONEL X750	-	19418.4	160.1	-	4176.0	1058.0	-	-	-	-	80
HAYNES 25	1.39	-	-	-	48.7	-	-	-	-	-	80

TABLE XLVIX

METAL DISSOLUTION IN MONOMETHYLHYDRAZINE - 2.6% H₂O

110 F - 15 Years

Density of MMH = 0.87 g/cc

Metal	μ g METAL IN SOLUTION										Vol. of MMH (cc)
	Co	Fe	Al	Mg	Cr	Ni	Ti	Cu	Mn	V	
AA6061-T6	-	-	27.8	-	-	-	-	22.3	-	-	80
304L SS	-	2749.2.	-	-	27.8	535.9	-	50.1	83.5	-	80
Ti6Al4V	-	522.0	27.8	-	-	-	11.1	-	-	-	80
INCONEL X750	-	-	14.0	-	27.8	-	-	-	-	-	80
HAYNES 25	6.26	-	-	-	-	-	-	-	-	-	80

TABLE L
METAL DISSOLUTION IN MONOMETHYLHYDRAZINE - 3.1% H₂O

110 F - 15 Years

Density of MMH = 0.87 g/cc

Metal	μ g METAL IN SOLUTION										Vol. of MMH (cc)
	Co	Fe	Al	Mg	Cr	Ni	Ti	Cu	Mn	V	
AA6061-T6	-	-	55.7	-	-	-	-	22.3	-	-	80
304L SS	-	243.6	-	-	48.7	11.1	-	2.78	-	-	80
Ti6Al4V	-	48.7	27.8	-	-	-	11.1	-	-	-	80
INCONEL X750	-	-	11.1	-	9.74	-	-	-	-	-	80
HAYNES 25	55.7	-	-	-	76.6	97.4	-	-	-	-	80

TABLE LI
METAL DISSOLUTION IN MONOMETHYLHYDRAZINE - CHLORIDE TESTS

50 F - 15 Years

Density of MMH = 0.87 g/cc

Metal	μ g METAL IN SOLUTION										Vol. of MMH (cc)
	Co	Fe	Al	Mg	Cr	Ni	Ti	Cu	Mn	V	
304L SS	-	570.0	-	-	69.6	52.9	-	104.0	-	-	80
INCONEL X750	-	654.0	34.8	-	-	-	34.8	-	-	-	80

TABLE LII
METAL DISSOLUTION IN MONOMETHYLHYDRAZINE - CHLORIDE TESTS

160 F - 15 Years

Density of MMH = 0.87 g/cc

Metal	μg METAL IN SOLUTION							Vol. of MMH (cc)
	Co	Fe	Al	Mg	Cr	Ni	Ti	
AA6061-T6	-	-	-	132.0	-	-	-	80
Ti6Al4V	-	570.0	-	-	-	-	577.0	80

TABLE LIII

SUMMARY OF METAL DISSOLUTION IN MONOMETHYLHYDRAZINE
AT THE 1 PPM SIGNIFICANCE LEVEL

Configuration	Metal	Elements	Metal Dissolution mg/cm ²
Baseline	AA5086	Cu	0.28
	304LSS	Co	0.19
	HASTELLOY B	Ni	2.41
	HAYNES 25	Co	0.64
Bimetallic Junction	304LSS-17-4PHSS	Co	0.78
	304LSS - Ti6Al4V	Ti	0.61
	HAYNES 25 - INCONEL X750	Ni	3.41
Stress	Ti6Al4V	Fe	0.49
Nonstress	AA6061-T6	Cr	0.54
	Ti6Al4V	Fe	0.49
Edge	304LSS	Co, Cu	1.88, 0.21
	HAYNES 25	Co	0.32
Electron Beam Weld	304LSS - 304LSS	Co	0.16
Crevice	Ti6Al4V	Cr	0.15
	HAYNES 25	Co	3.90
Impurities	Ti6Al4V - 2.1% H ₂ O	Fe	0.49
	INCONEL X750 - 2.1% H ₂ O	Fe, Al, Cr, Ni	38.8, 0.32, 8.35, 2.12
	304LSS - 2.6% H ₂ O	Fe, Ni, Mn	5.50, 1.07, 0.17
	Ti6Al4V - 2.6% H ₂ O	Fe	1.04
	304LSS - 3.1% H ₂ O	Fe	0.487
	HAYNES 25 - 3.1% H ₂ O	Cr, Ni	0.15, 0.192
	304LSS 10 ppm Cl (50 F)	Fe, Cr, Cu	1.14, 0.14, 0.21
	AA6061-T6 - 10 ppm Cl (160 F)	Cu, Mg	0.38, 0.26
	Ti6Al4V - 30 ppm Cl (160 F)	Fe, Ti	1.14, 1.15
	INCONEL X750 - 30 ppm Cl (50 F)	Fe	1.31
Metal Pretreatment	AA6061-T6-A	Mg	0.20
	304LSS - A	Fe, Cr, Ni, Mn	0.25, 0.96, 0.28, 0.18
	INCONEL X750 - A	Fe, Cr, Ni	4.79, 0.96, 0.72
	AA6061-T6 - B	Al, Cr	0.17, 1.14
	304LSS - B	Fe	0.36
	AA6061 - C	Mg	0.15
	304LSS - C	Fe, Cr, Ni	1.28, 0.31, 0.17
	INCONEL X750 - C	Ni	0.600

TABLE LIV

STORAGE TANK DIMENSIONS AND
PHYSICAL PROPERTIES OF PROPELLANTS

Spherical Tank Volume (20 inch diameter) - 68642 cm³
1% Ullage - 682 cm³
Volume of Propellant - 67956 cm³
Surface Area Exposed to Propellant - 7630 cm²

Property	Propellant Properties at 430	
	Hydrazine	Monomethylhydrazine
Density (g/cm ³)	0.9875	0.8535
Vapor Pressure (atm)	0.0505	0.162
Mass of Propellant (gram)	67107	58000
Moles of Propellant	2094	1259
Molecular wgt (g/g mole)	32.05	46.08

TABLE LV

PRESSURE REQUIRED TO DISSOLVE AMMONIA IN HYDRAZINE

$$x_{\text{NH}_3} = K P_{\text{NH}_3} \quad (K = 0.05283 \text{ atm}^{-1} \text{ @ } 40 \text{ C})$$

Metal	Time (Yr)	Moles NH_3	Mole Fraction	P (atm)
AA6061-T6	1	0.047	0.2323×10^{-4}	0.44×10^{-3}
	5	0.265	1.3	2.48
	9	0.362	1.70	3.39
	15	0.599	2.96	5.61
Ti6Al4V	1	0.023	0.1137×10^{-4}	0.215×10^{-3}
	5	0.125	0.173	0.328
	9	0.247	1.22	2.31
	15	0.408	2.02	3.83
304LSS	1	0.136	0.6722×10^{-4}	1.27×10^{-3}
	5	0.431	2.13	4.03
	9	0.599	2.86	5.40
	15	0.875	4.323	8.19

TABLE LVI

CALCULATED PRESSURE RISE IN N_2H_4 TANK
(43C)

Metal	Time (Years)	N_2H_4 Decomposed mg/cm ²	Moles N_2H_4 Decomposed	Moles NH_3 Formed	Moles N_2 Formed	P_{TOT} atm
AA6061-T6	1	0.144	0.0343	0.0457	0.0114	0.301
	5	0.818	0.1947	0.2596	0.0649	1.478
	9	1.12	0.2666	0.3554	0.0889	2.006
	15	1.85	0.4404	0.5872	0.1468	3.280 (48 psia)
Ti6Al4V	1	0.071	0.0169	0.0225	0.0056	0.174
	5	0.416	0.0990	0.1320	0.0330	0.776
	9	0.762	0.1814	0.2419	0.0605	1.382
	15	1.26	0.3000	0.4000	0.1000	2.251 (33.1 psia)
304LSS	1	0.505	0.1202	0.1603	0.0401	0.933
	5	1.33	0.3166	0.4221	0.1055	2.372
	9	1.85	0.4404	0.5872	0.1468	3.280
	15	2.70	0.6428	0.8507	0.2142	4.763 (70 psia)

TABLE LVII

CALCULATED PRESSURE RISE IN MMH TANK
(43C)

Metal	Time (Years)	MMH Decomp. mg/cm ²	Initial			Final Complete CH ₄ Solubility	Final No CH ₄ Solubility
			Moles MMH	Moles CH ₄	Moles N ₂	PT atm	PT atm
AA6061-T6	1	0.032	0.0053	0.0018	0.0018	0.171	0.239
	5	0.165	0.0273	0.0091	0.0091	0.206	0.550
	9	0.391	0.0647	0.0216	0.0216	0.266	1.082
	15	0.673	0.1114	0.0371	0.0371	0.341	1.743
							(25.6 psia)
Ti6Al4V	1	0.139	0.0230	0.0077	0.0077	0.199	0.490
	5	0.484	0.0802	0.0267	0.0267	0.281	1.300
	9	0.900	0.1490	0.0497	0.0497	0.401	2.280
	15	1.31	0.2169	0.0723	0.0723	0.510	3.243
							(47.6 psia)
304LSS	1	0.273	0.0452	0.0151	0.0151	0.235	0.806
	5	0.996	0.1649	0.0550	0.0550	0.427	2.506
	9	1.95	0.3229	0.1076	0.1076	0.678	4.745
	15	3.53	0.5846	0.1949	0.1949	1.10	8.470
							(124.5 psia)
							(16.2 psia)

TABLE LVIII

METAL DISSOLUTION IN N_2H_4
(Baseline Tests)

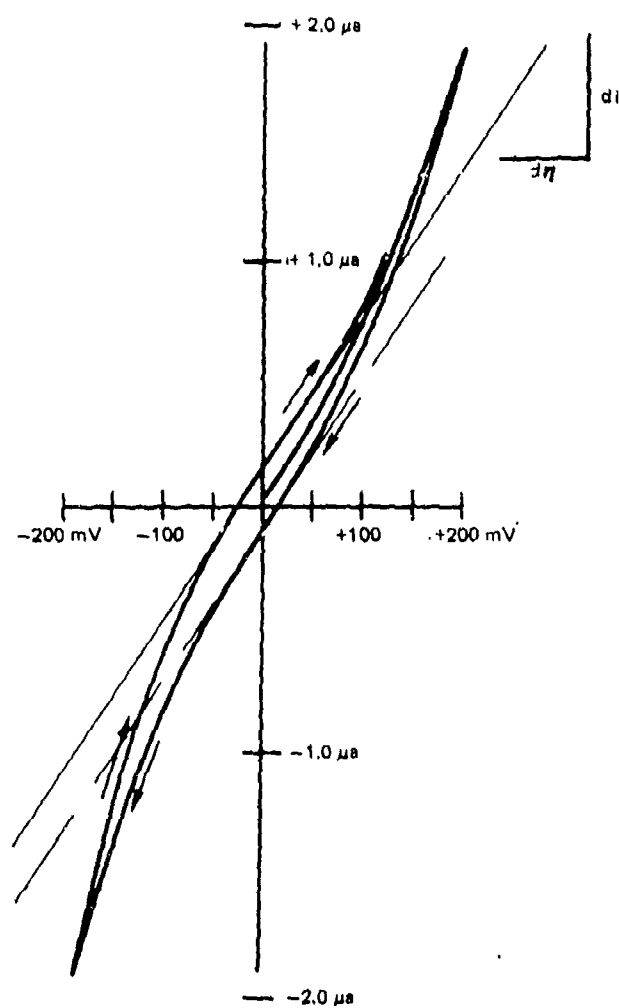
Metal	Density (grams/cm ³)	Total Metal In Solution (grams)	Penetration	
			(mils)	(cm)
AA1100	2.71	27.2×10^{-6}	0.008	2.00×10^{-5}
AA6061-T6	2.72	214.4×10^{-6}	0.062	1.58×10^{-4}
AA2219	2.70	285.9×10^{-6}	0.084	2.12×10^{-4}
AA5086	2.70	1884.6×10^{-6}	0.551	1.40×10^{-3}
304LSS	7.90	43.2×10^{-6}	0.004	1.10×10^{-5}
430SS	7.90	1059.2×10^{-6}	0.106	2.68×10^{-4}
17-4PHSS	7.90	135.0×10^{-6}	0.013	3.42×10^{-5}
Ti6Al4V	4.50	746.2×10^{-6}	0.131	3.32×10^{-4}
INCONEL X750	8.39	1323.0×10^{-6}	0.124	3.15×10^{-4}
HASTELLOY B	8.50	50.4×10^{-6}	0.005	1.19×10^{-5}
HAYNES 25	8.50	730.8×10^{-6}	0.068	1.72×10^{-4}

TABLE LIX

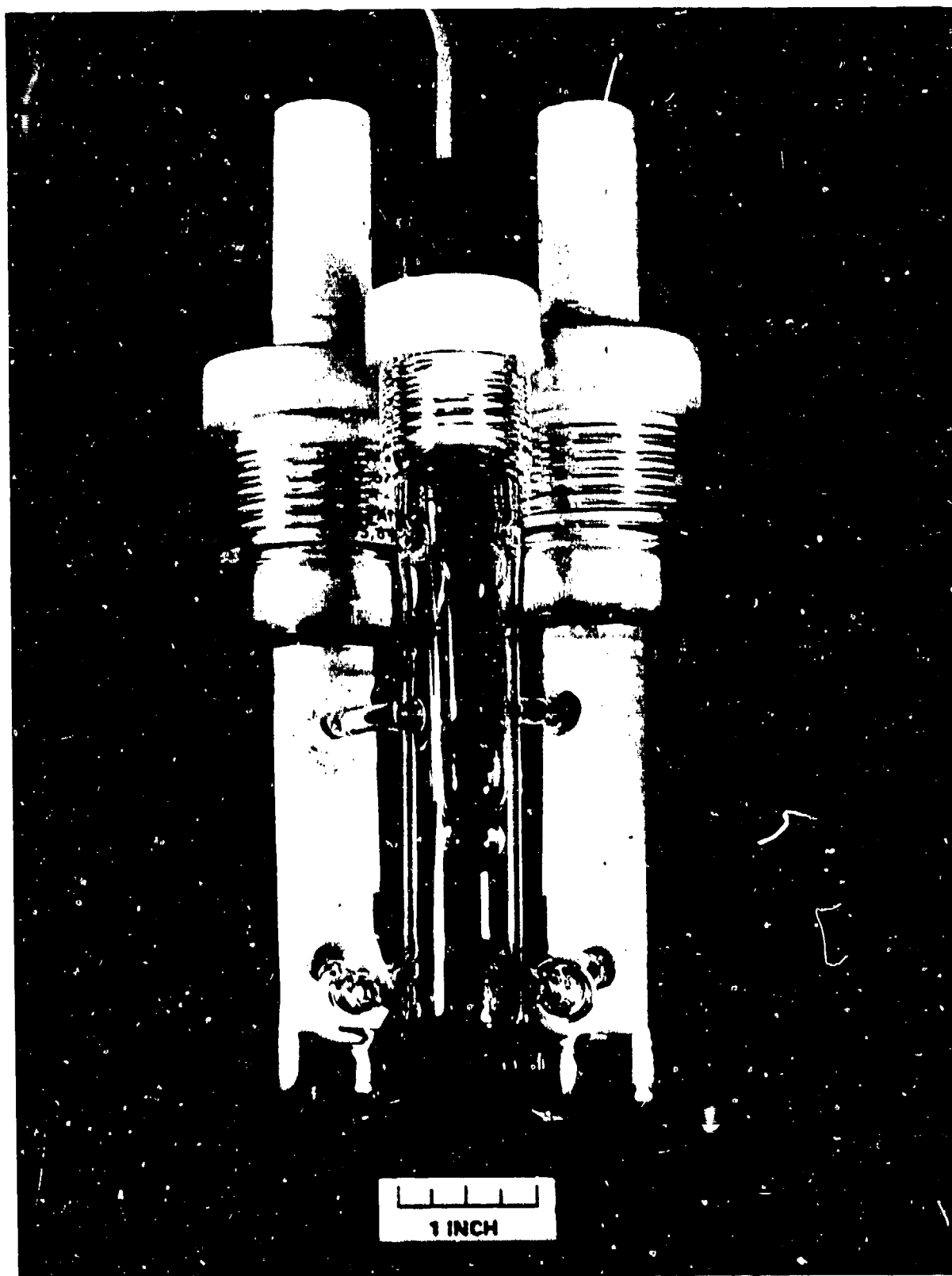
METAL DISSOLUTION IN MMH
(Baseline Tests)
(15 Years Simulated time)

Metal	Density (grams/cm ³)	Total Metal In Solution (grams)	Penetration (mils)	Penetration (cm)
AA1100	2.71	0		0
AA6061-T6	2.72	57.1×10^{-6}	0.016	4.20×10^{-5}
AA2219	2.70	58.7×10^{-6}	0.017	4.35×10^{-5}
AA5086	2.70	166.4×10^{-6}	0.048	1.23×10^{-4}
304LSS	7.90	148.7×10^{-6}	0.015	3.76×10^{-5}
430SS	7.90	32.3×10^{-6}	0.003	8.18×10^{-6}
17-4PHSS	7.90	54.8×10^{-6}	0.005	1.39×10^{-5}
T16A14V	4.50	37.0×10^{-6}	0.006	1.64×10^{-5}
INCONEL X750	8.39	27.8×10^{-6}	0.003	6.62×10^{-6}
HASTELLOY B	8.50	1254.8×10^{-6}	0.116	2.95×10^{-4}
HAYNES 25	8.50	328.5×10^{-6}	0.030	7.73×10^{-5}

TYPICAL EXPERIMENTAL CURRENT-VOLTAGE SCAN
(PT-10%Ir IN PROPELLENT GRADE HYDRAZINE)

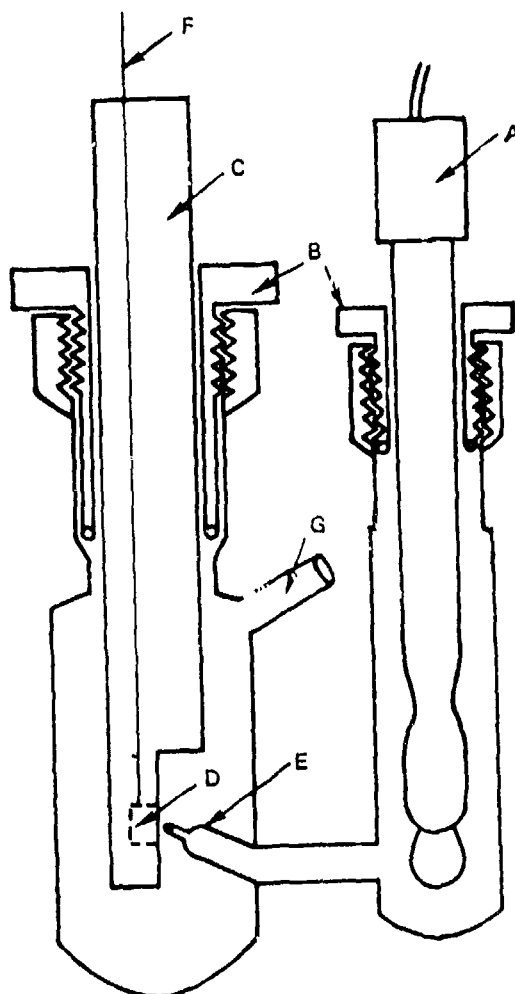


78-00-106-1



MATERIAL COMPATIBILITY TEST CELL

(CROSS SECTION)

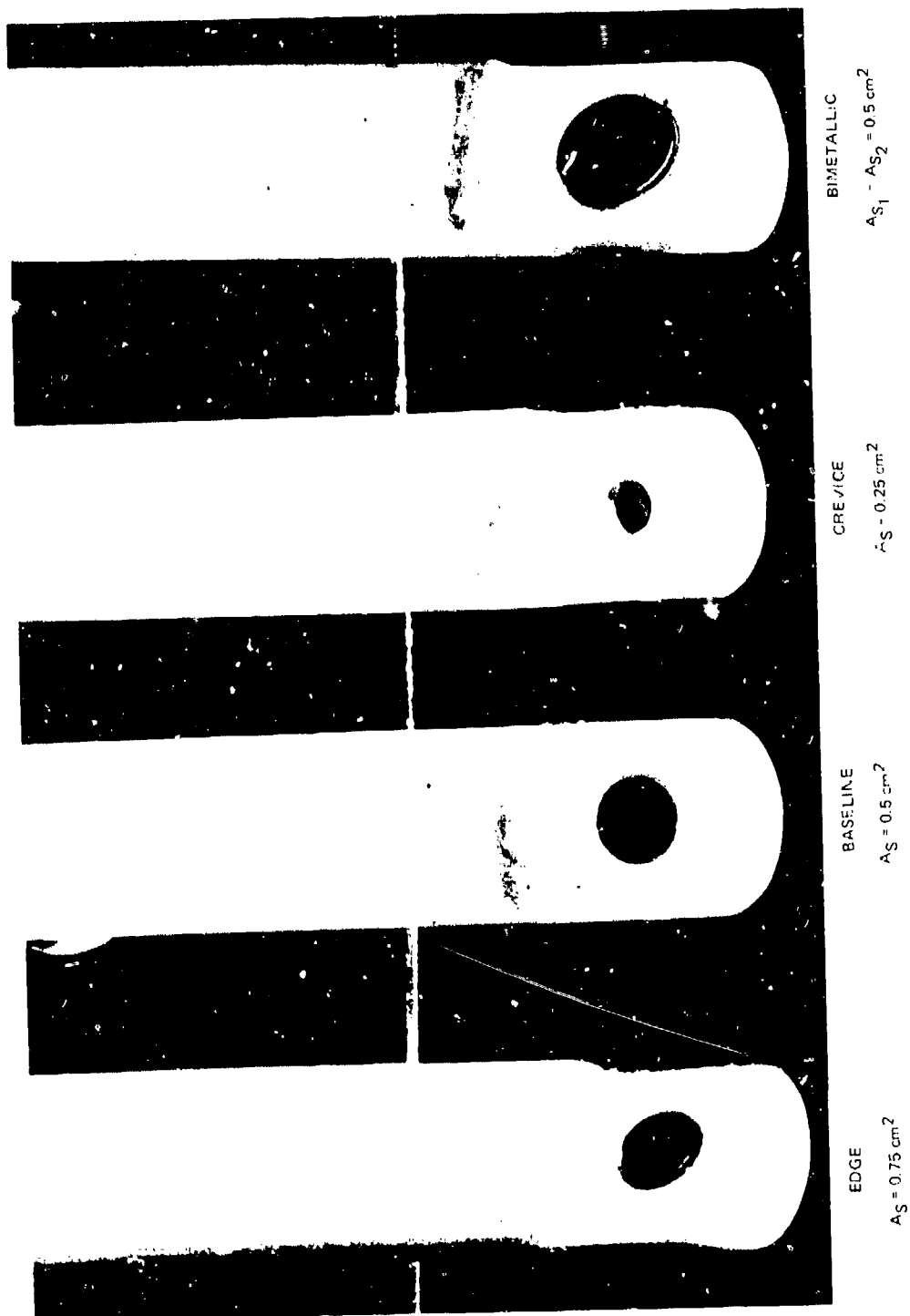


KEY

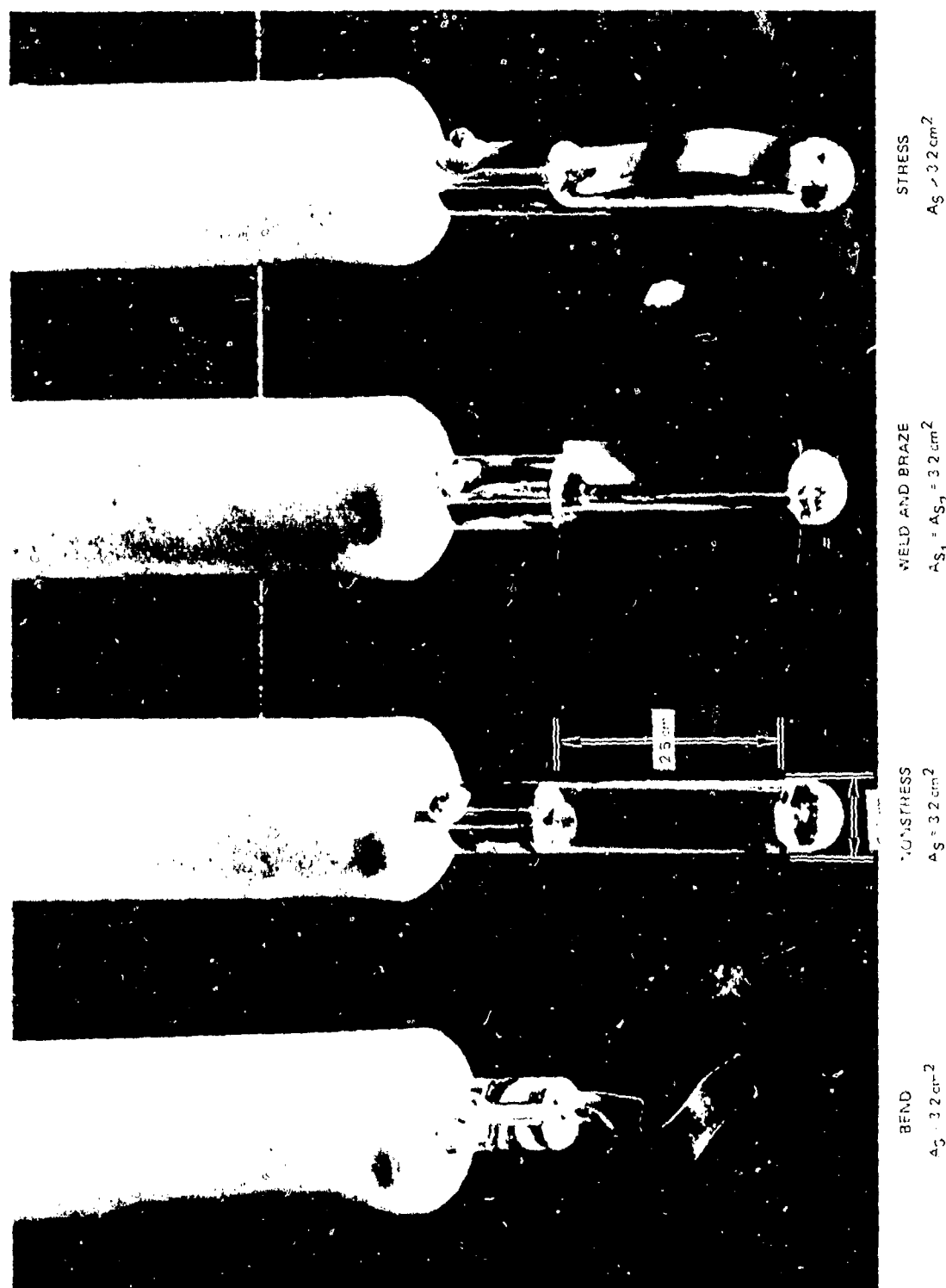
- A - GLASS REFERENCE ELECTRODE
- B - TEFLON ELECTRODE HOLDERS WITH O-RING SEALS
- C - TEFLON HOLDER FOR TEST SPECIMEN (WORKING ELECTRODE)
- D - TEST SPECIMEN
- E - LUGGEN PROBE (IR-FREE CONNECTOR TO REFERENCE ELECTRODE)
- F - LEAD TO TEST SPECIMEN
- G - GAS EXIT

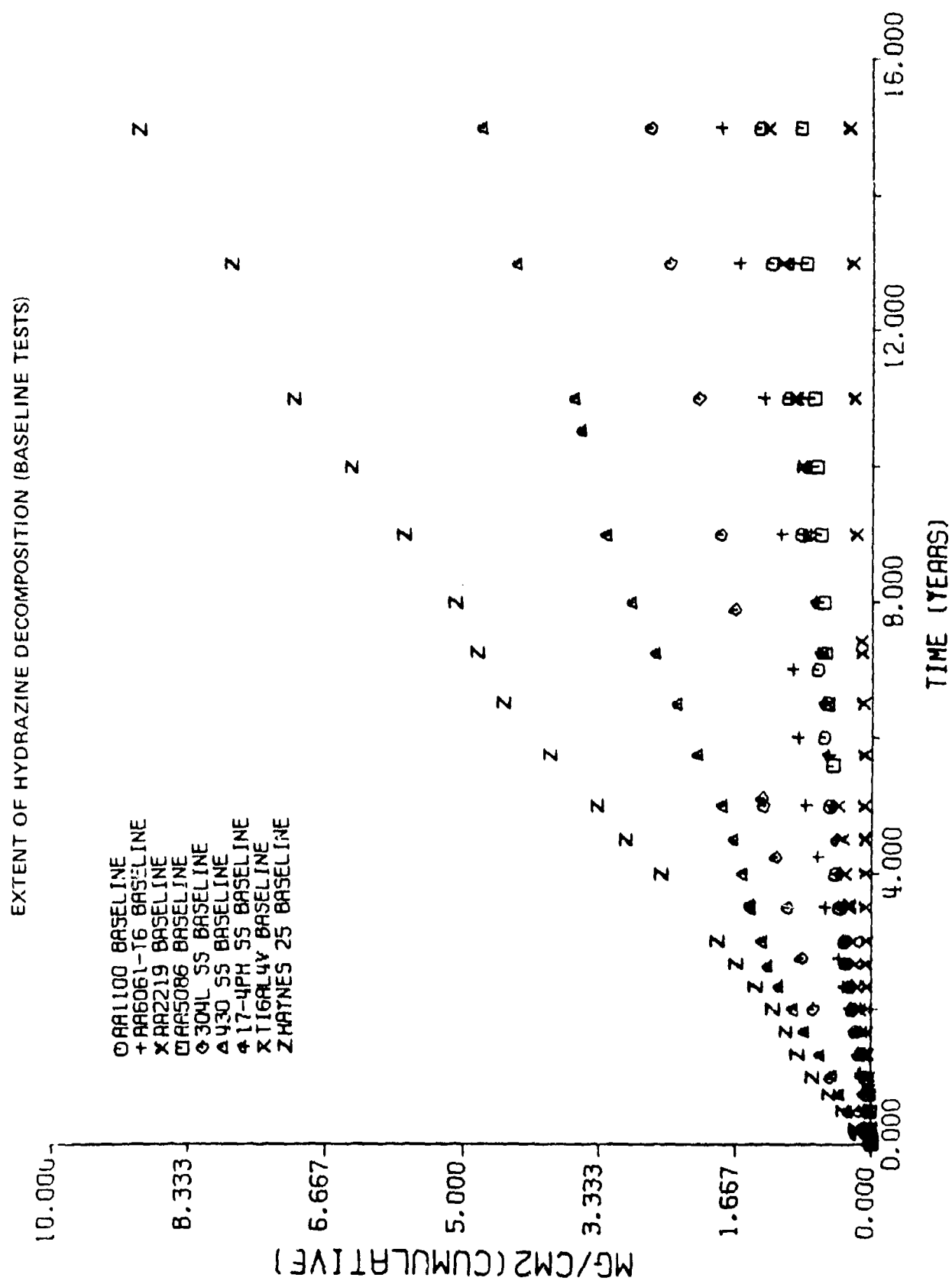
N08-66-1

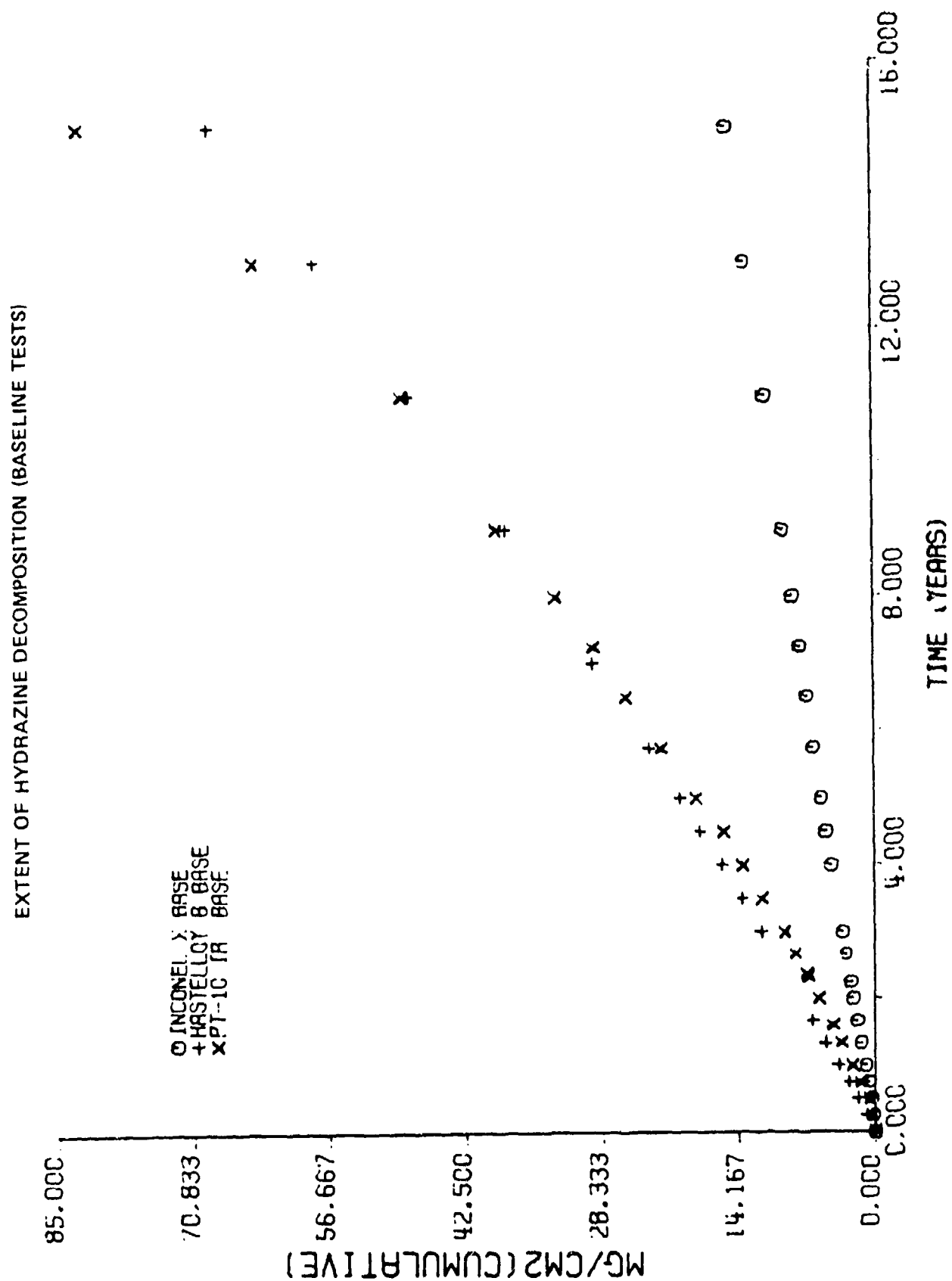
MATERIAL COMPATIBILITY TEST SPECIMENS - SLUG CONFIGURATIONS



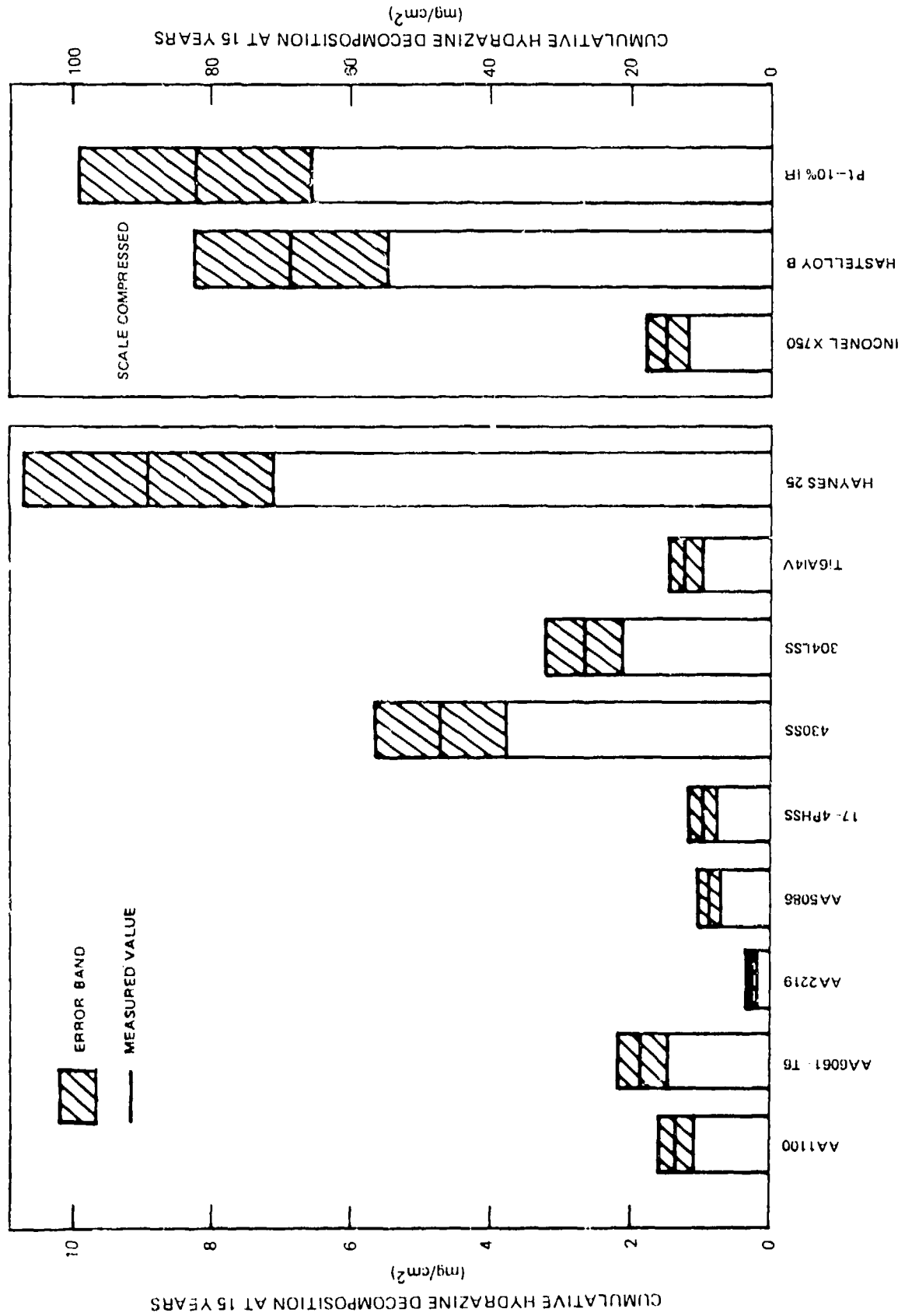
MATERIAL COMPATIBILITY TEST SPECIMENS - STRIP CONFIGURATIONS





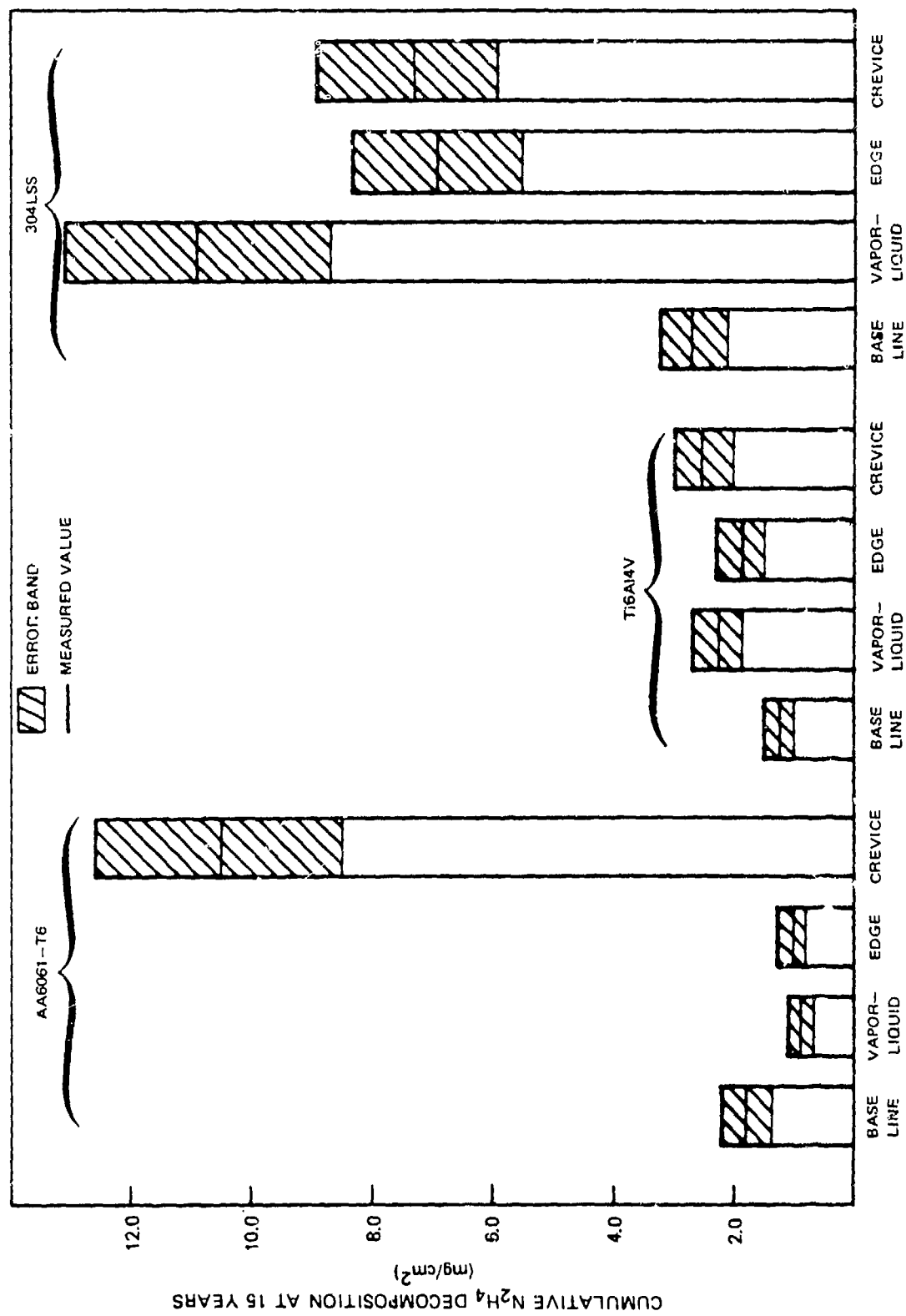


EXTENT OF HYDRAZINE DECOMPOSITION ON SELECTED METALS AT 110F



EXTENT OF HYDRAZINE DECOMPOSITION VAPOR-LIQUID, EDGE AND CREVICE CONFIGURATIONS AT 110 F

(a) AA6061-T6, Ti6Al4V AND 304LSS



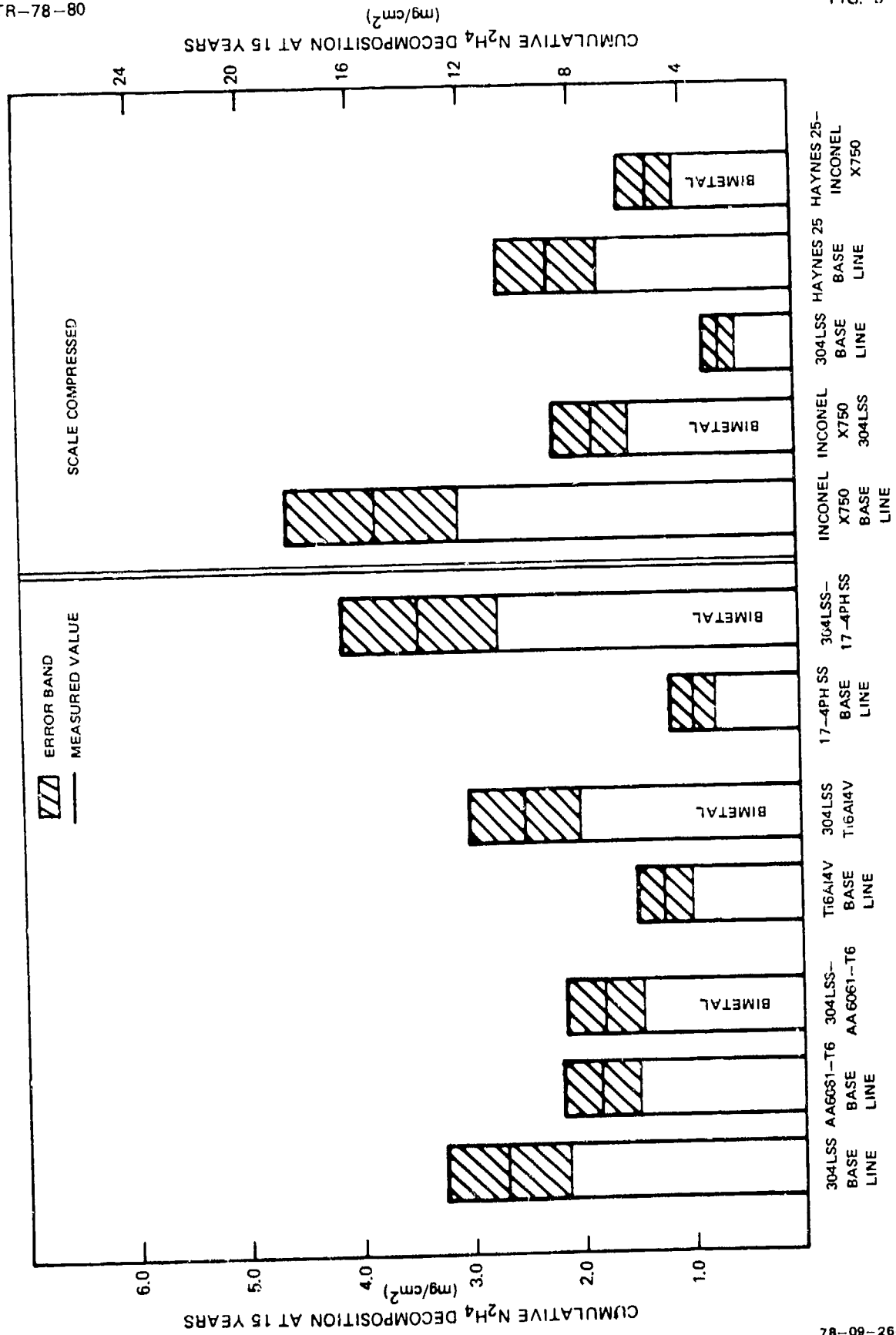
78-09-26-2

(b) HAYNES 25 AND INCONEL X750



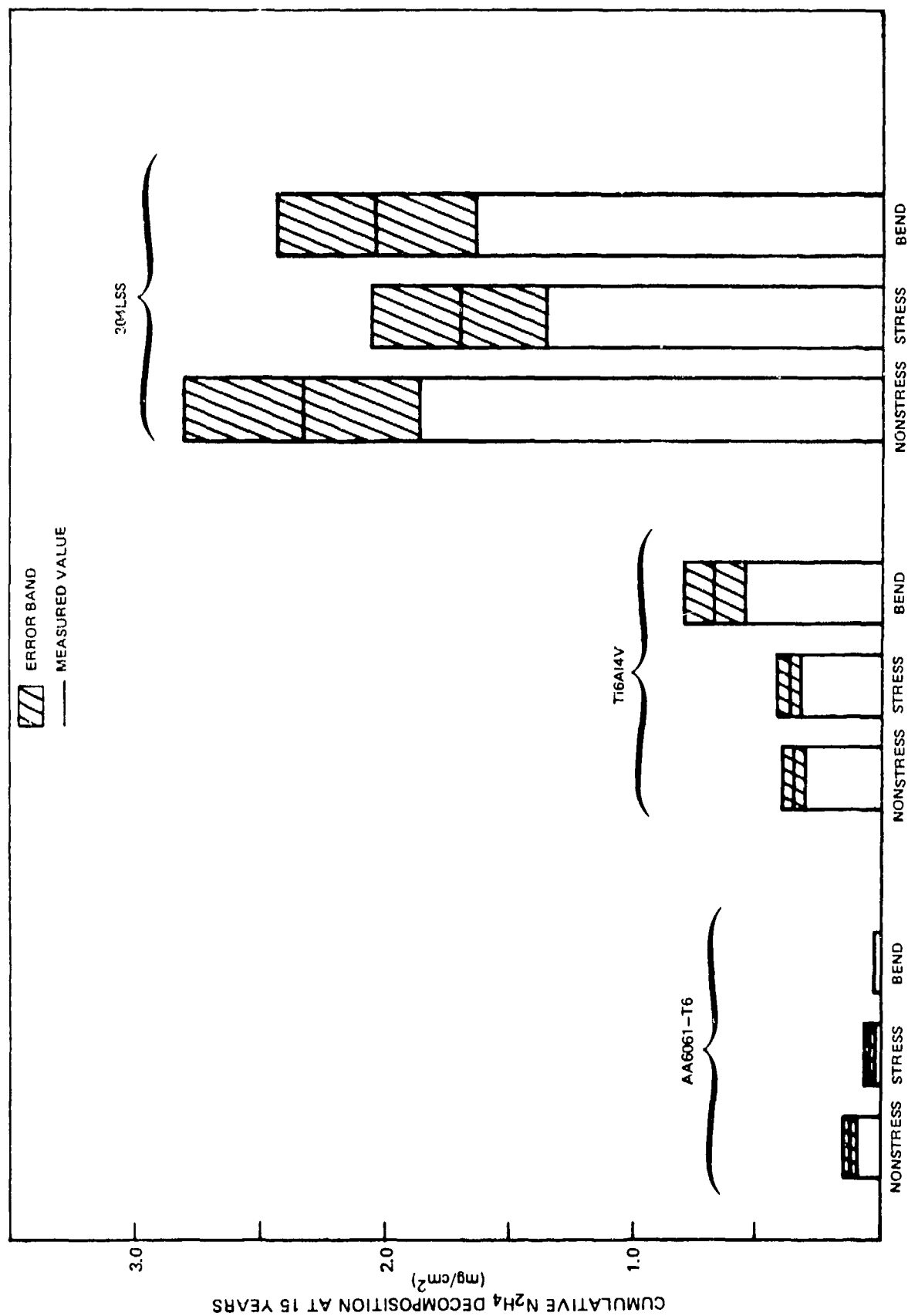
78-09-26-3

EXTENT OF HYDRAZINE DECOMPOSITION ON BIMETALLIC JUNCTIONS AT 110F



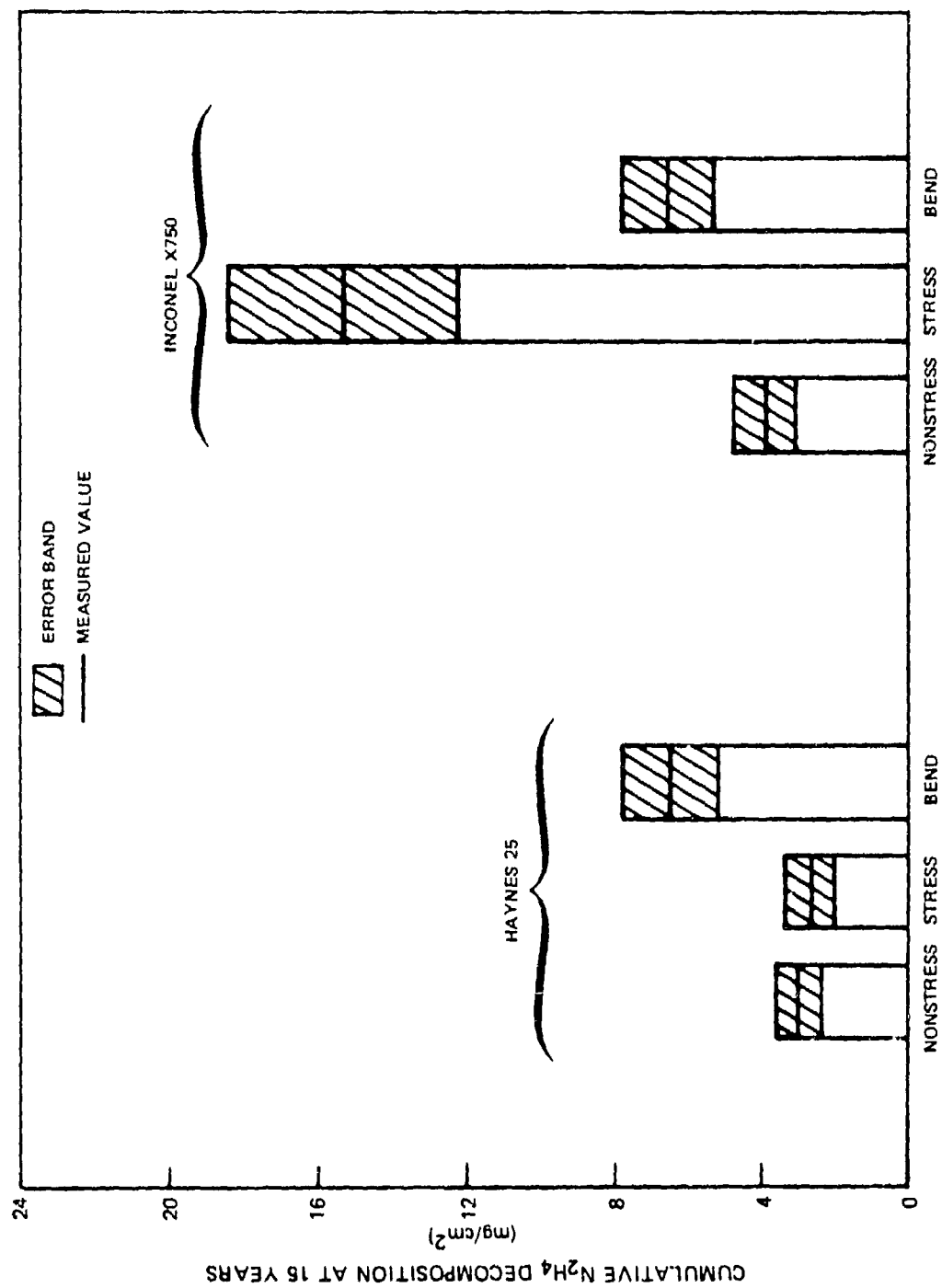
EFFECT OF METAL STRESS AND BENDS ON HYDRAZINE DECOMPOSITION AT 110 F

(a) AA6061-T6, Ti6Al4V AND 304LSS

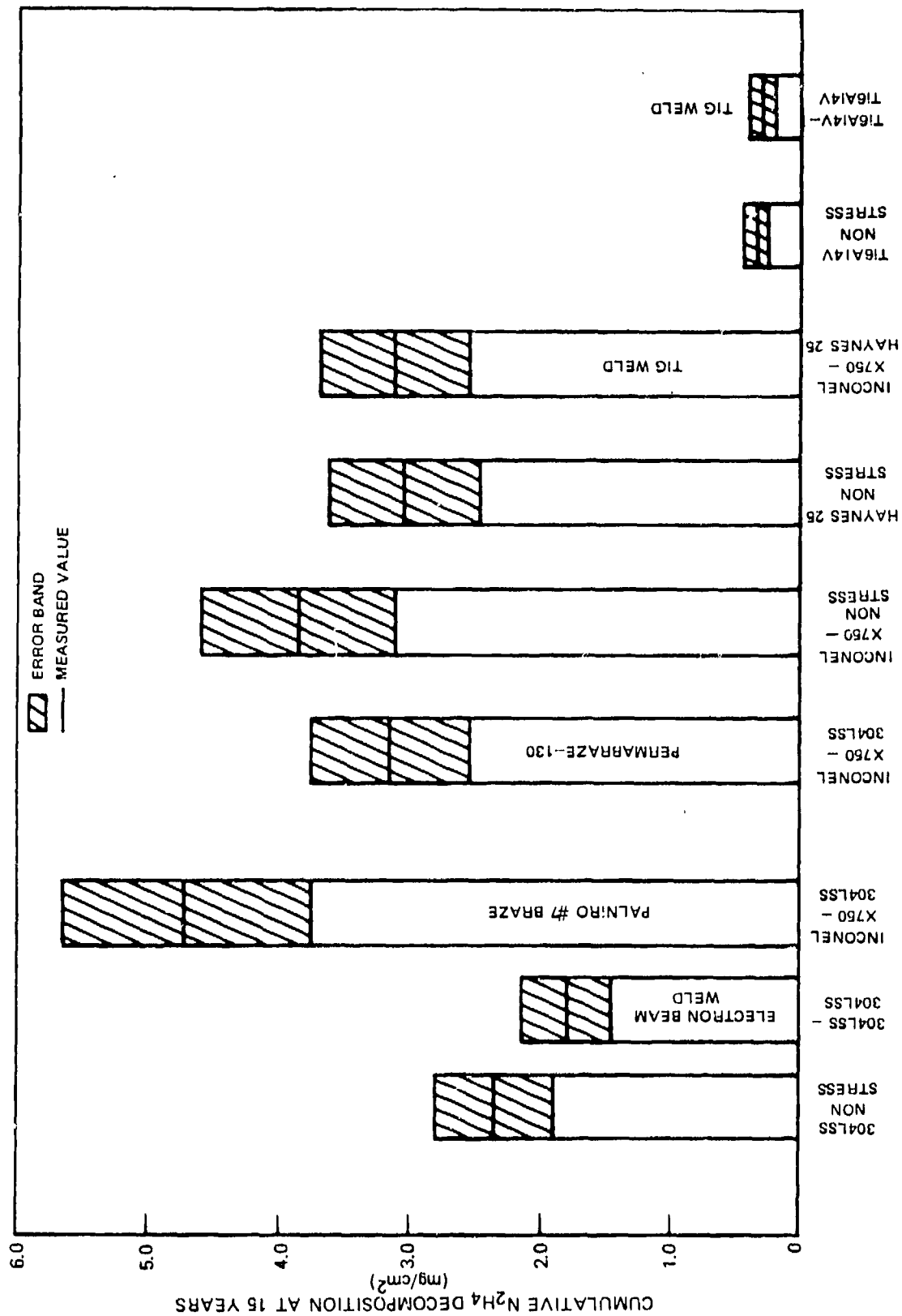


78-09-26-5

(b) HAYNES 25 AND INCONEL X750



EXTENT OF HYDRAZINE DECOMPOSITION ON WELDS AND BRAZES AT 110 F



78-60-26-7

TEST MATRIX FOR EVALUATING CLEANING PROCEDURES FOR USE WITH HYDRAZINE

METALS

GROUP I: AA1100, AA6061-T6, AA5086

(1) (2) (3)

GROUP II: 17-4PH, 430SS, 304LSS

(4) (5) (6)

GROUP III: T16A14V, HAYNES 25, INCONEL X750

(7) (8) (9)

TEST MATRIXES

GROUP I CLEANING PROCEDURE

METAL	CLEANING PROCEDURE		
	A	B	C
	1	α	β
	2	β	γ
	3	γ	α

GROUP II: CLEANING PROCEDURE

METAL	CLEANING PROCEDURE		
	A	B	C
	4	β	γ
	5	γ	α
	6	α	β

GROUP III: CLEANING PROCEDURE

METAL	CLEANING PROCEDURE		
	A	B	C
	7	γ	α
	8	α	β
	9	β	γ

TEMPERATURES

α - 50 F

β - 110 F

γ - 160 F

TEST MATRIX FOR EVALUATING EFFECTS OF IMPURITIES IN HYDRAZINE

METALS	IMPURITY		
	CO ₂	H ₂ O	Cl ⁻
	50 ppm	.0%	10 ppm
1. HAYNES 25 (Co)	IMPURITY LEVELS A B C	0%	20 ppm
2. INCONEL X (Ni)		1.5%	30 ppm
3. Ti6Al4V (Ti)		2.0%	
4. 304L (Fe)			
5. AA2219 (Al)			
6. AA1100 (Al)			
7. AA6061-T6 (Al)			
8. 430 (Fe)			
9. 17-4PH (Fe)			

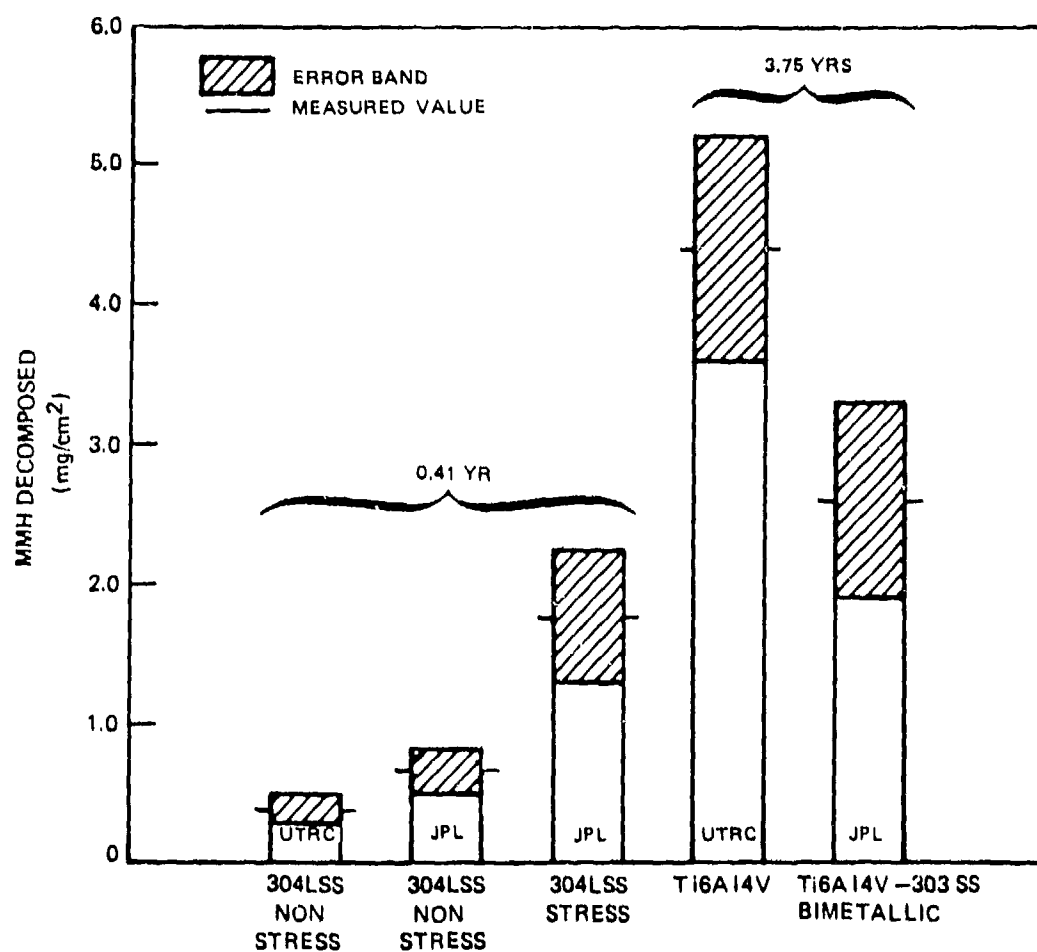
IMPURITY LEVEL		
A	B	C
5	8	2
9	3	6
4	7	1

IMPURITY LEVEL		
A	B	C
6	9	3
7	1	4
8	2	5

IMPURITY LEVEL		
A	B	C
1	4	7
2	5	8
3	6	9

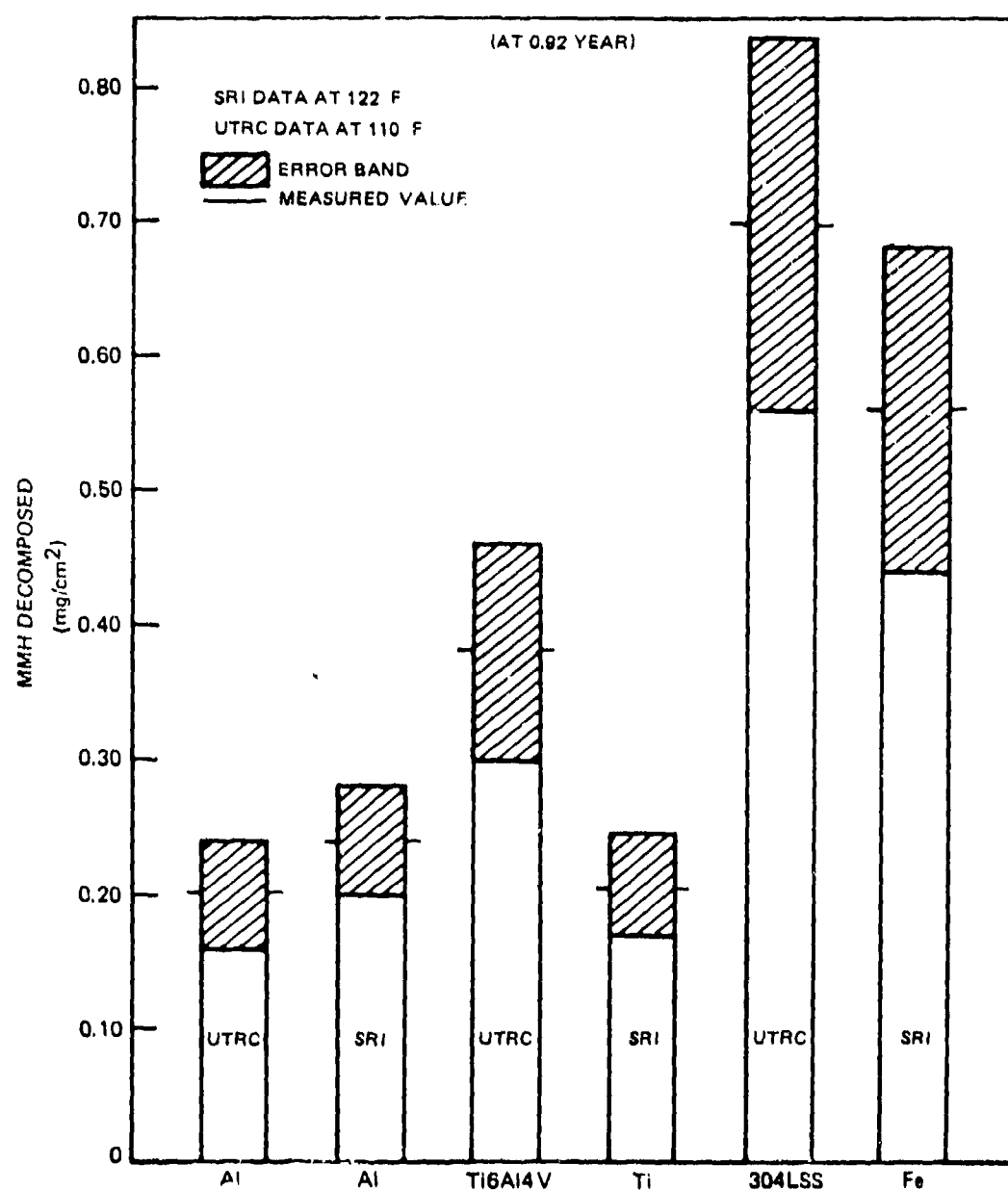
IMPURITY LEVEL		
A	B	C
5	8	2
9	3	6
4	7	1

77-08-64-1

COMPARISON OF UTRC AND JPL COMPATIBILITY DATA
IN MONOMETHYLHYDRAZINE AT 110 F

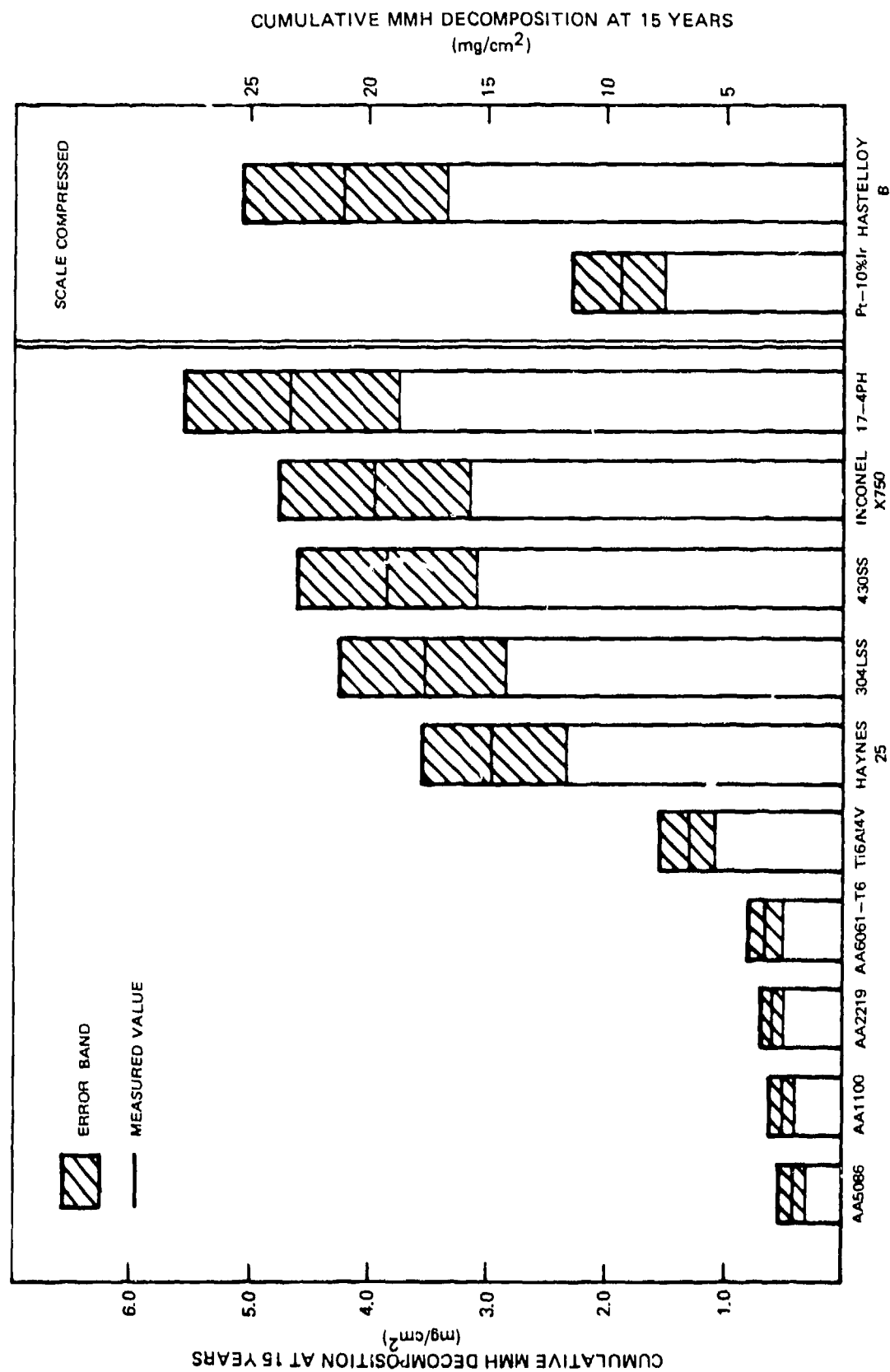
77-12-97-1

COMPARISON OF UTRC AND SRI COMPATIBILITY DATA IN MONOMETHYLHYDRAZINE



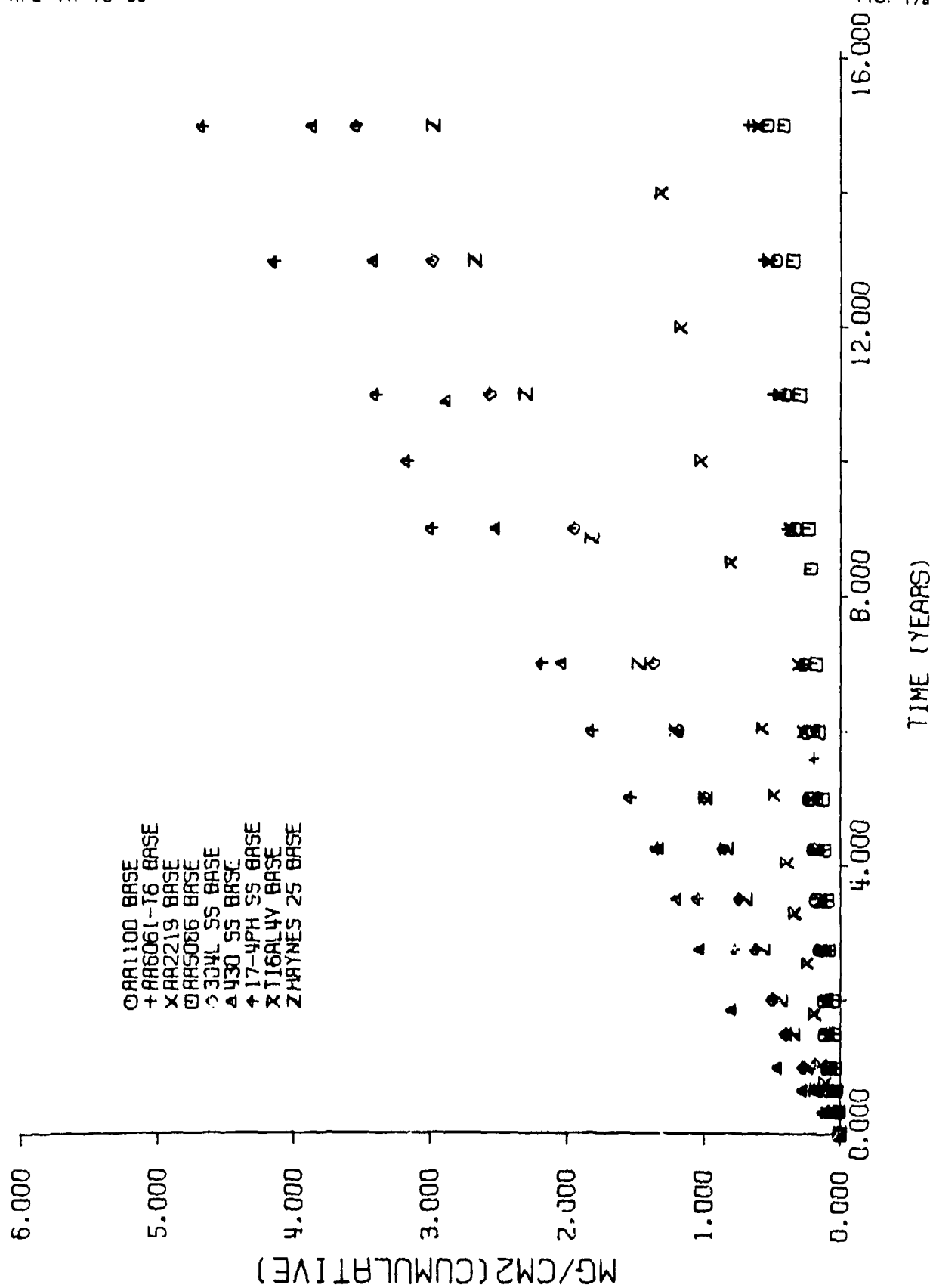
77-12-97-2

EXTENT OF MONOMETHYLHYDRAZINE DECOMPOSITION ON SELECTED METALS AT 110 F
(BASELINE TESTS)

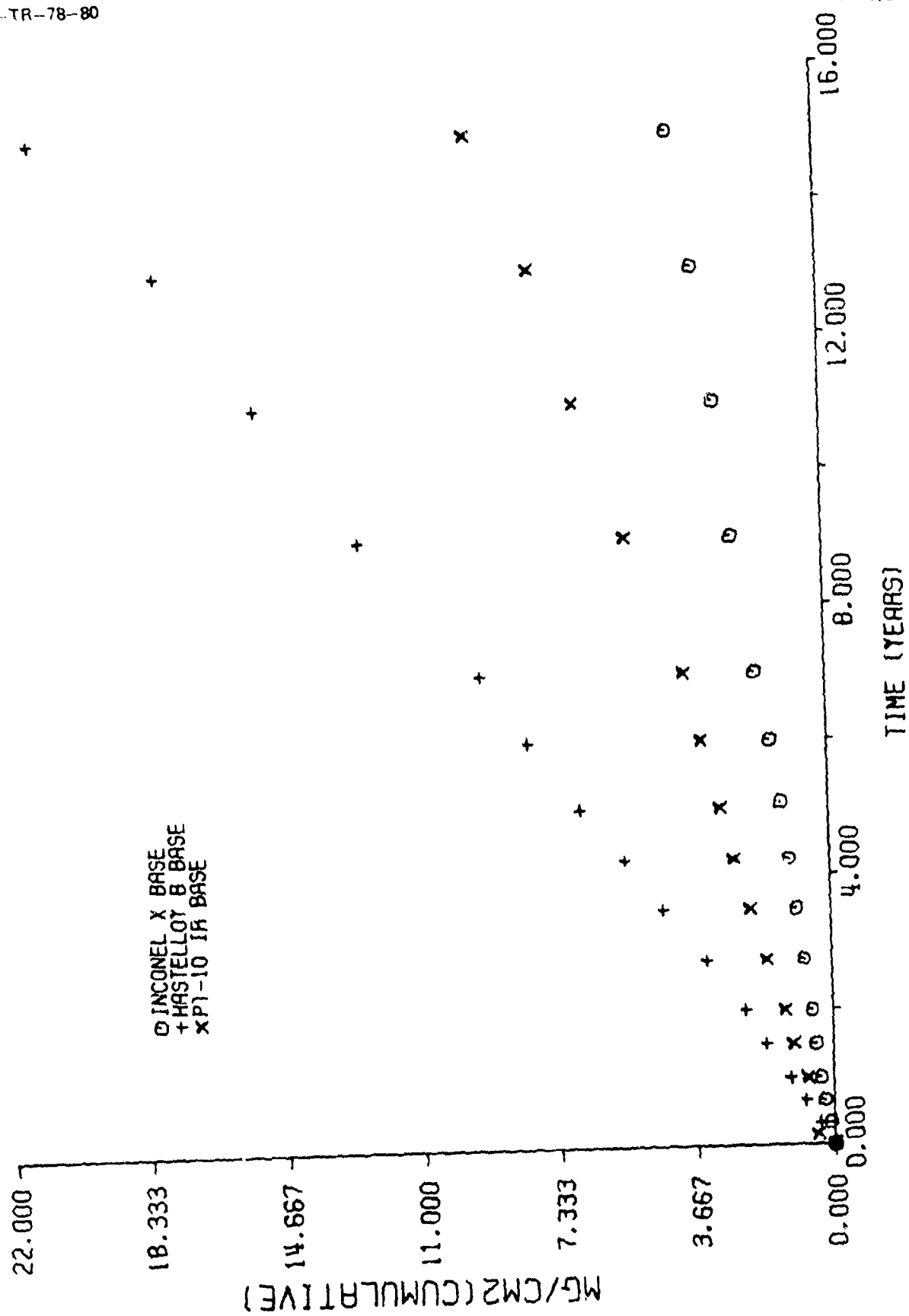


78-09-28-8

EXTENT OF MONOMETHYLHYDRAZINE DECOMPOSITION (BASELINE TESTS)

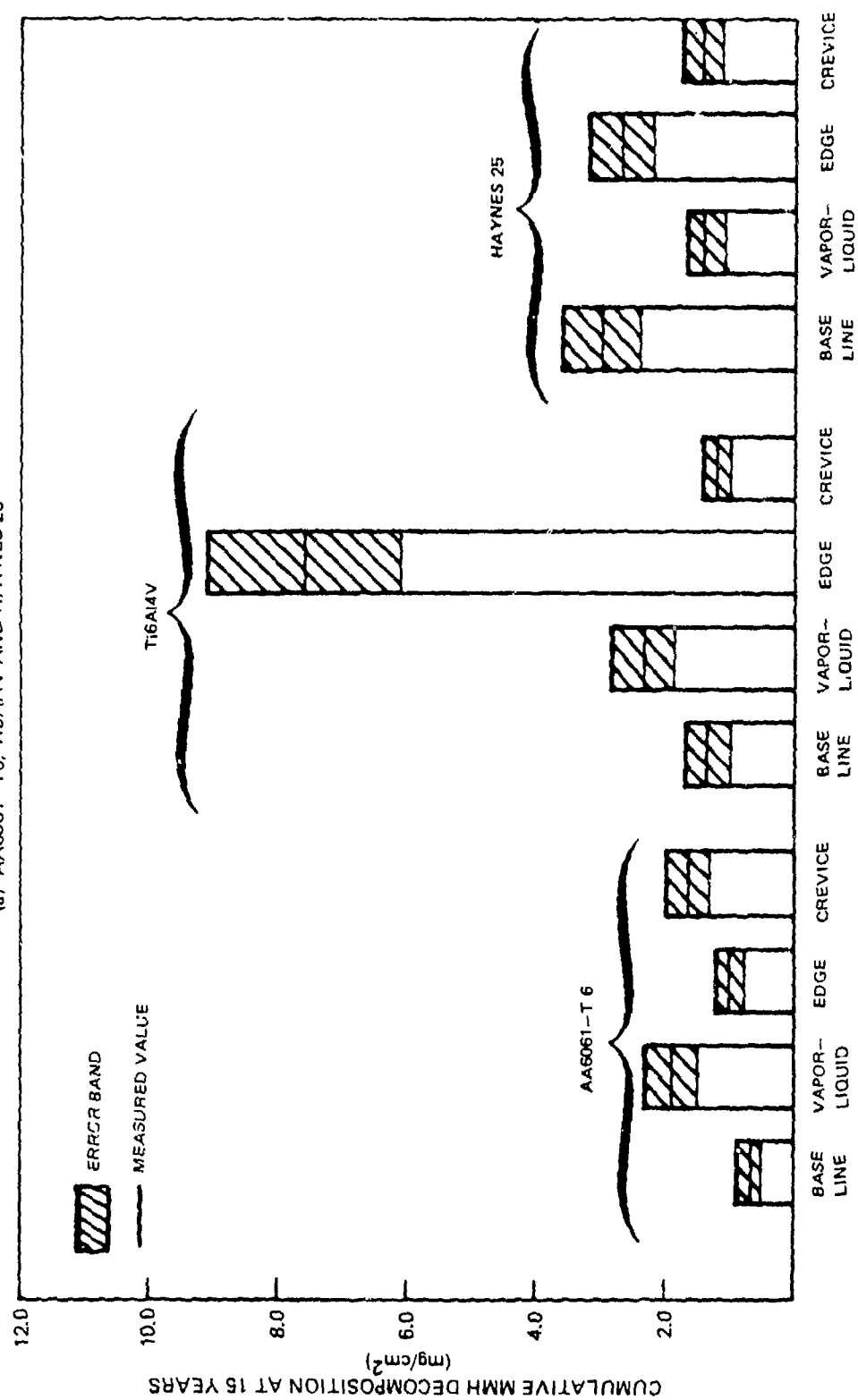


EXTENT OF MONOMETHYLHYDRAZINE DECOMPOSITION (BASELINE TESTS)



EXTENT OF MONOMETHYLHYDRAZINE DECOMPOSITION ON VAPOR-LIQUID, EDGE AND CREVICE CONFIGURATIONS AT 110 F

(a) AA6061-T6, Ti6Al4V AND HAYNES 25



78-09-26-9

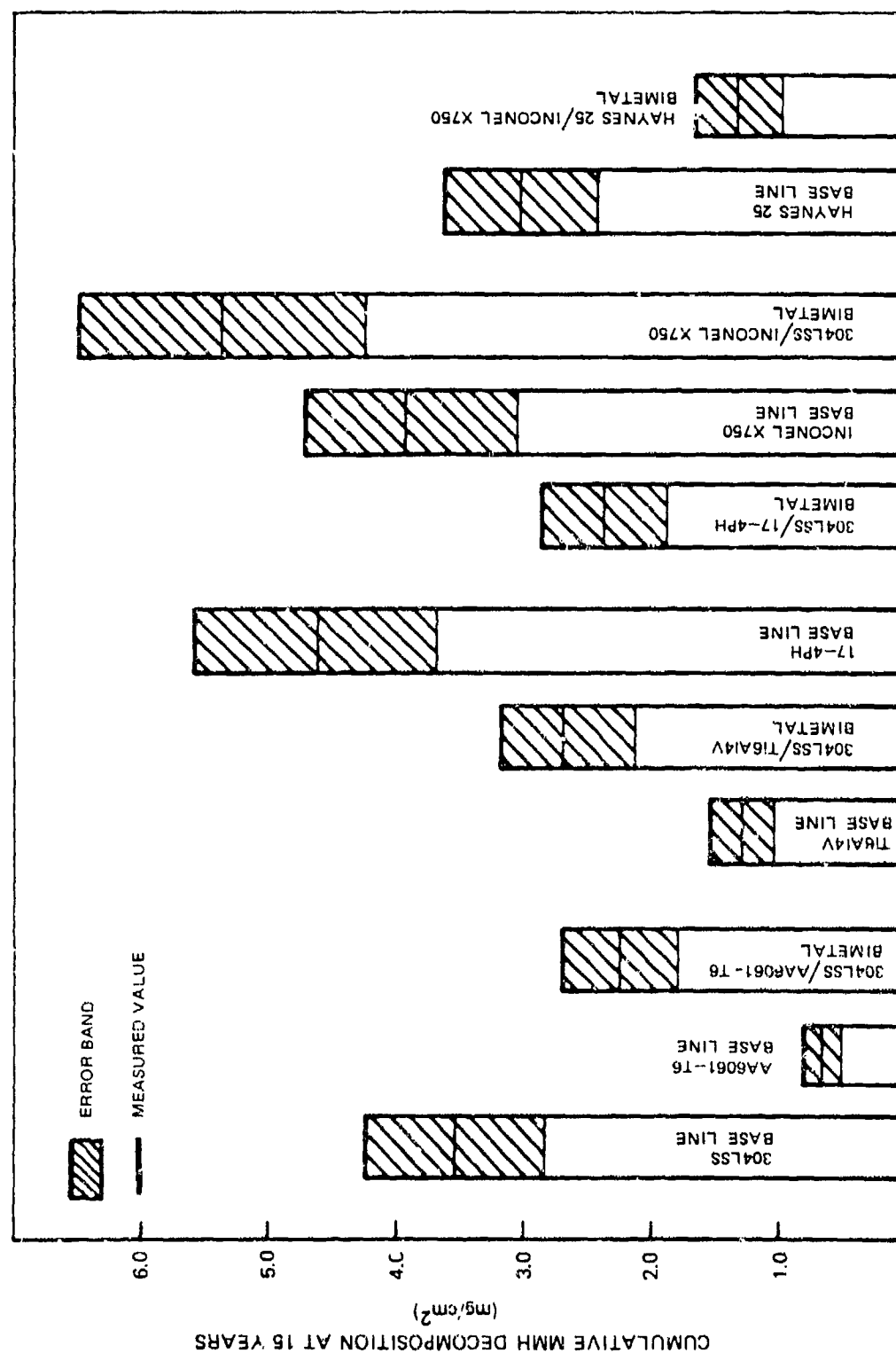
EXTENT OF MONOMETHYLHYDRAZINE DECOMPOSITION ON VAPOR-LIQUID, EDGE AND CREVICE CONFIGURATIONS AT 110 F

(b) 304LSS AND INCONEL X750



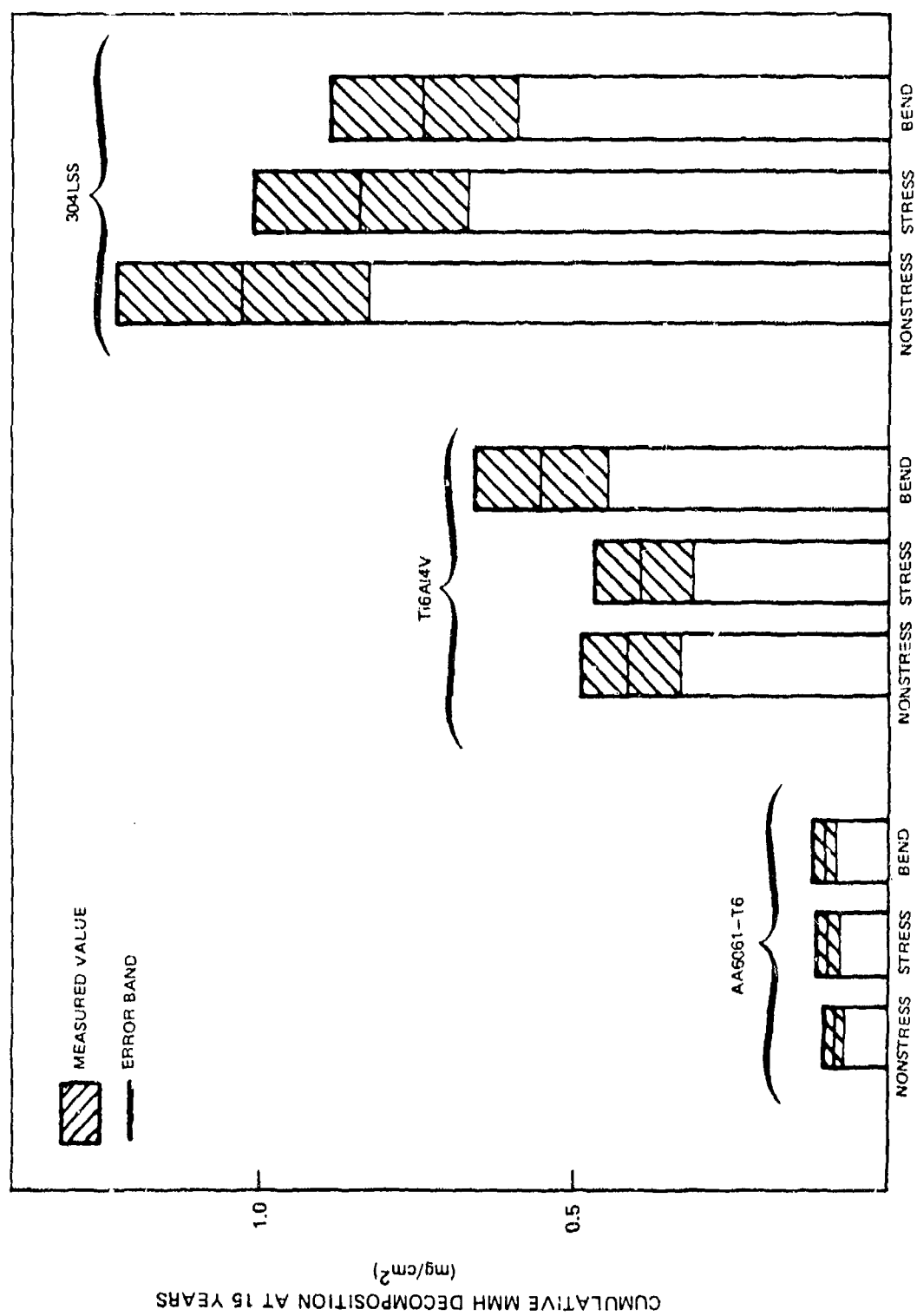
78-09-26-10

EXTENT OF MONOMETHYLHYDRAZINE DECOMPOSITION
ON BIMETALLIC JUNCTIONS AT 110 F



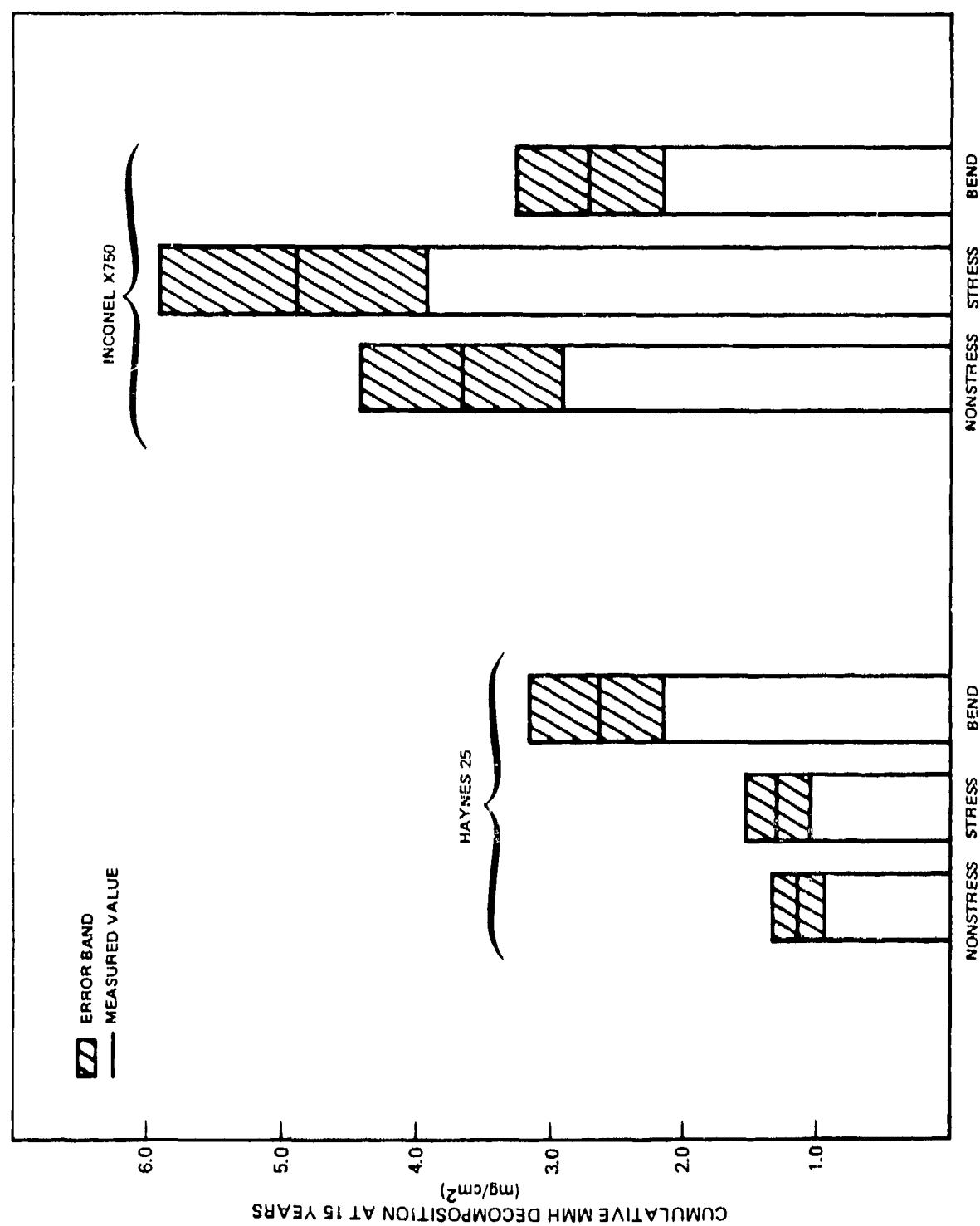
EFFECT OF METAL STRESS AND BENDS ON MMH DECOMPOSITION AT 110F

(a) AA6061-T6, T6Al4V AND 304LSS



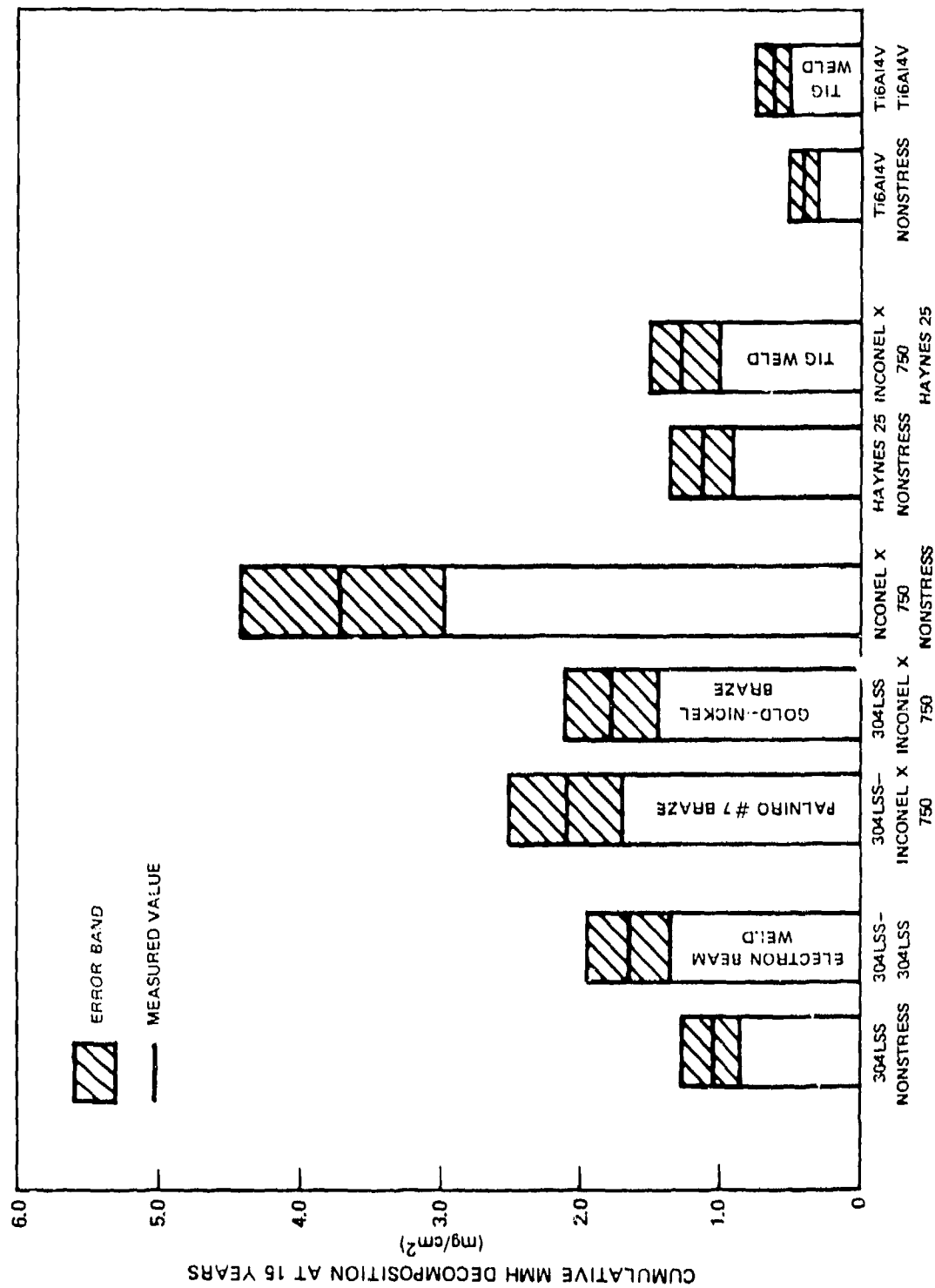
EFFECT OF METAL STRESS AND BENDS ON MMH DECOMPOSITION AT 110 F

(b) HAYNES 25 AND INCONEL X750



78-09-26-13

EXTENT OF MONOMETHYLHYDRAZINE DECOMPOSITION ON WELDS AND BRAZES AT 110 F



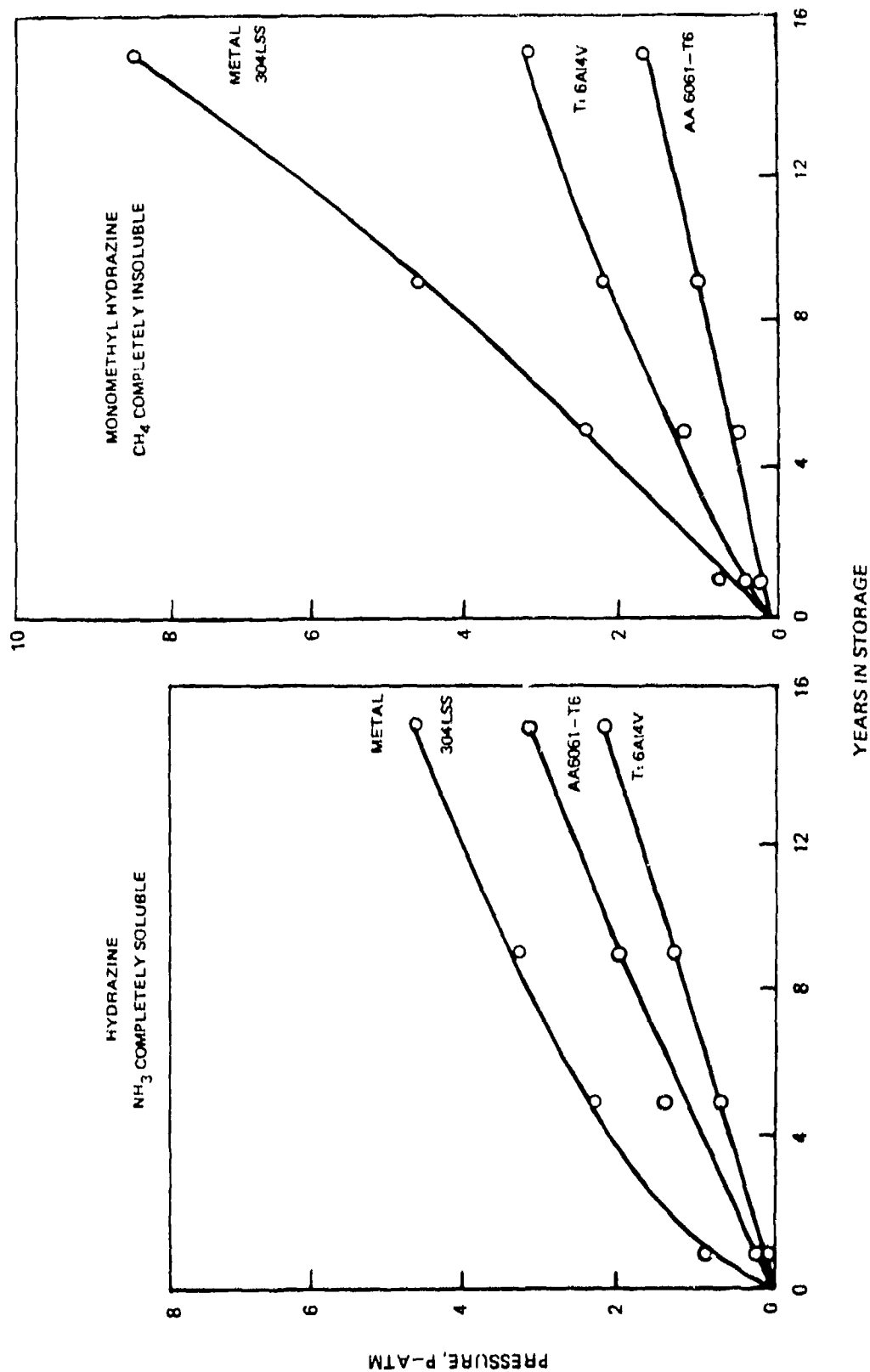
78-09-26-14

PRESSURE BUILD-UP IN FUEL STORAGE TANKS

29 IN. DIAM. SPHERICAL TANK

1% ULLAGE

TEMPERATURE -43C



78-10-217-1

APPENDIX A

EQUIPMENT AND TEST PROCEDURES

Experimental Test Cell

The experimental test cell, shown in Figs. A-1 and A-2, was designed to provide a closed system for the tests using fabrication materials known to be relatively inert in hydrazine and monomethylhydrazine. These include pyrex glass and a Teflon/ethylene-propylene terpolymer. The glass reference electrode (A) was found to maintain a stable potential once the glass membrane was saturated with hydrazine. This potential was measured with respect to a standard calomel electrode over a long period of time while in contact with hydrazine. The absolute potential of this electrode is not known, since the solvent effects on the calomel electrode are uncertain. However, as long as a constant potential is maintained, changes in the potential of the test piece with respect to the glass electrode are absolute. Since all voltage measurements are in terms of a ΔE (polarization), an absolute reference potential is not necessary.

Two identical test pieces and test piece holders were used in each cell. Threaded Teflon holders (B) are used for both the test piece and reference electrodes. The test electrode holders and the reference electrode are sealed in the cell by means of ethylene-propylene "O" rings at the base of the threaded Teflon fittings (B). A vent tube (G) is provided for each test electrode compartment. This tubing is connected to a Teflon plug stopcock and is vented to a hood.

Drawings of the threaded Teflon caps are shown in Figs. A-3 and A-4. They were designed to fit threaded glass fittings from chromatographic columns which include a seat for the "O" ring. The "O" ring sizes are 2-210 for the 25 mm caps (for the test piece holders) and 2-111 for the 15 mm cap (for the glass electrode).

The main sections of the cell are fabricated from 35 mm OD pyrex tubing and are 8.9-cm long, as measured from the "O" ring seat. The reference electrode section is fabricated from 20 mm OD pyrex tubing and is 10.2-cm long, as measured from the "O" ring seat. The main sections of the cell are joined by means of a short piece (approximately 1.9-cm) of 10 mm OD pyrex tubing to provide for current flow. The three sections of the cell are braced by 5 mm glass rod and are spaced so there is ample room for the three Teflon caps. The two capillary probes from the reference section of the cell are fabricated from 6 mm OD pyrex tubing which are ring-sealed through the walls of the main

chambers finally terminating in the capillary probes. The capillary probes were positioned so that the tip of the capillary was at the vertical centerline of the main sections of the cell. Because of the nature of the glass blowing process there was some latitude in the exact dimensions of the cell. The only critical considerations are; the position of the capillaries, so that proper spacing is achieved between the capillary tips and the test pieces, and the spacing of the compartments to ensure room for the Teflon caps.

The test piece holder is shown in Fig. A-5. The dimensions are such that the proper spacing can be achieved between the reference capillary and the surface of the test piece. Because of the flexibility of Teflon, it is possible to adjust the spacing by slightly bending the test piece holder. Since there is a minimal current flow between the reference and the test pieces ($< \text{one microamp}$) the only voltage drop in the system is between the tip of the capillary and the test piece. This is the only area in which significant current flow takes place. This voltage drop must be added to the ΔE imposed on the system. However, with proper design, the voltage drop is minimized to the point where it can be neglected. A series of experiments was performed in which a movable capillary was employed and it was determined that the reference ΔE was minimized with a 2.0 mm outside x 1.0 mm inside diameter capillary placed 2.0 mm from the surface of the test piece.

Two test pieces are employed because of the nature of the metal-propellant interaction and also because the tests require that one electrode be polarized anodically and, therefore, the other must be polarized cathodically. Normally reactions take place at micro-anodic and micro-cathodic sites on the same macro-surface; however, these processes are necessarily separated when potential is imposed to accelerate the surface reactions. Thus, if one test piece is always used as the anode (working electrode) and the other as the cathode (counter electrode), the total products of reaction during a test should be the same as those on the normal unpolarized surface. This would not be the case if one electrode was the material to be studied and the second electrode was on inert material such as platinum. The counter electrode, which is the cathode during current-voltage measurement, was the baseline slug configuration in all cases, regardless of the anode test piece configuration.

Instrumentation

A photograph of the instrumentation required for accelerated compatibility testing is shown in Fig. A-6. The instrument for determining i_0 is a device known as a potentiostat (A). This device is designed to provide a potential difference between the reference and working (test) electrode. A feedback system in the potentiostat provides the current flow necessary to maintain the set potential difference. The potential difference may be set manually, but

the standard practice is to automatically scan through a desired potential range at some predetermined rate. For the present application it was desirable to use low scan rates, since the kinetics of the process are such that low reaction rates were expected. The potential is scanned by means of a Universal Programmer (B). The resulting voltage and current signals were fed to an X-Y Recorder (C), where the voltage (ΔE) was plotted on the Y-axis and the current response on the X-axis (see Figure 1).

Once the current versus voltage plot is recorded and i_0 is determined, the system under test is electrolyzed using one of the constant current power supplies (D). Several constant temperature baths (E) are used in order to run tests at a variety of temperatures simultaneously. Tests performed below room temperature were controlled by means of a Porta-Cool refrigeration unit, while standard thermostatic heaters were used for the elevated temperatures. The specific equipment required is listed in Table A-I.

Experimental Procedures

In order to obtain accurate values of the exchange current density (i_0) it is necessary to perform the experiments in accordance with the following procedure:

- a) The voltage difference between the test piece and the reference (glass) electrode is nulled so that there will be no net current flow when the potentiostat is placed in the operate position.
- b) The program limits are set so that on placing the potentiostat in the operate position, the voltage is scanned 50 mv in both the anodic and cathodic direction. The slope of the current-voltage plot at the equilibrium potential is used to obtain $di/d\eta$, which in turn is used to calculate i_0 according to the low field approximation (Eq. 4 - Section II). A current-voltage plot for platinum-10% Iridium is shown in Fig. 1. This scan was deliberately extended to ± 200 mv in order to determine the linear voltage range which could be used to determine the slope $di/d\eta$. The straight line portions of both the anodic and cathodic scans are limited to approximately ± 50 mv overpotential which is typical for the metals studied in this program.
- c) The rate at which the voltage is scanned is an important parameter. It has been determined that rates much above 20 mv/min yield high values of $di/d\eta$ due to failure to maintain equilibrium conditions. Thus, this rate has been selected as a maximum.
- d) Once i_0 has been determined and the decomposition rate ($\text{mg}/\text{cm}^2\text{yr}$) has been calculated, the time-base of the test is extended by electrolysis of

the system at a current which is some multiple of i_0 . The ratio of the electrolysis current density to the exchange current density is the time-base simulation factor. It has been determined experimentally that electrolysis currents should be less than 100 μa in order to obtain reproducible values for exchange current density (Ref. 4). In actual practice, the electrolysis current is determined by the desired simulated time increment and the magnitude of the exchange current density. Metals such as the aluminum alloys and Ti6Al4V have relatively low exchange current densities, and electrolysis currents on the order of 10 to 20 μa are sufficient to obtain reasonable time simulation ratios. The stainless steels require currents on the order of 30 to 50 μa in order to simulate time to a reasonable degree without sacrificing accuracy. It was necessary to electrolyze at currents approaching 100 μa only in the case of highly active metals such as Pt-10%Ir, Hastalloy B, Inconel X750 and Haynes 25 due to the much higher exchange current densities associated with these metals.

e) Each simulated time increment is used in conjunction with its associated decomposition rate to calculate the incremental amount of decomposition in mg/year. These values are then summed to provide a cumulative measure of the extent of propellant decomposition as a function of simulated time.

f) It has been found that the most accurate data is obtained when the simulated time increments are relatively short; for example, during the early stages of a particular test. Fairly rapid changes in the electrochemical activity of the propellant-metal interface are usually evident during the first several years of simulated time. After that period there appears to be a passivation effect in most cases so that the remainder of data is relatively linear. Thus, the recommended procedure is to determine the exchange current density for a period of three to four days without electrolysis, followed by simulation of the time base in increments of 0.33, 0.67, 1.0, 1.5, 2.0, 2.75, 3.50, 4.25, 5.0, 6.0, 7.0, 9.0, 11.0, 13.0 and 15.0 years. This procedure was followed for all baseline and nonstress tests. For all special metal configuration tests (bend, edges, crevices, etc), the simulated time sequence was 0.5, 1.0, 2.0, 3.0, 5.0, 7.0, 9.0, 12.0 and 15.0 years. These sequences gave accurate time profiles for the decomposition rates of both hydrazine and monomethylhydrazine, as a function of simulated time, without disturbing the natural propellant-material interactions that would be experienced under real-time situations.

TABLE A-I

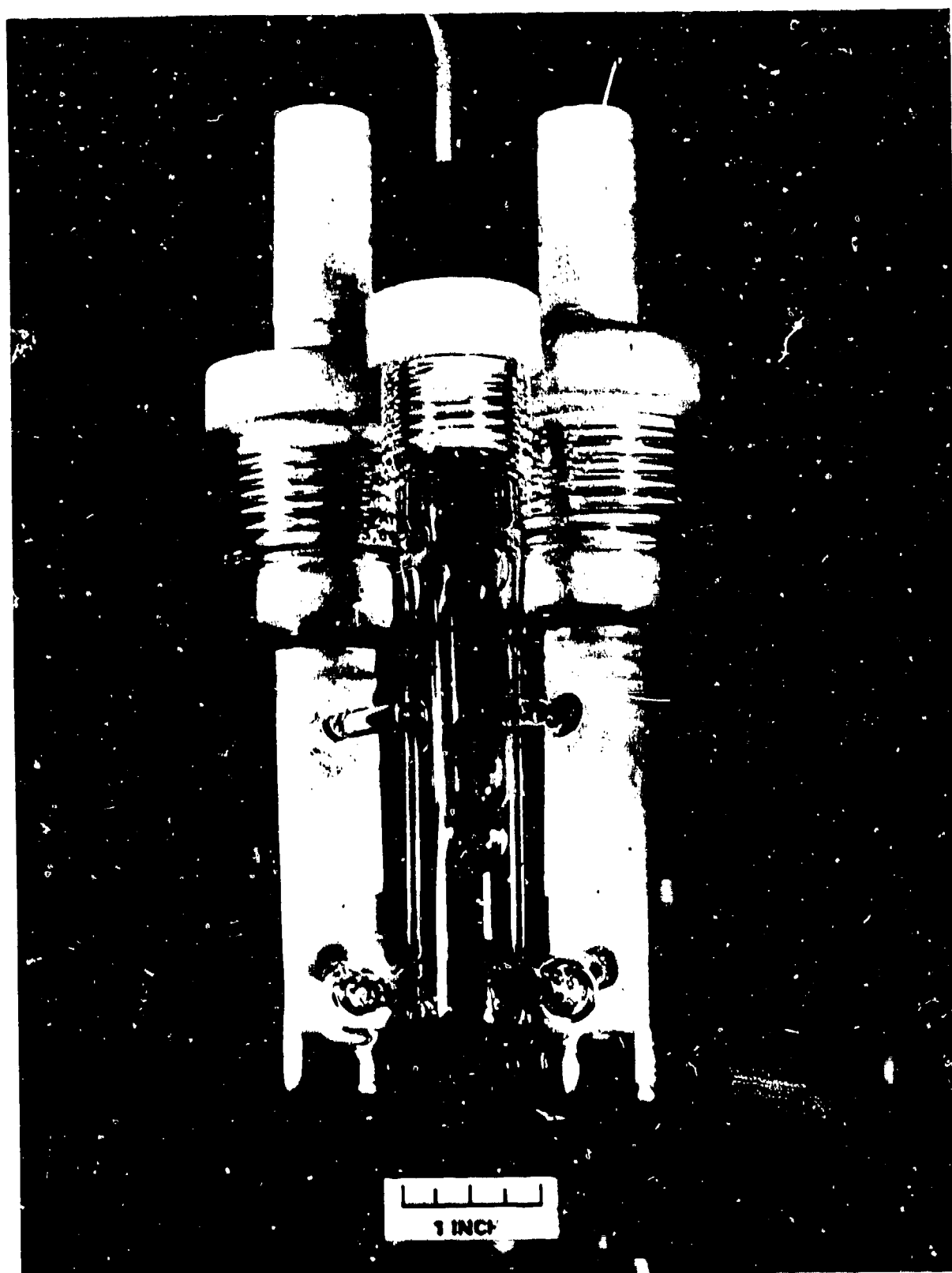
LIST OF EQUIPMENT

I. Electronic Apparatus

- a) Potentiostat-Galvanostat, PAR Model 173 or Equivalent
- b) Universal Programmer PAR Model 175 or Equivalent
- c) X-Y Recorder, Mosley Model 135 AM or Equivalent
- d) Power Supplies - Kepco Model PC-2 (Constant Current) (100v-200 ma max.) or Electronic Measurements Model C612 (300v-100 ma max.) or Equivalent

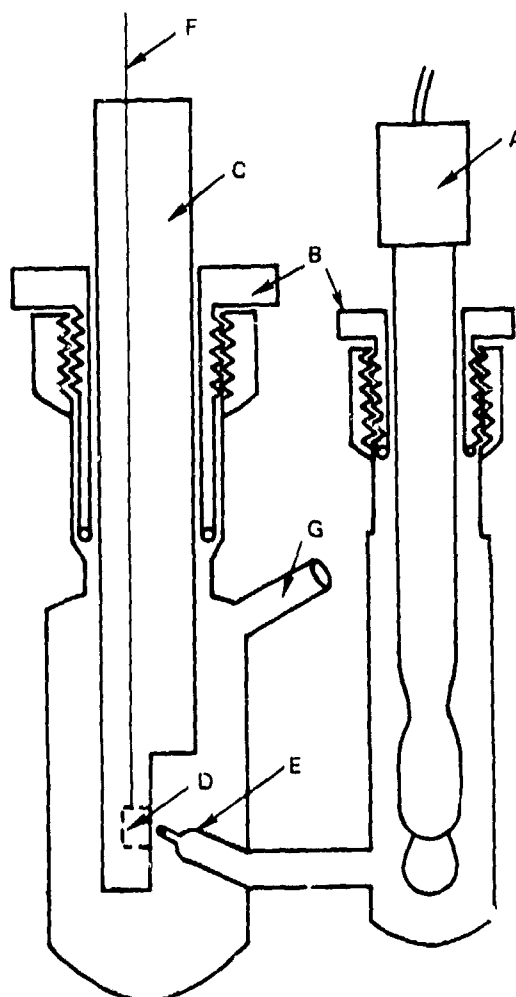
II. Constant Temperature Apparatus

- a) Heating and Control - Precision Scientific Porta-Temp or Equivalent
- b) Cooling and Control - Precision Scientific Porta-Cool or Equivalent



MATERIAL COMPATIBILITY TEST CELL

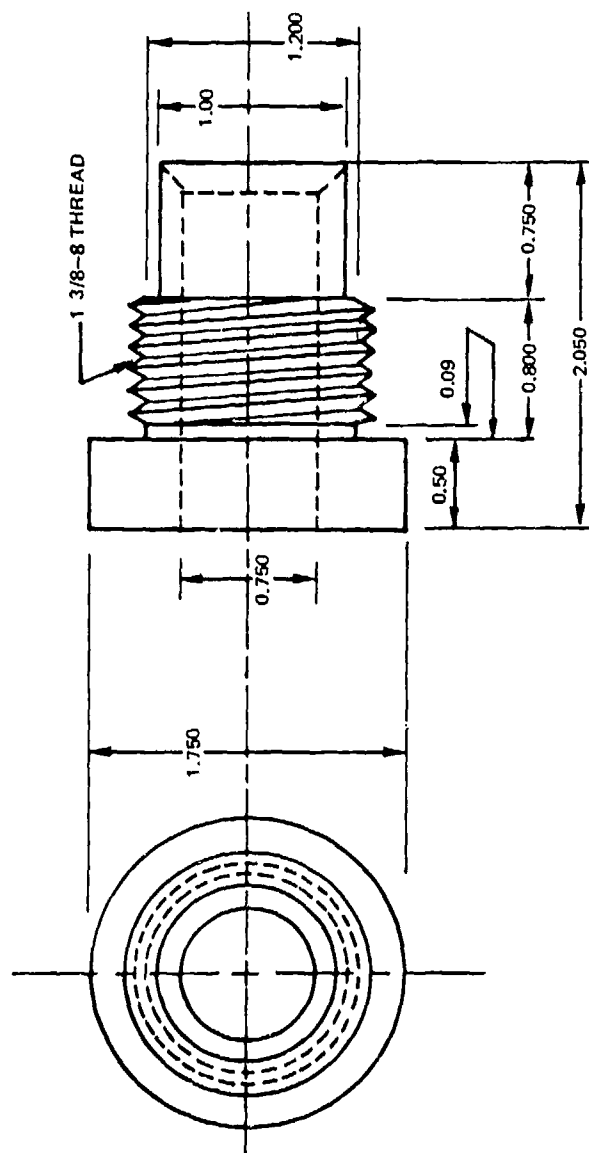
(CROSS SECTION)



KEY

- A - GLASS REFERENCE ELECTRODE
- B - TEFLON ELECTRODE HOLDERS WITH O-RING SEALS
- C - TEFLON HOLDER FOR TEST SPECIMEN (WORKING ELECTRODE)
- D - TEST SPECIMEN
- E - LUGGEN PROBE (IR-FREE CONNECTOR TO REFERENCE ELECTRODE)
- F - LEAD TO TEST SPECIMEN
- G - GAS EXIT

THREADED TEFLON CAP
(25 mm)



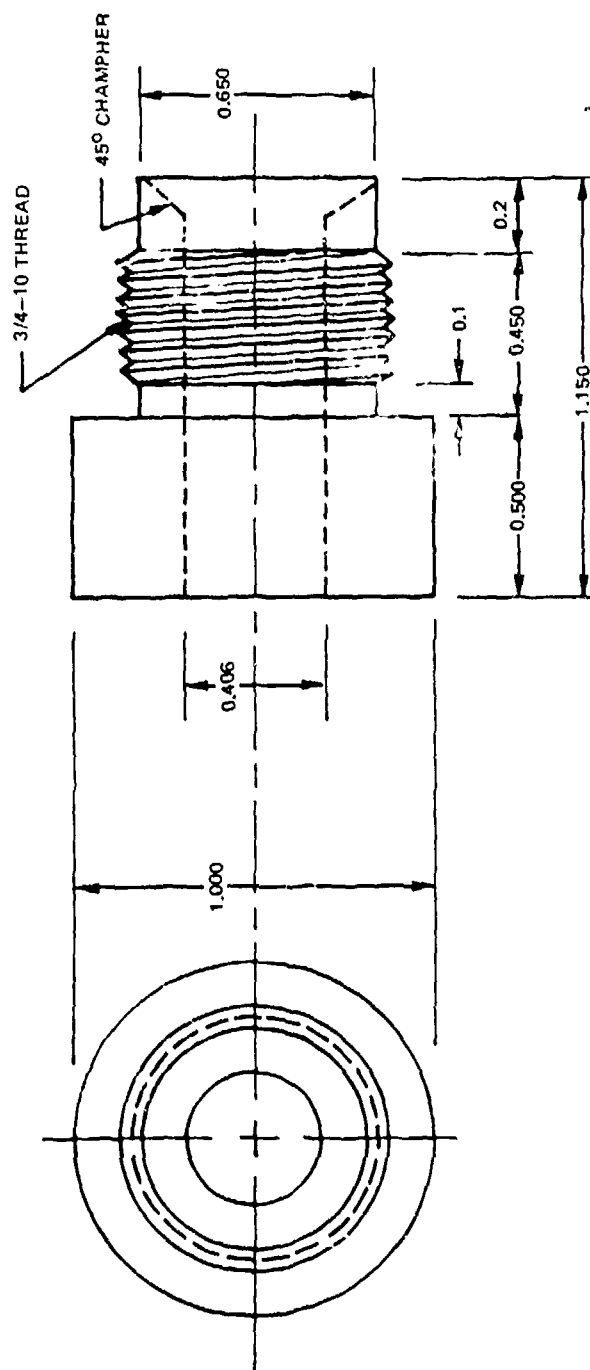
MATERIAL: TEFLON

TOLERANCE: ± 0.010

SCALE = FULL

ALL DIMENSIONS IN INCHES

THREADED TEFLON CAP
(15 mm)



MATERIAL : TEFLON

TOLERANCE : ± 0.010

SCALE = 1:2

ALL DIMENSIONS IN INCHES

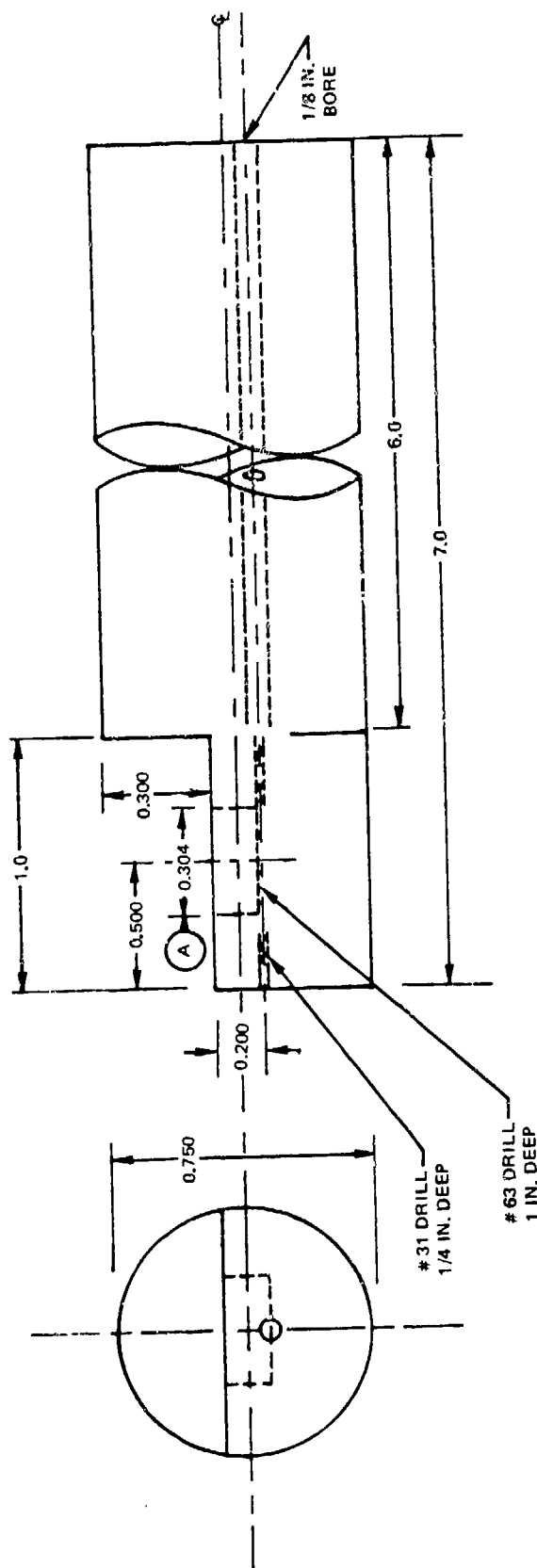
ELECTRODE HOLDER

MAT'L

TOLERANCE: ± 0.010

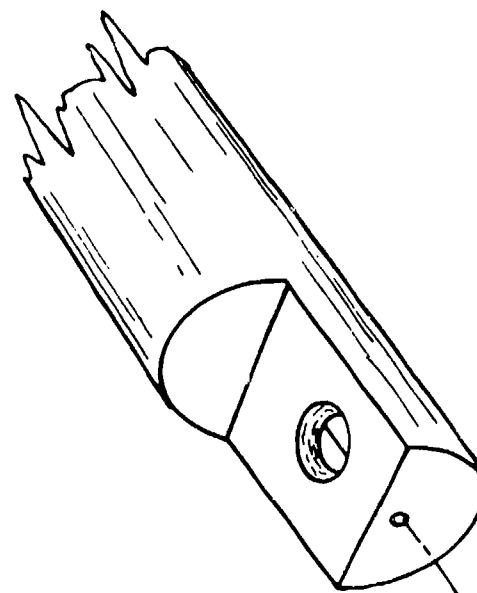
SCALE: 1:2

ALL DIMENSIONS IN INCHES

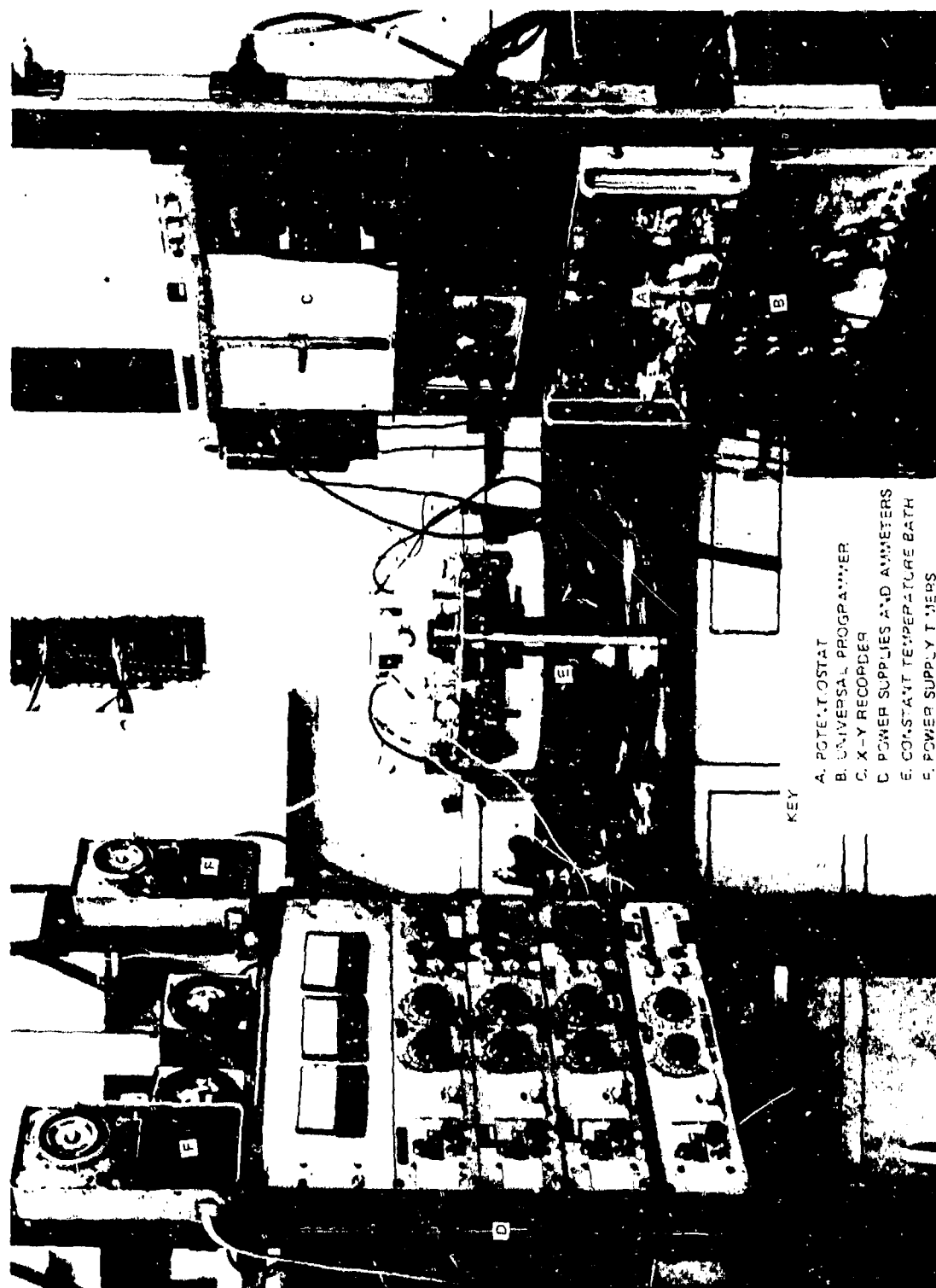


NOTE:

(A) MUST BE HELD TO
+ 0.000 AND -0.002



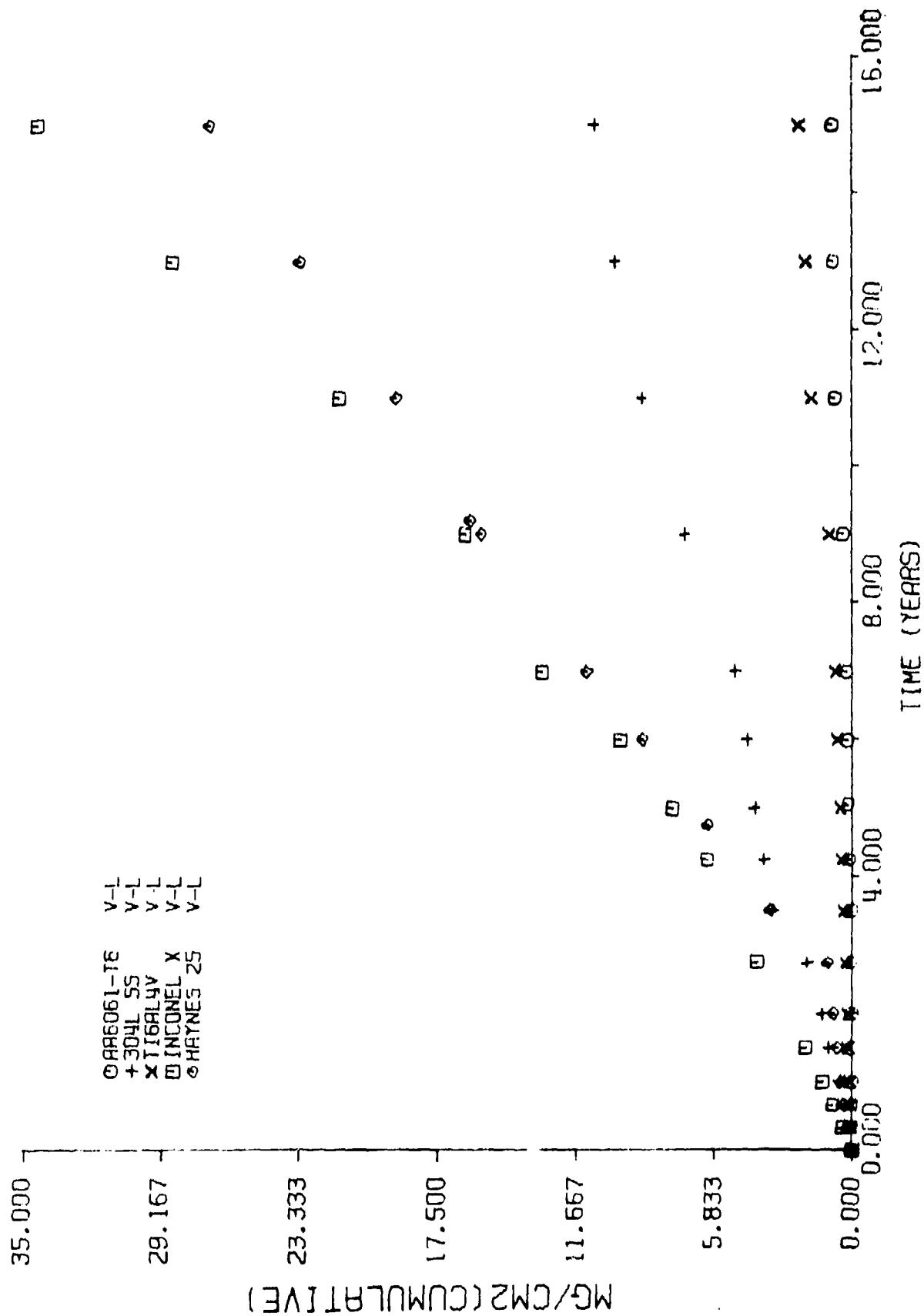
ELECTROCHEMICAL TESTING APPARATUS



APPENDIX B

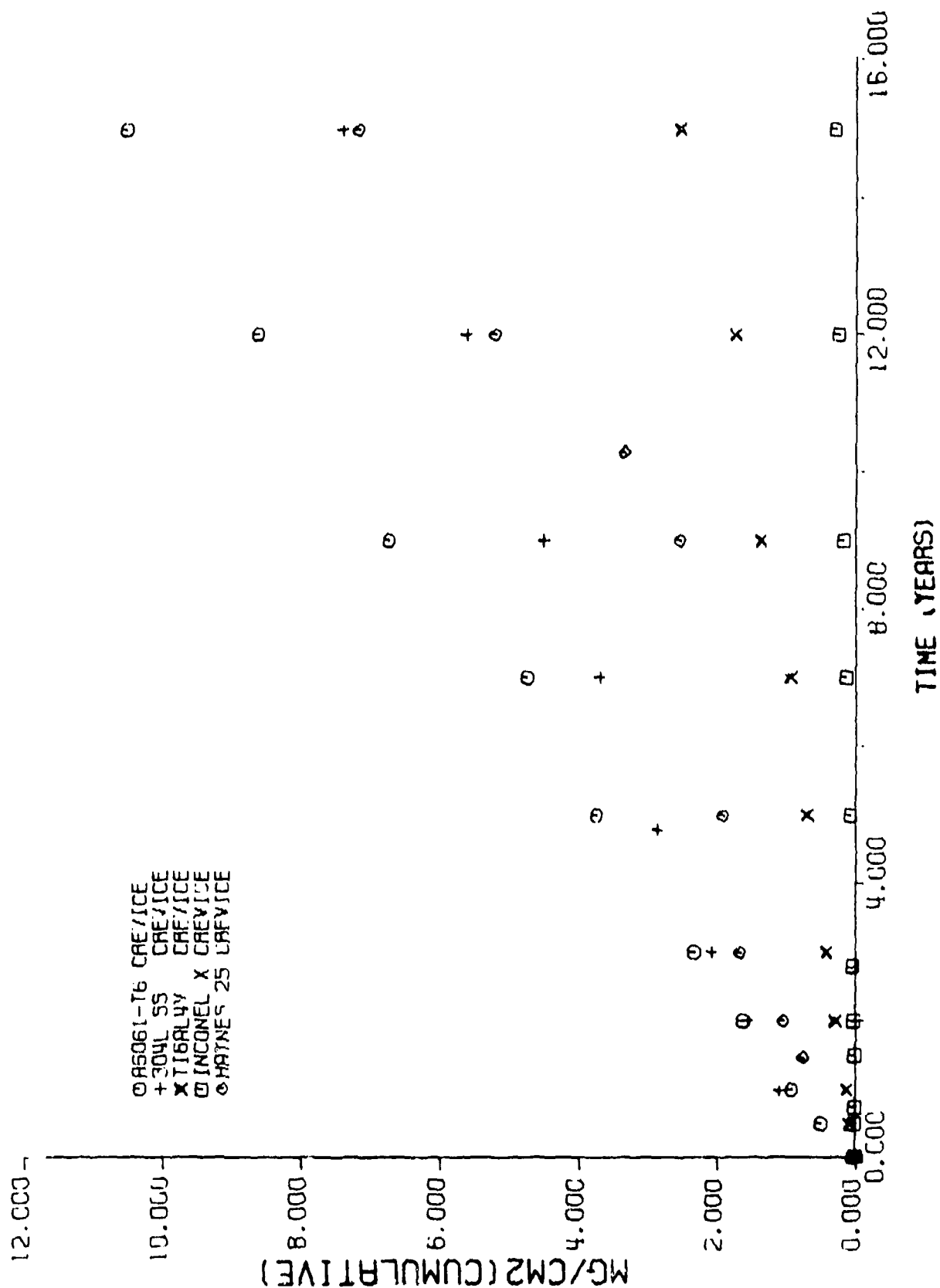
EXTENT OF HYDRAZINE DECOMPOSITION

EFFECT OF VAPOR-LIQUID INTERFACE ON HYDRAZINE DECOMPOSITION

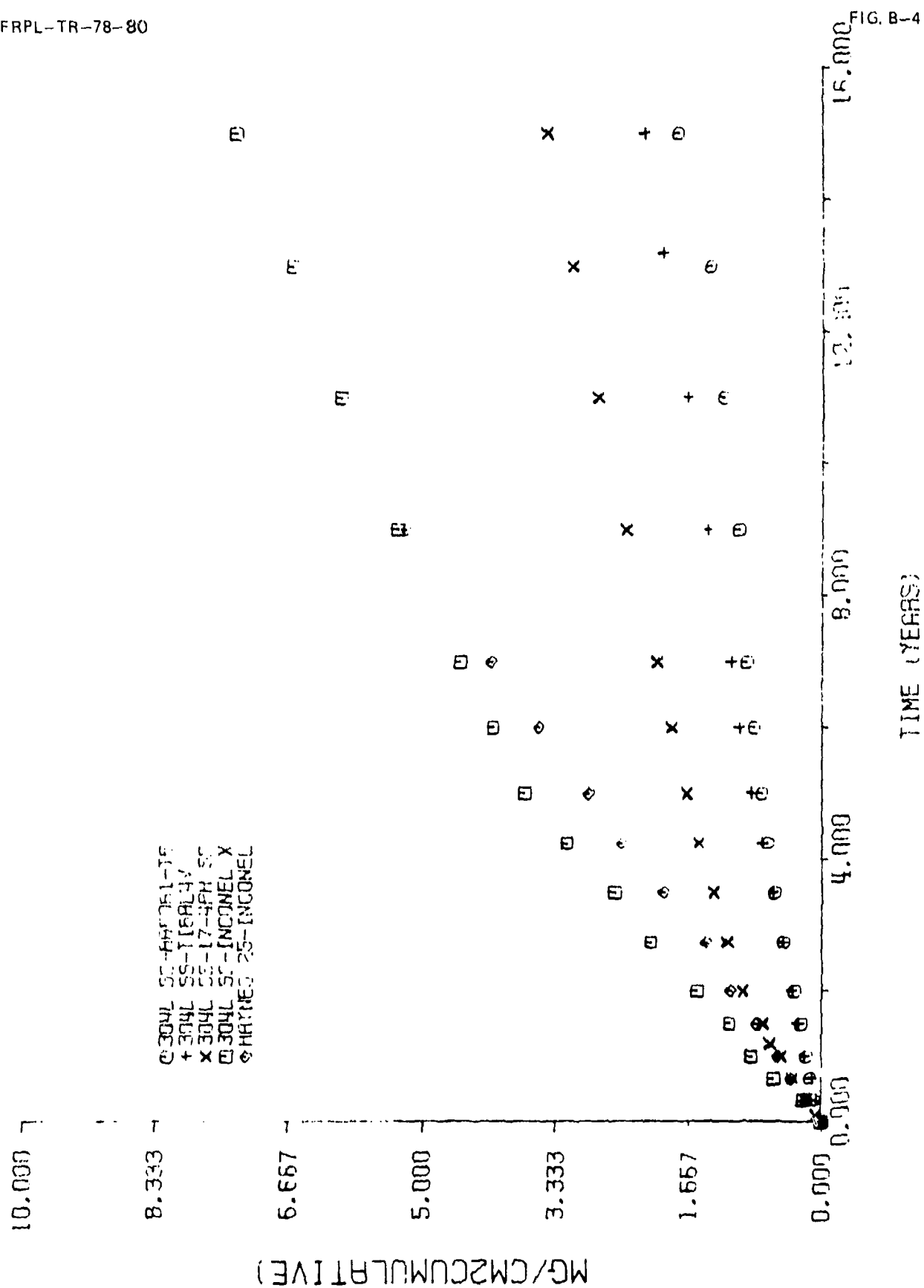


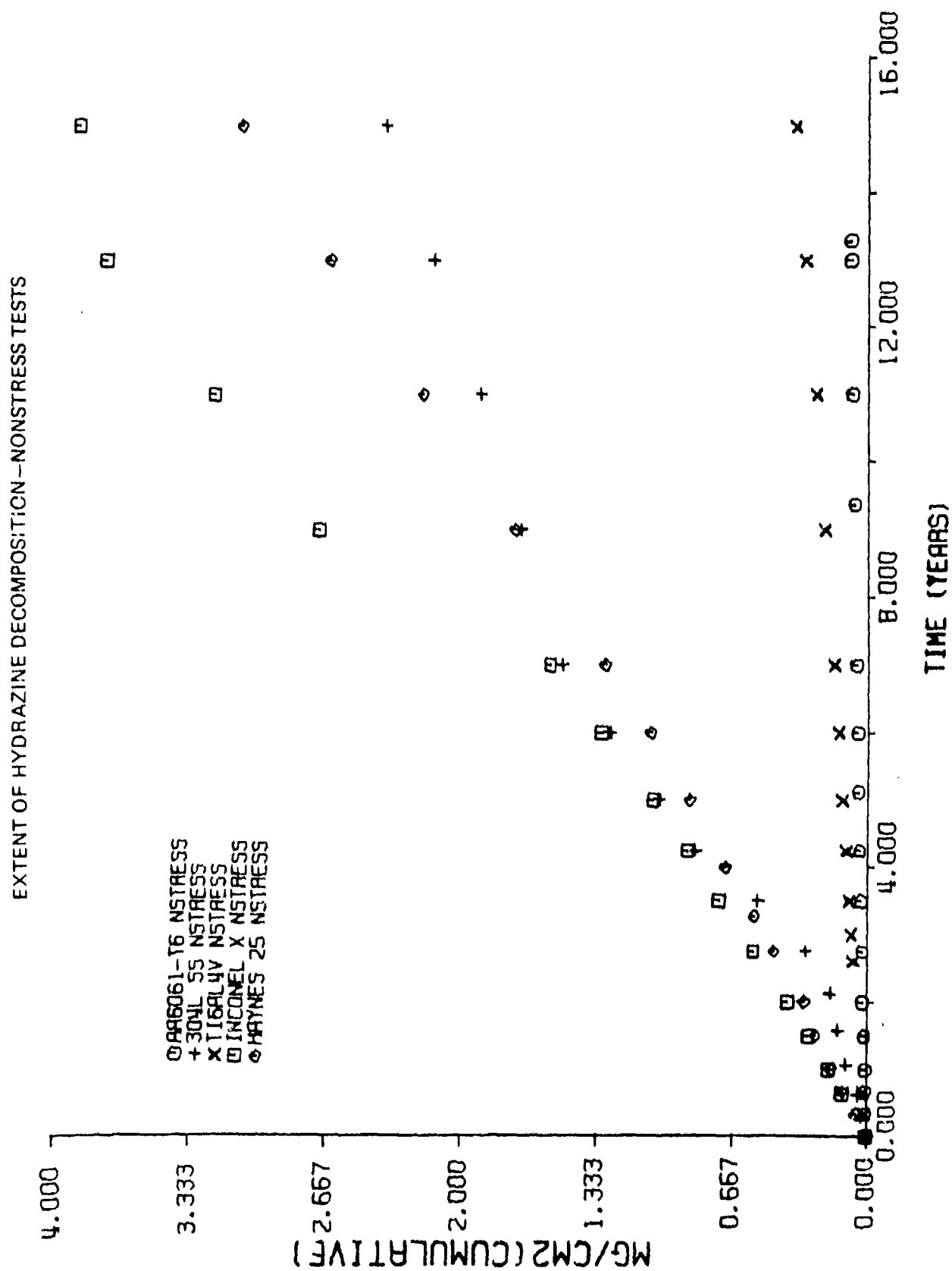


EFFECT OF CREVICES ON HYDRAZINE DECOMPOSITION



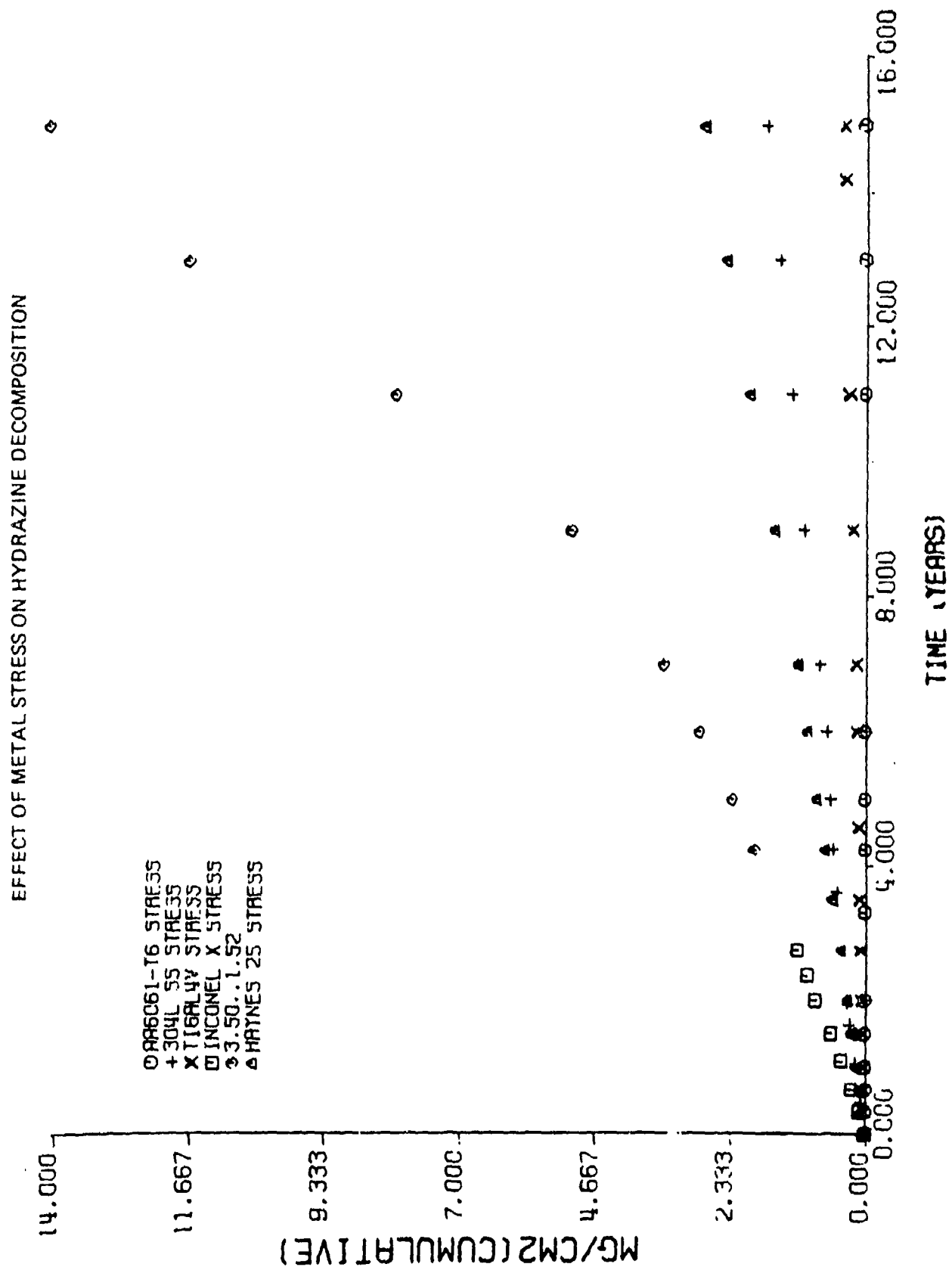
EFFECT OF BIMETALLIC JUNCTION ON HYDRAZINE DECOMPOSITION

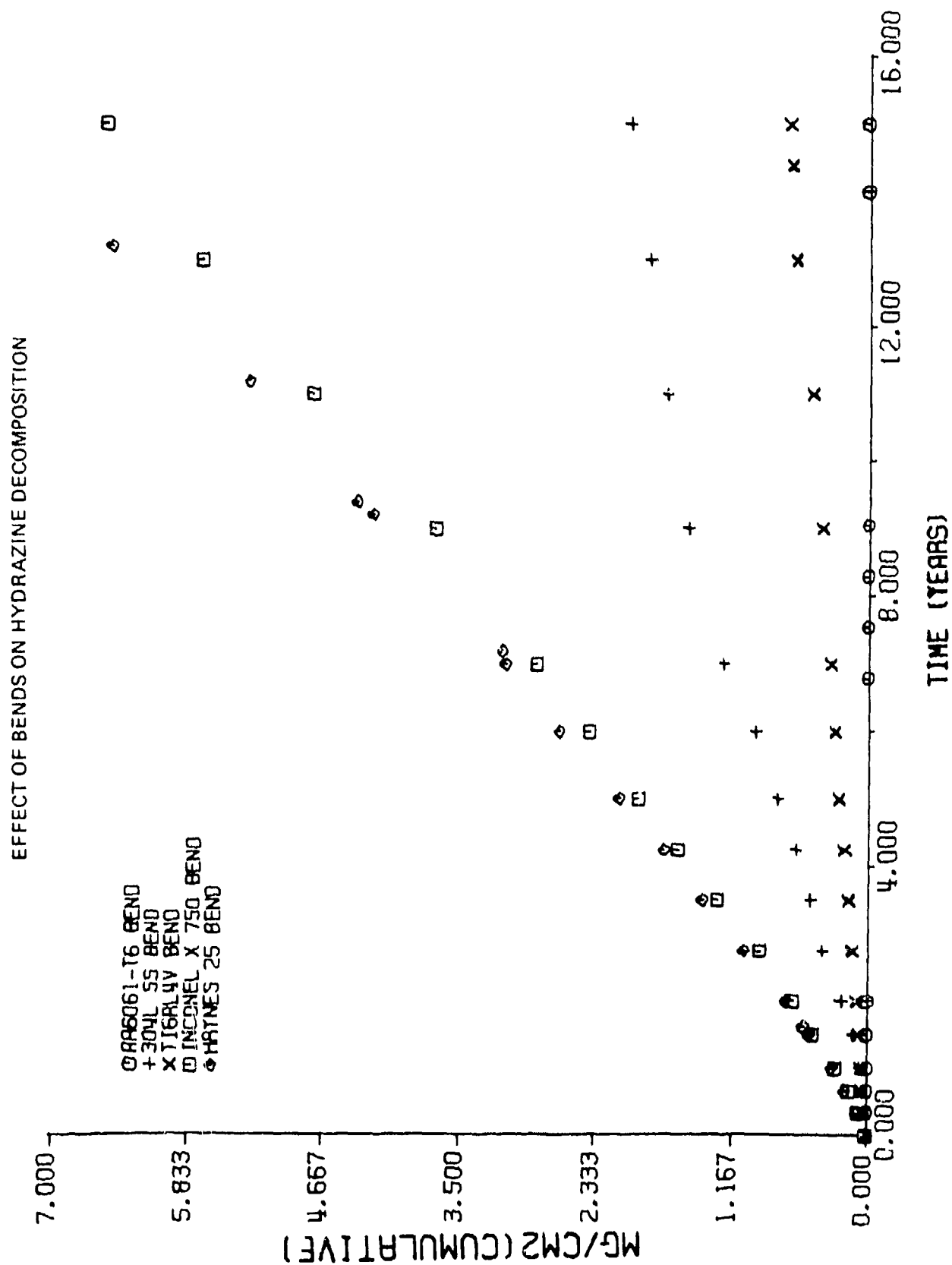


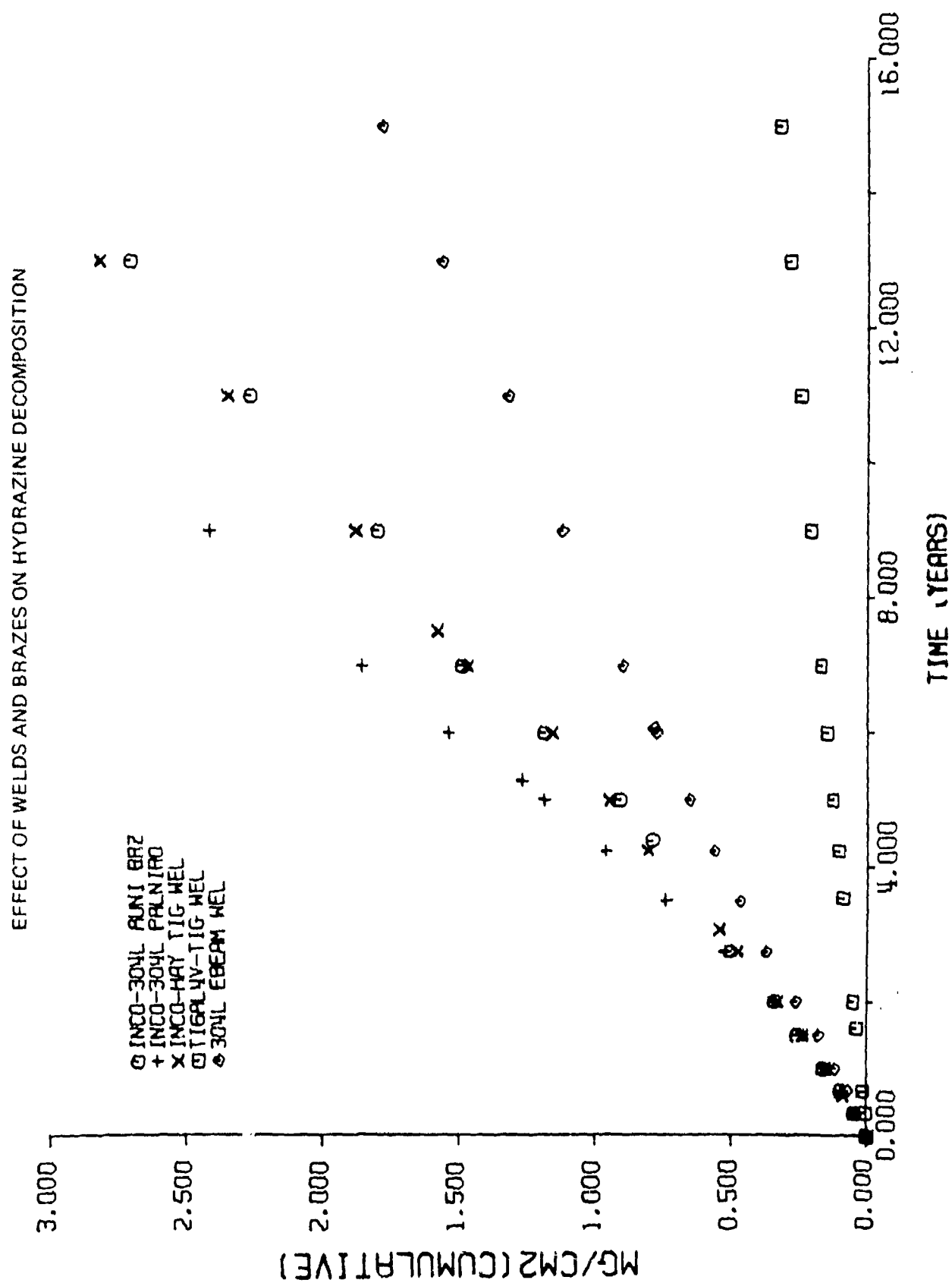


096061-16 NSTRESS
+304L 55 NSTRESS
X118AL4V NSTRESS
0 INCONEL X NSTRESS
0 HAYNES 25 NSTRESS

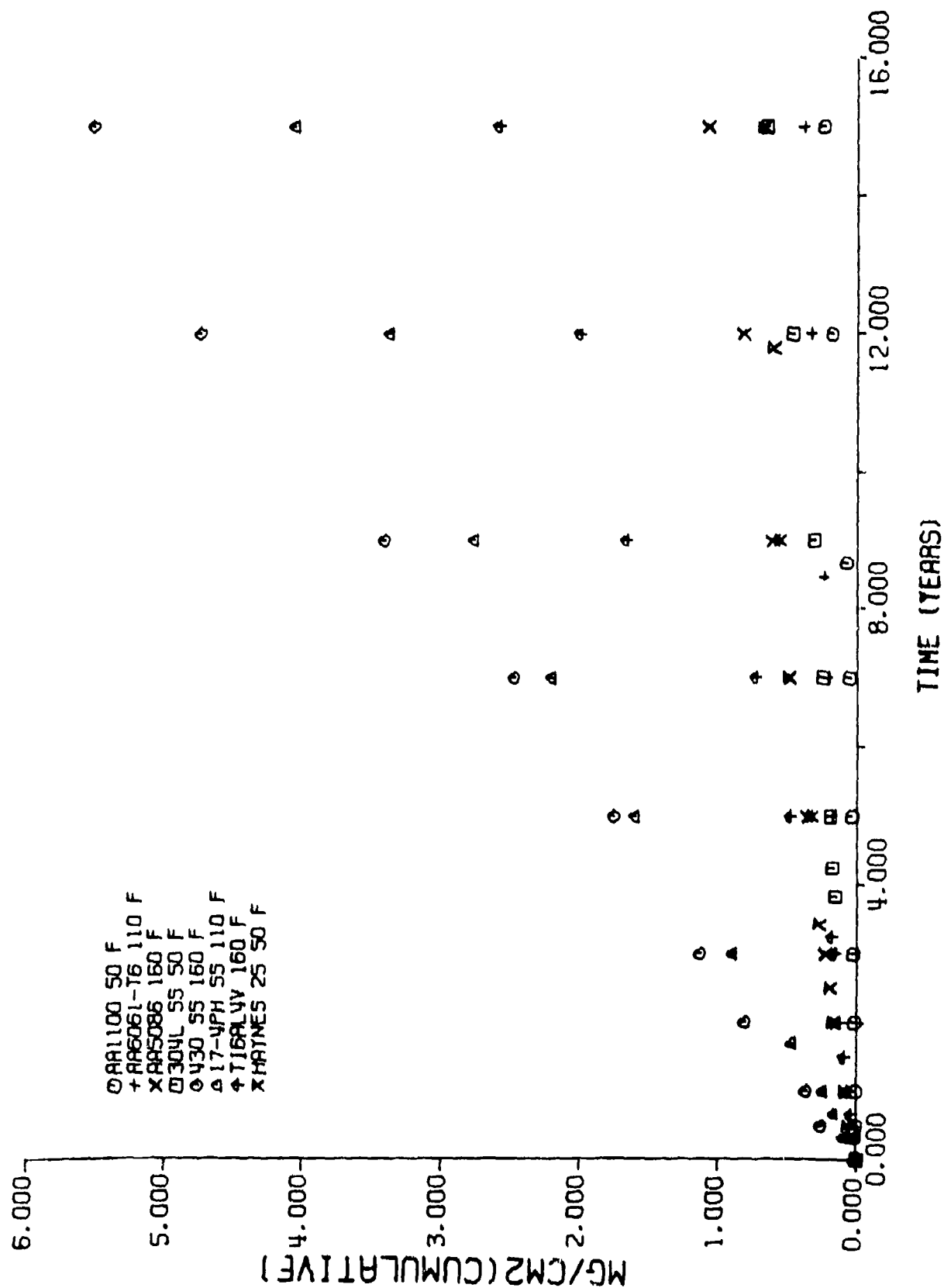
H-6



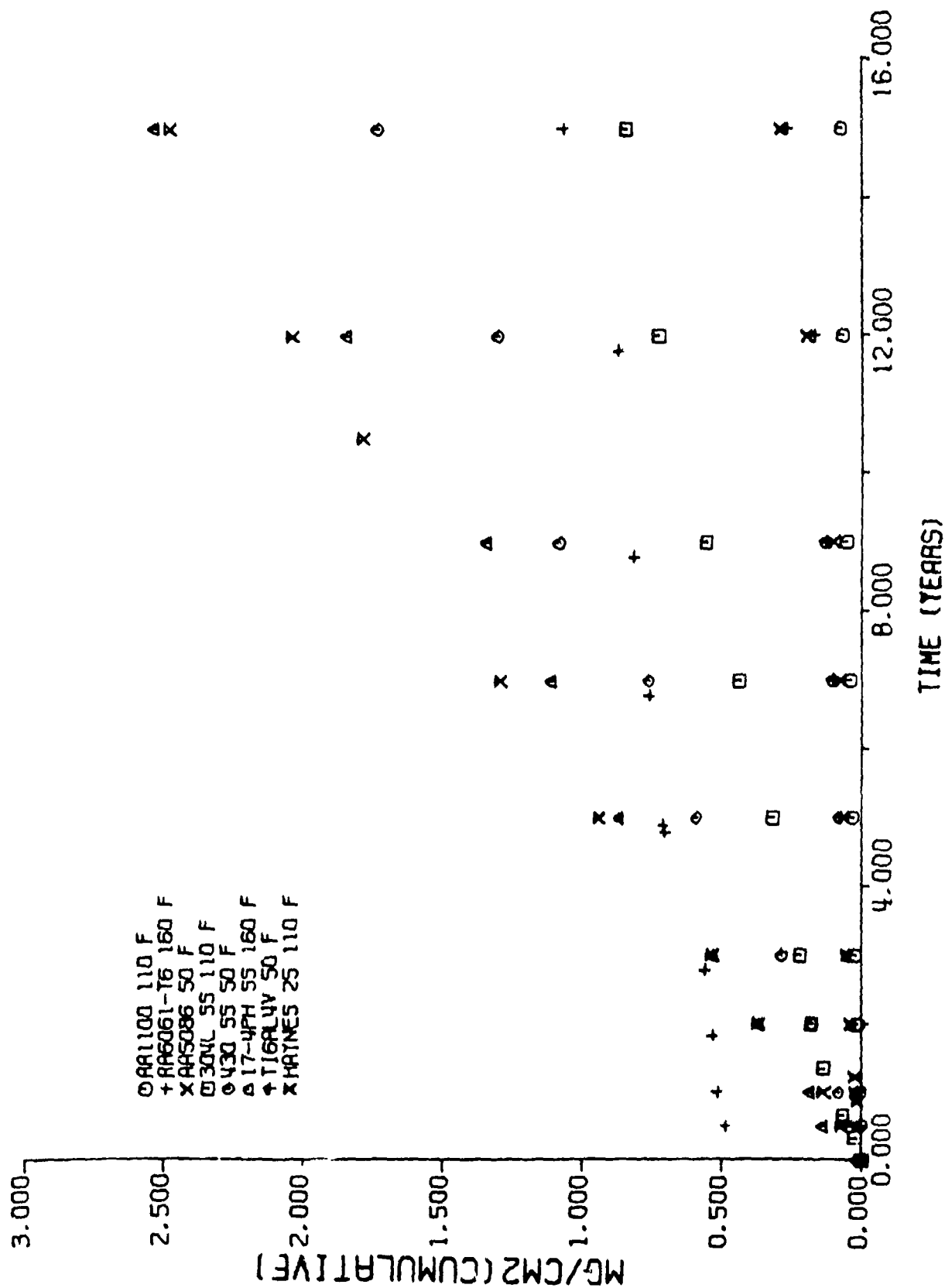




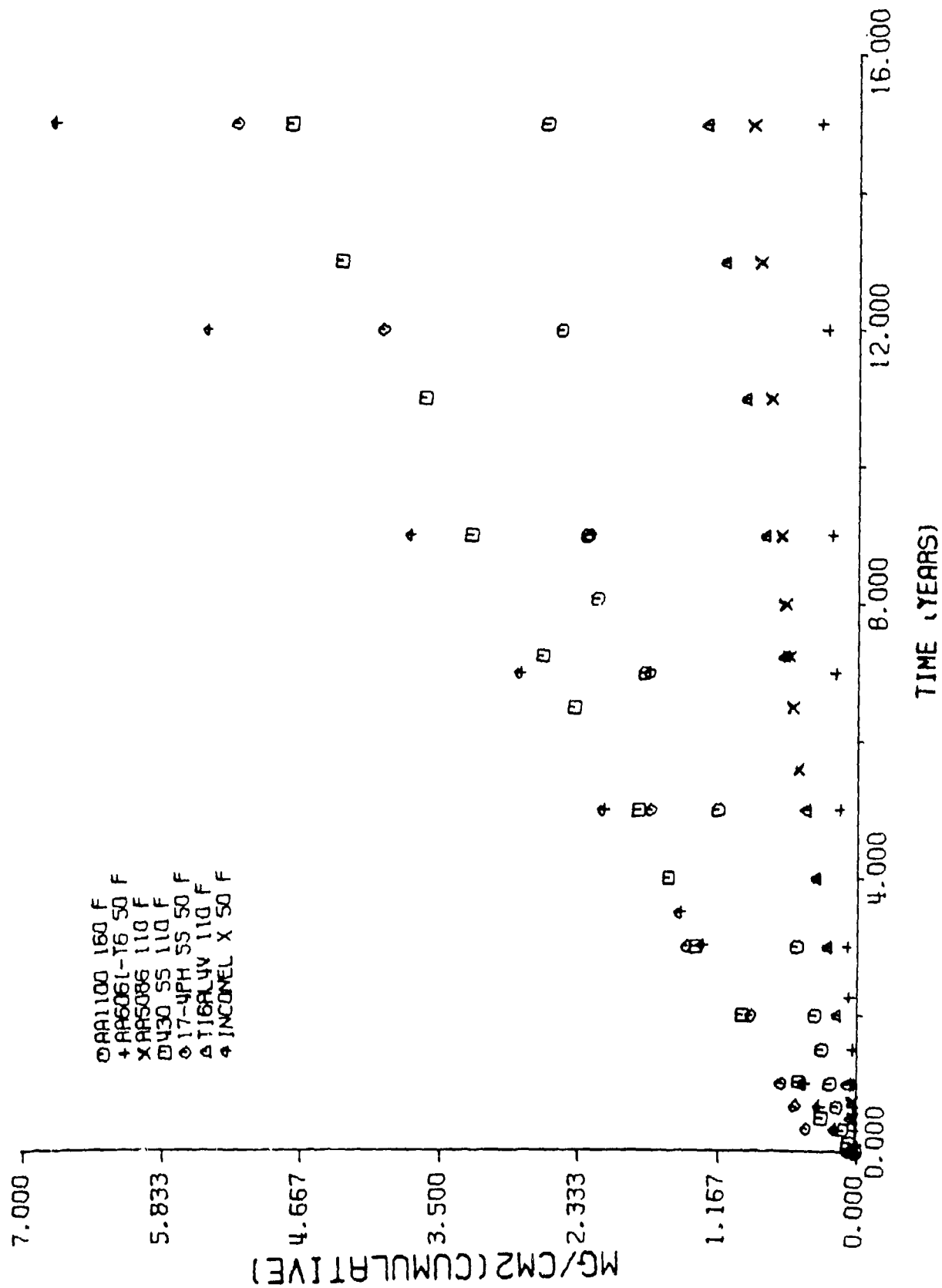
EFFECT OF METAL PRETREATMENT (A) ON HYDRAZINE DECOMPOSITION

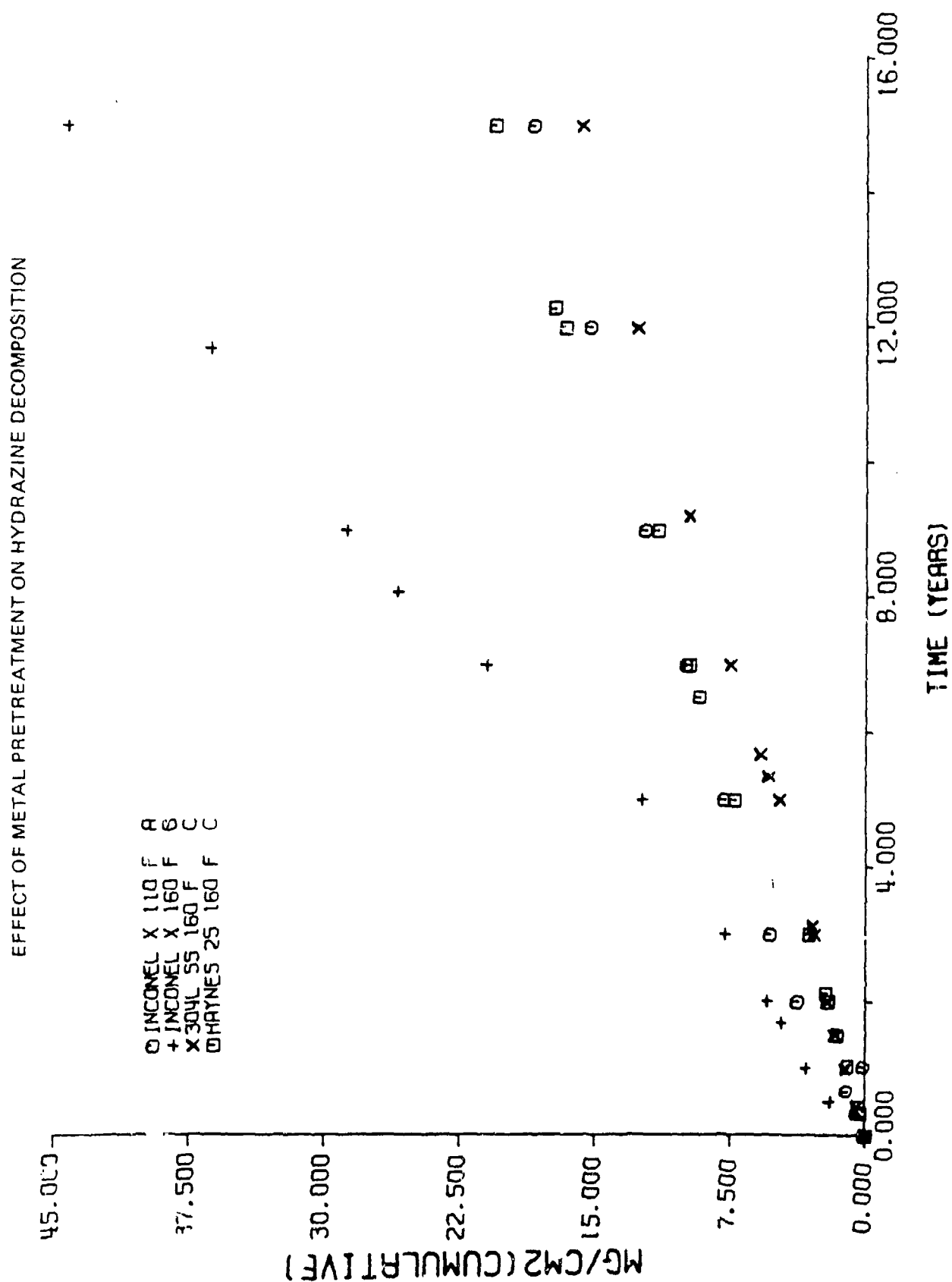


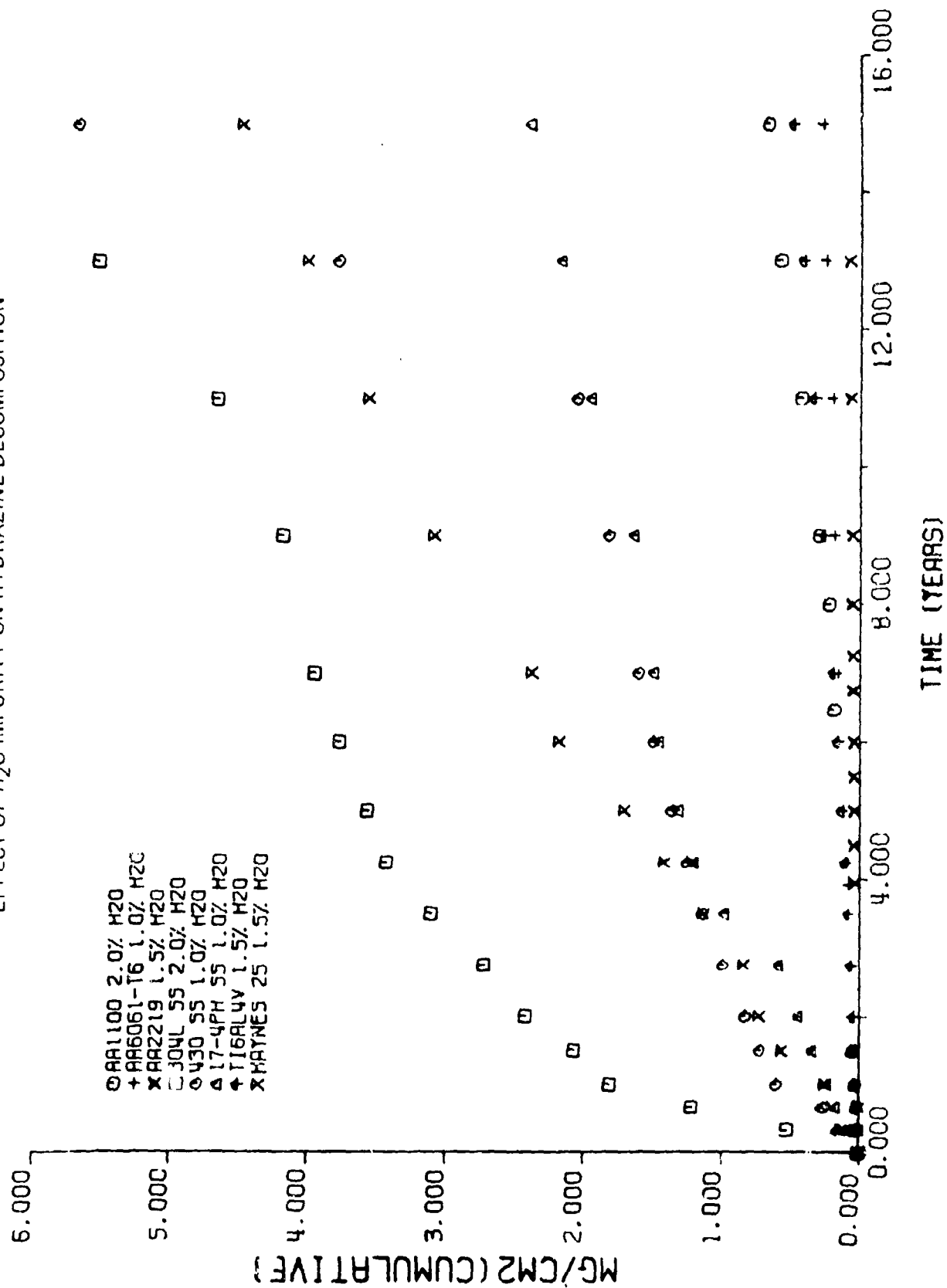
EFFECT OF METAL PRETREATMENT (B) ON HYDRAZINE DECOMPOSITION

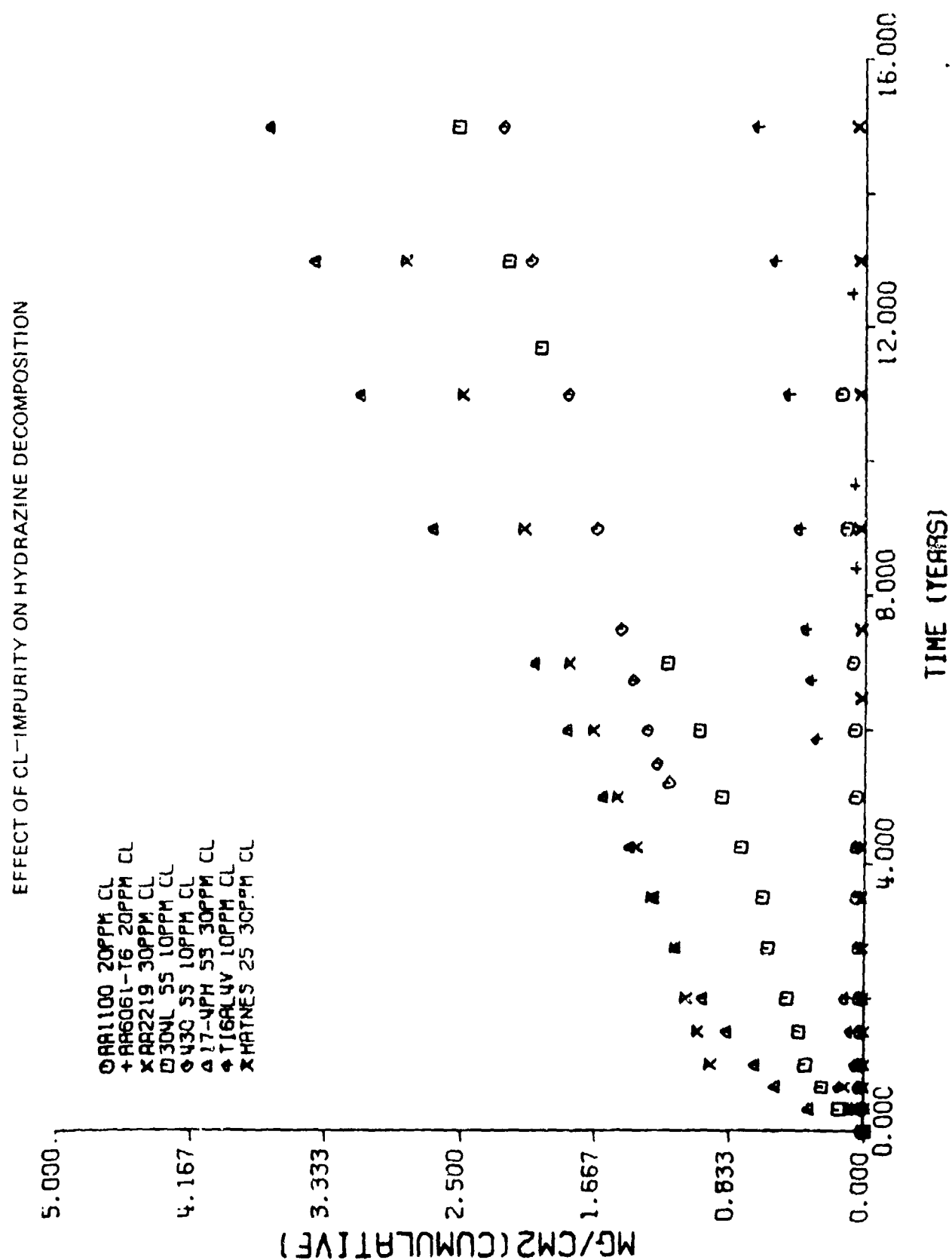


EFFECT OF METAL PRETREATMENT (C) ON HYDRAZINE DECOMPOSITION



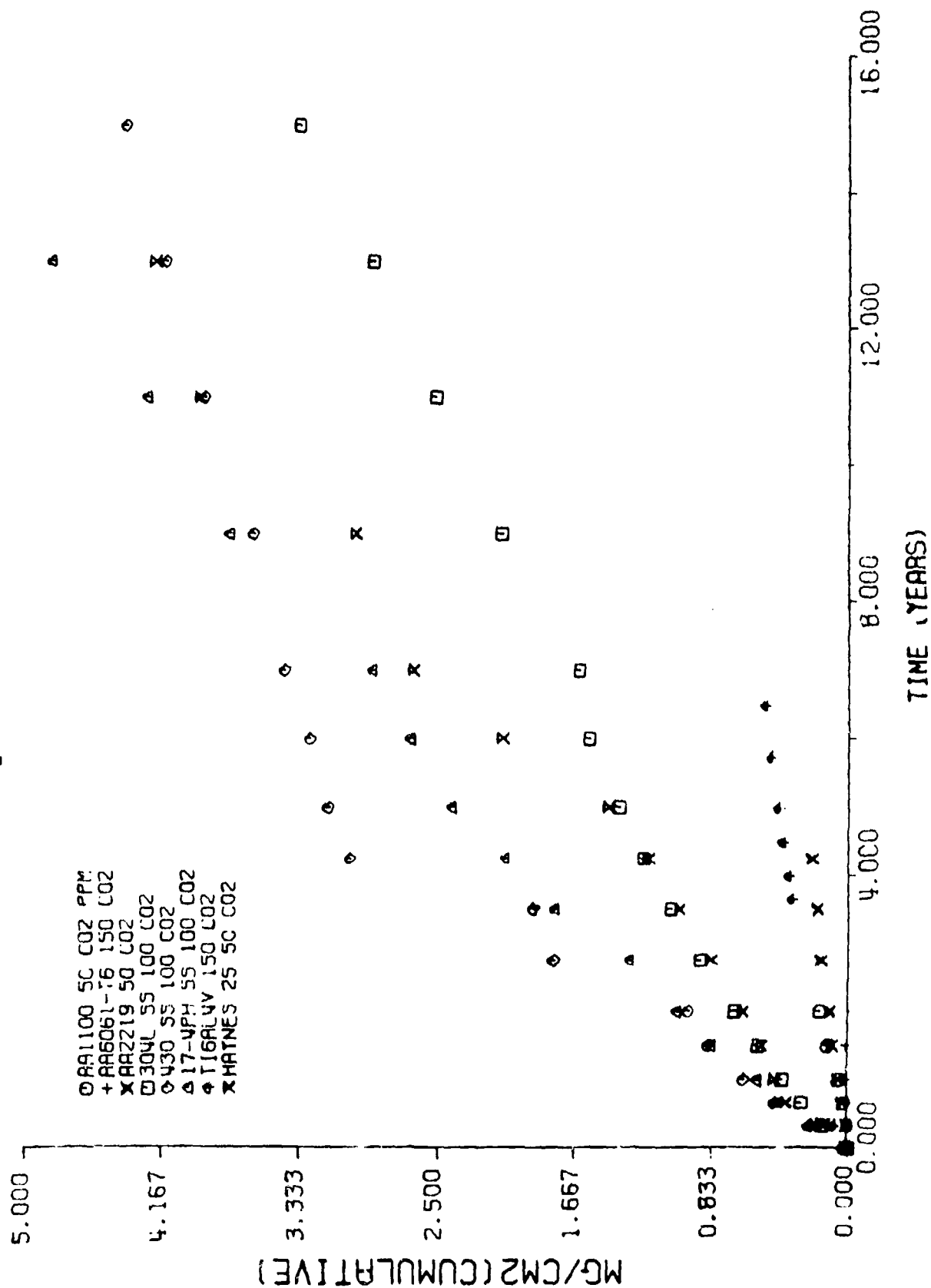


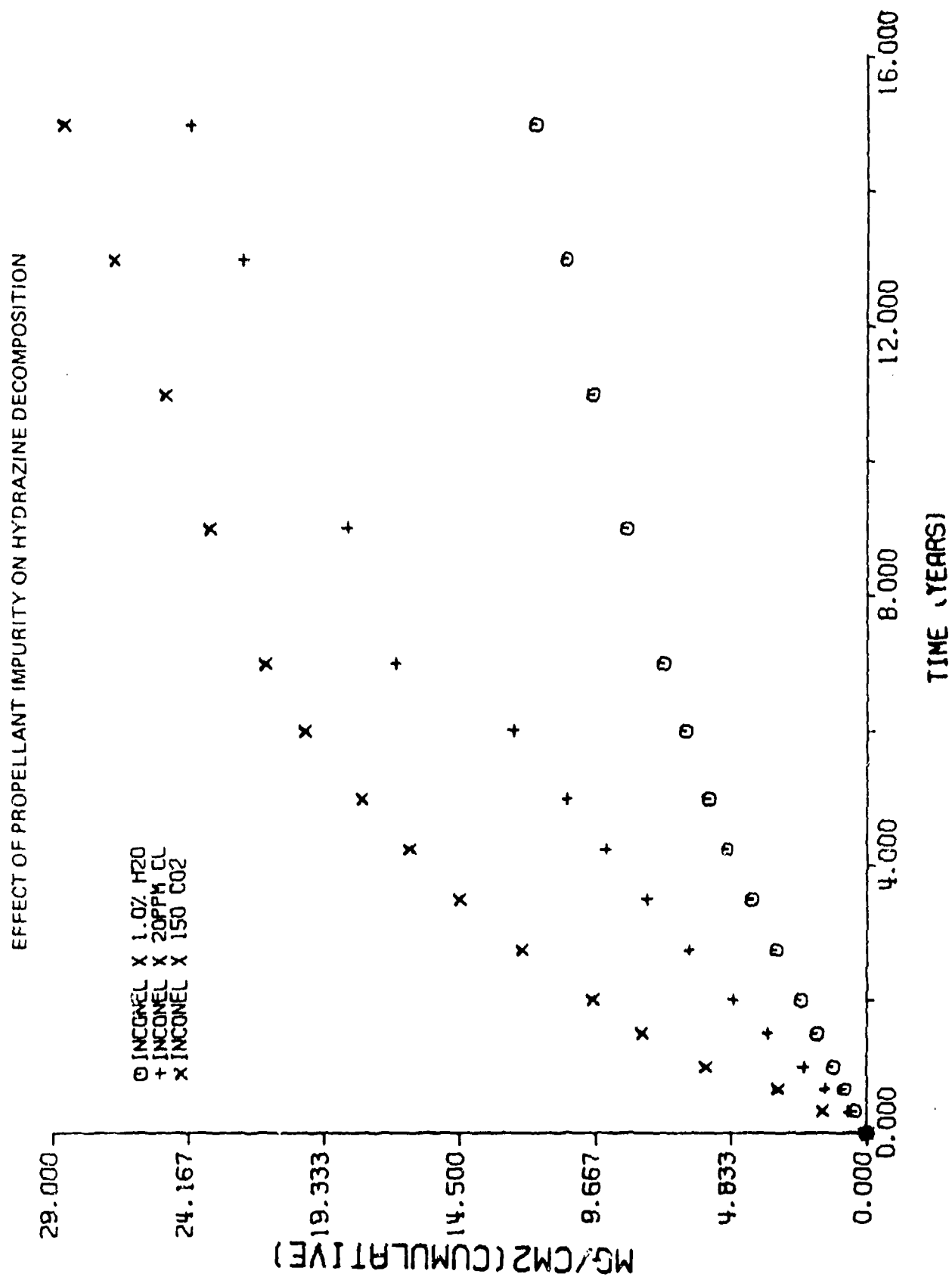
EFFECT OF H₂O IMPURITY ON HYDRAZINE DECOMPOSITION



@A1100 20PPM CL
 + AR6061-T6 20PPM CL
 X AR2219 30PPM CL
 @304L 55 10PPM CL
 @430 55 10PPM CL
 @ 17-4PH 55 30PPM CL
 @ T16AL4V 10PPM CL
 X HAINES 25 30PPM CL

B-15

EFFECT OF CO₂ IMPURITY ON HYDRAZINE DECOMPOSITION

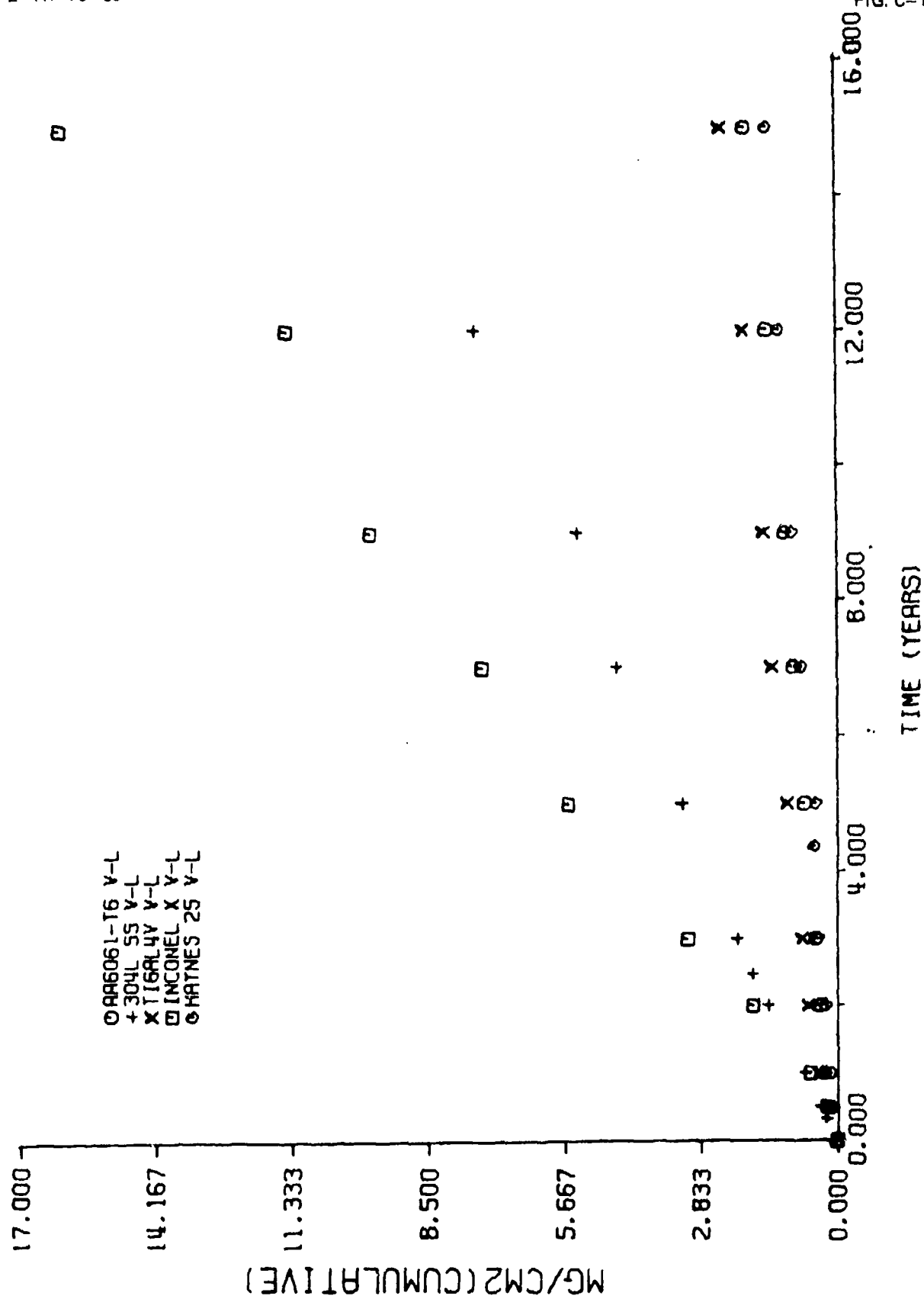


AFRPL-TR-78-80

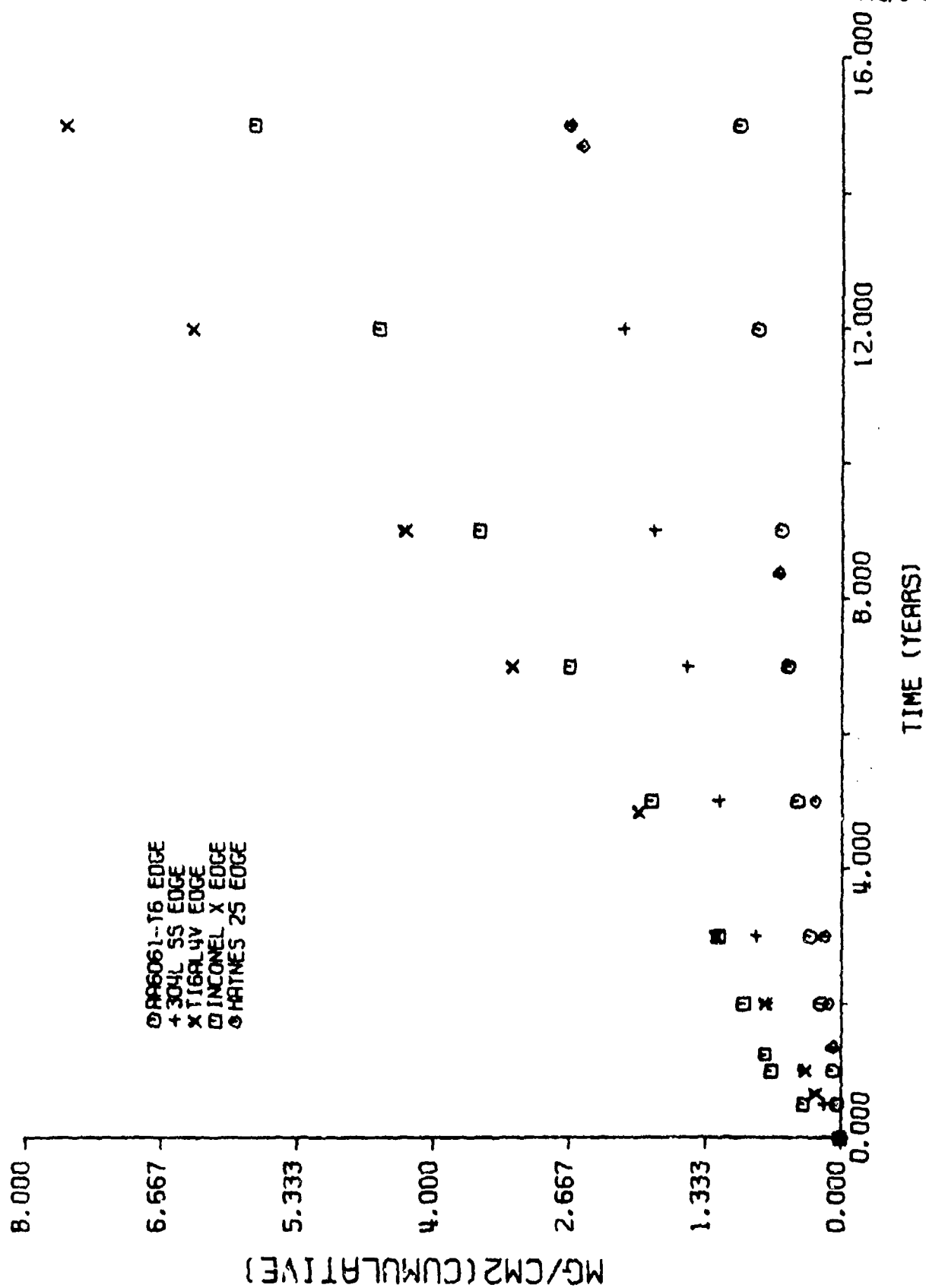
APPENDIX C

EXTENT OF MONOMETHYLHYDRAZINE DECOMPOSITION

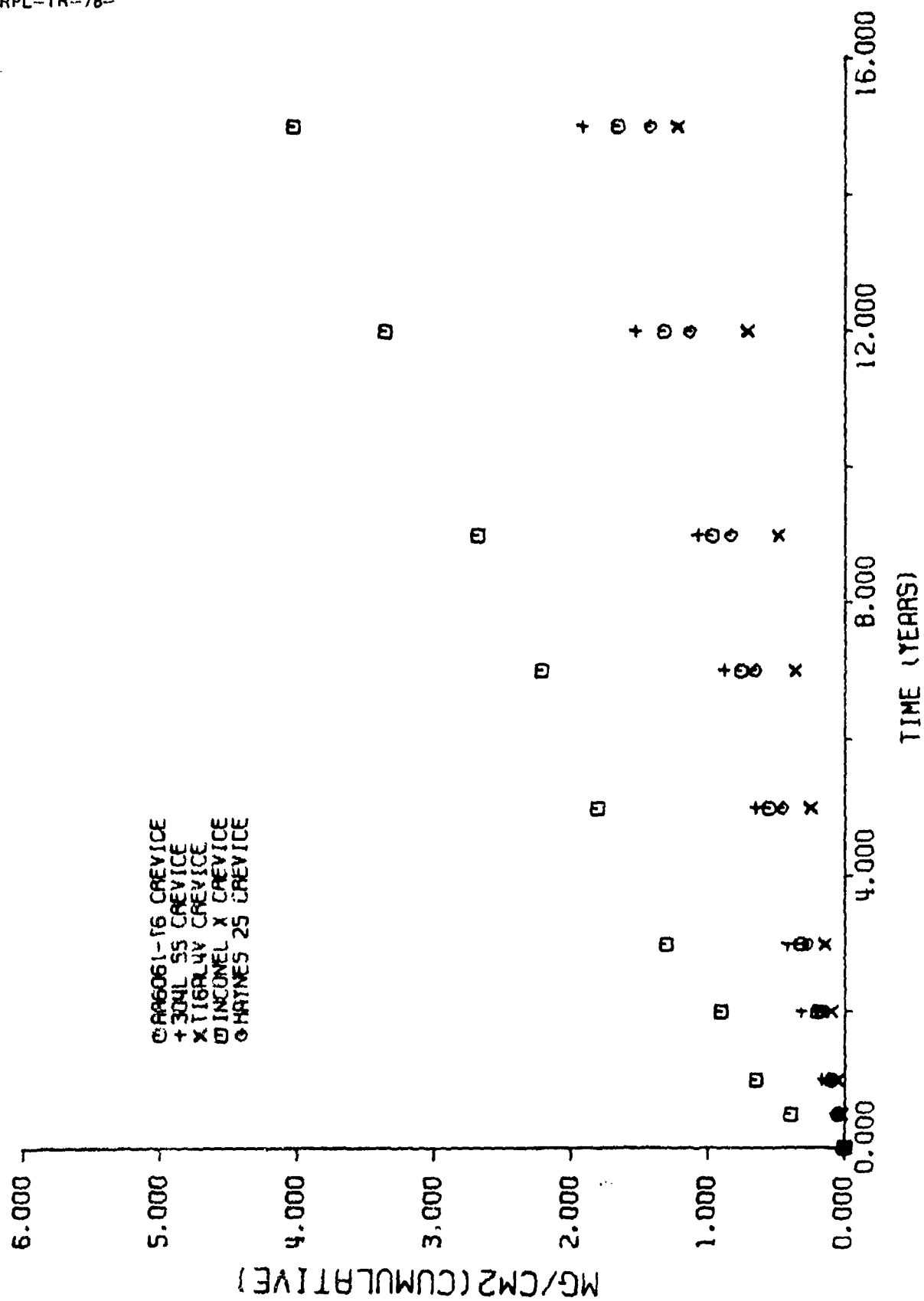
EXTENT OF MONOMETHYLHYDRAZINE DECOMPOSITION (EFFECT OF VAPOR-LIQUID INTERFACE)



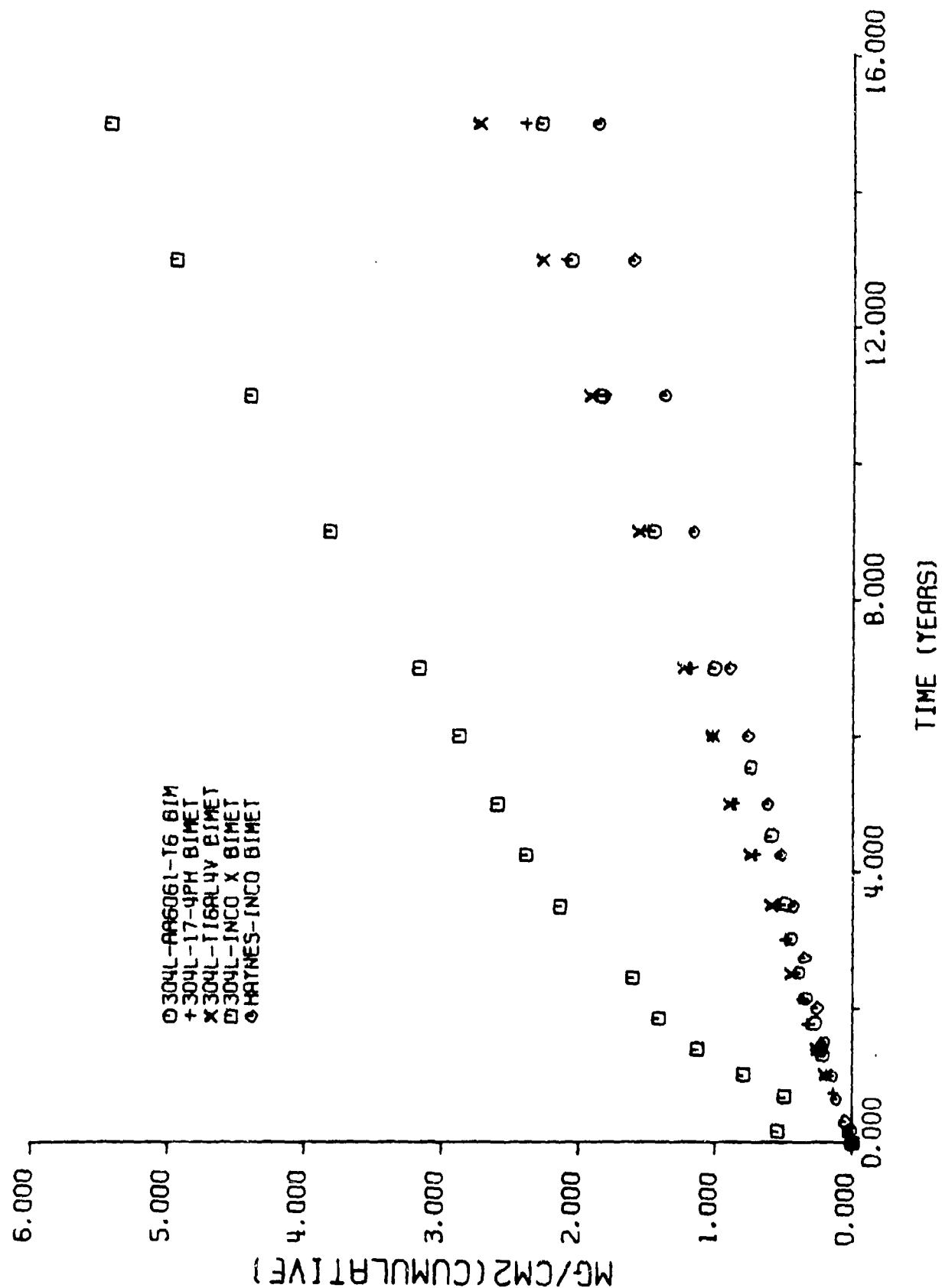
EXTENT OF MONOMETHYLHYDRAZINE DECOMPOSITION (EDGE EFFECT)



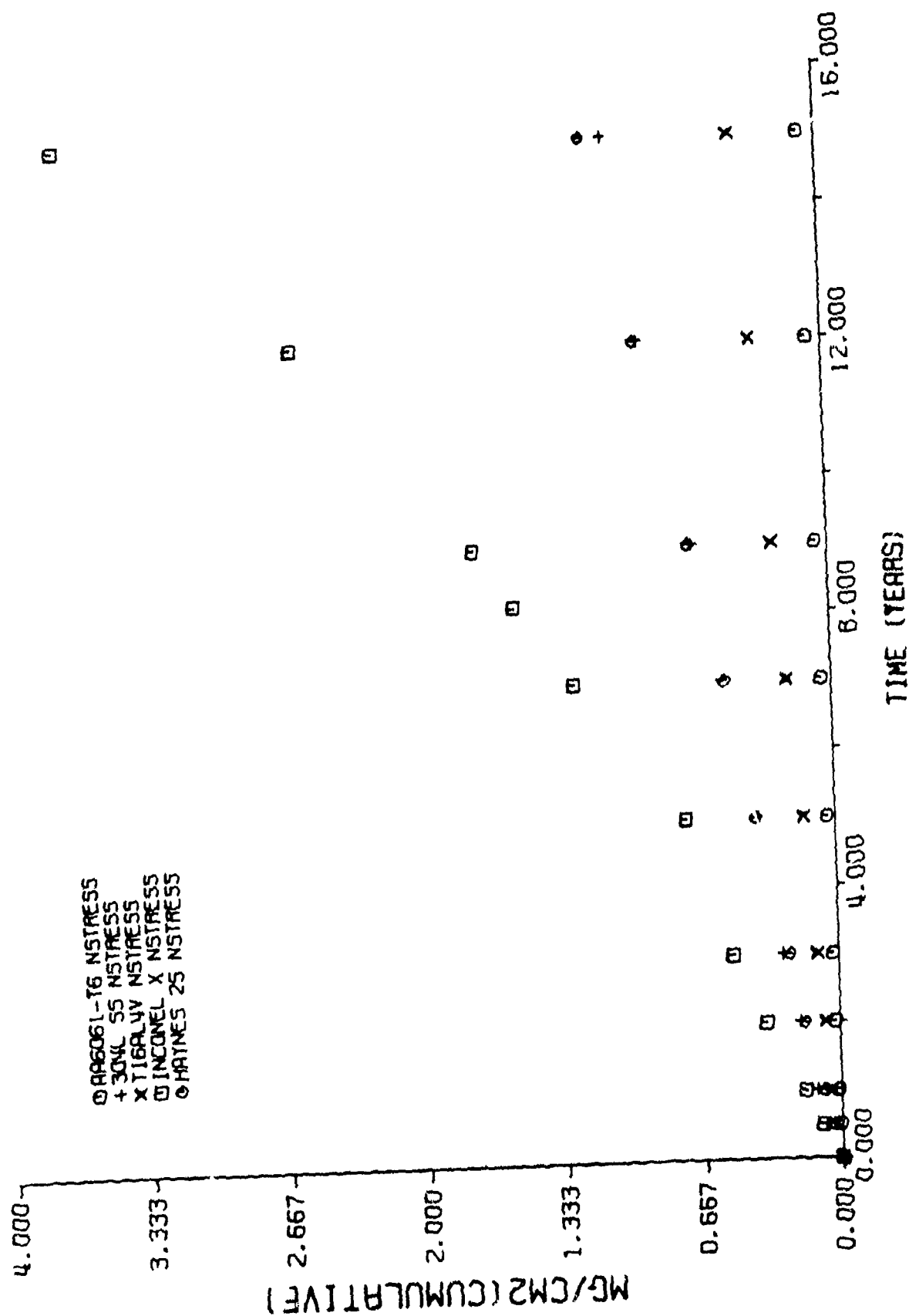
EXTENT OF MONOMETHYLHYDRAZINE DECOMPOSITION (CREVICE EFFECT)

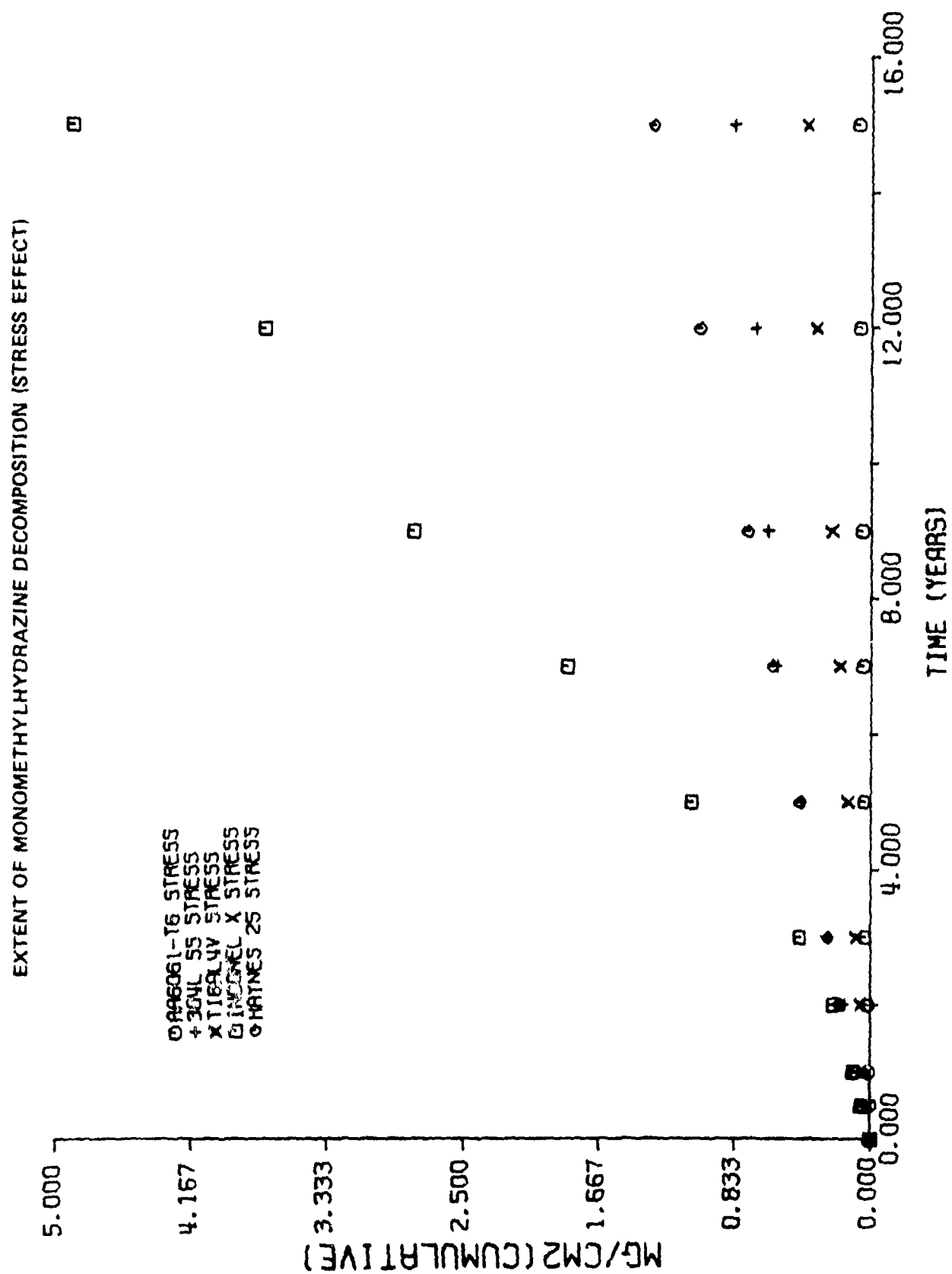


EXTENT OF MONOMETHYLHYDRAZINE DECOMPOSITION (EFFECT OF BIMETALLIC JUNCTION)

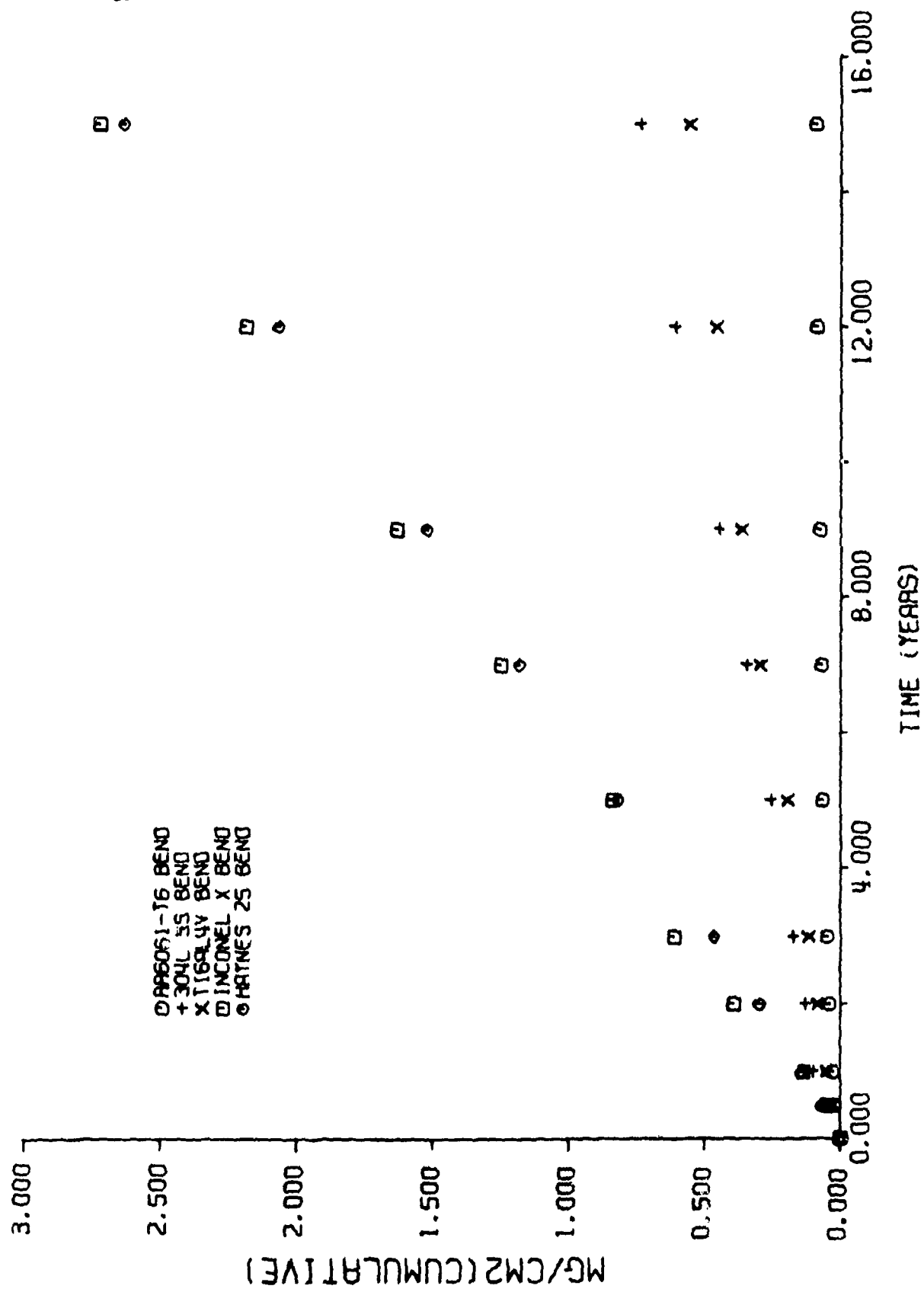


EXTENT OF MONOMETHYLHYDRAZINE DECOMPOSITION (NONSTRESS TESTS)

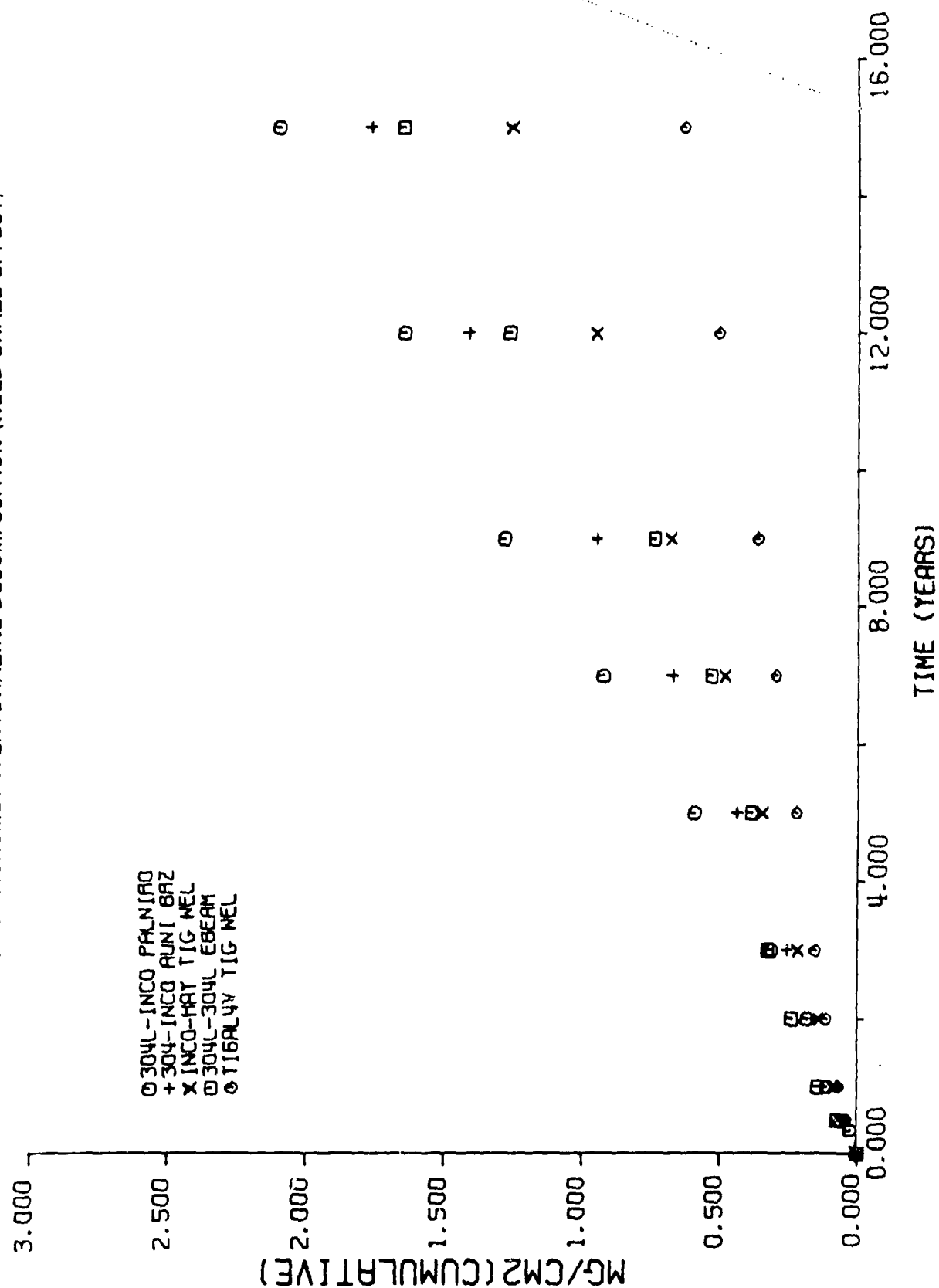




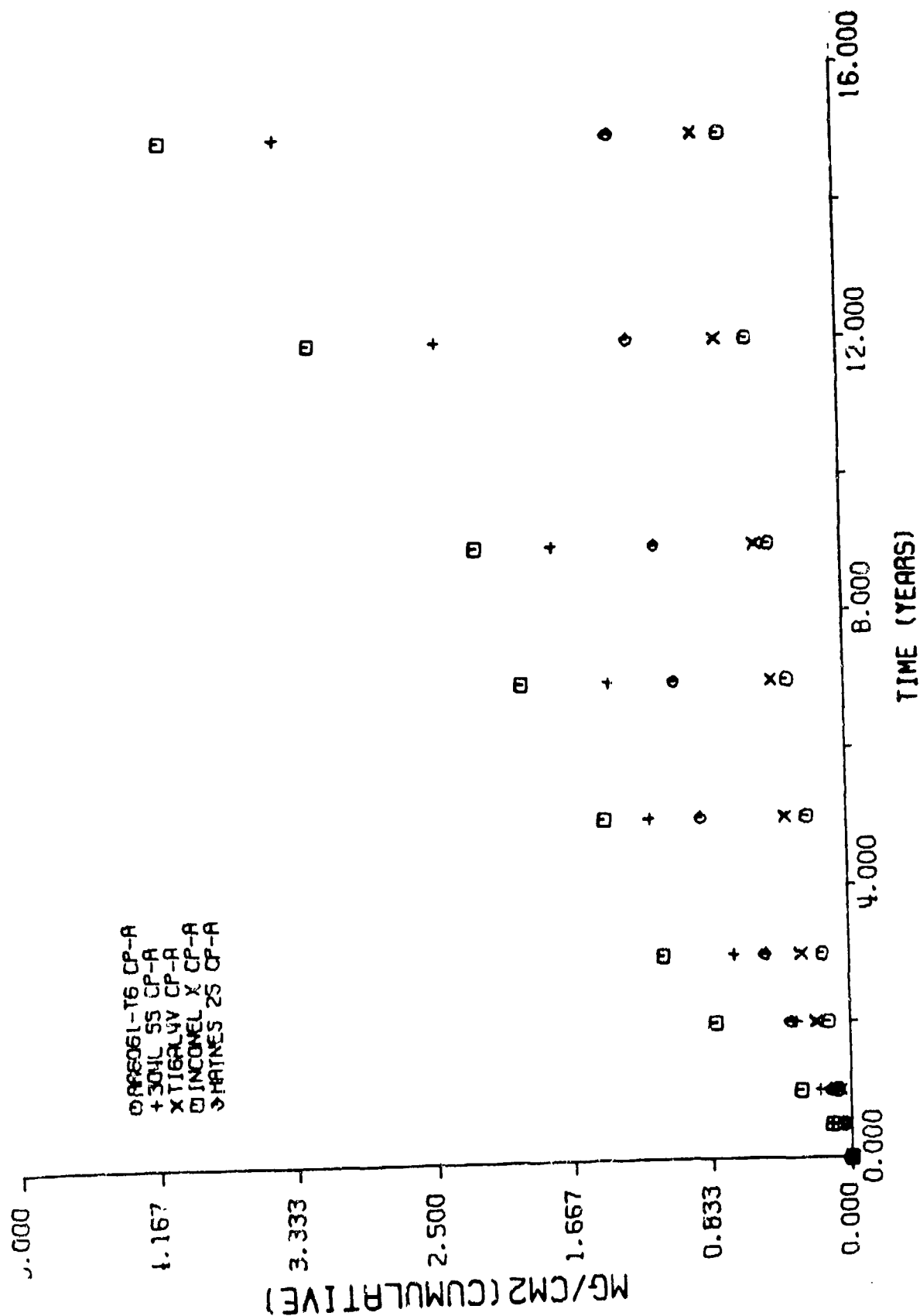
EXTENT OF MONOMETHYLHYDRAZINE DECOMPOSITION (BEND EFFECT)



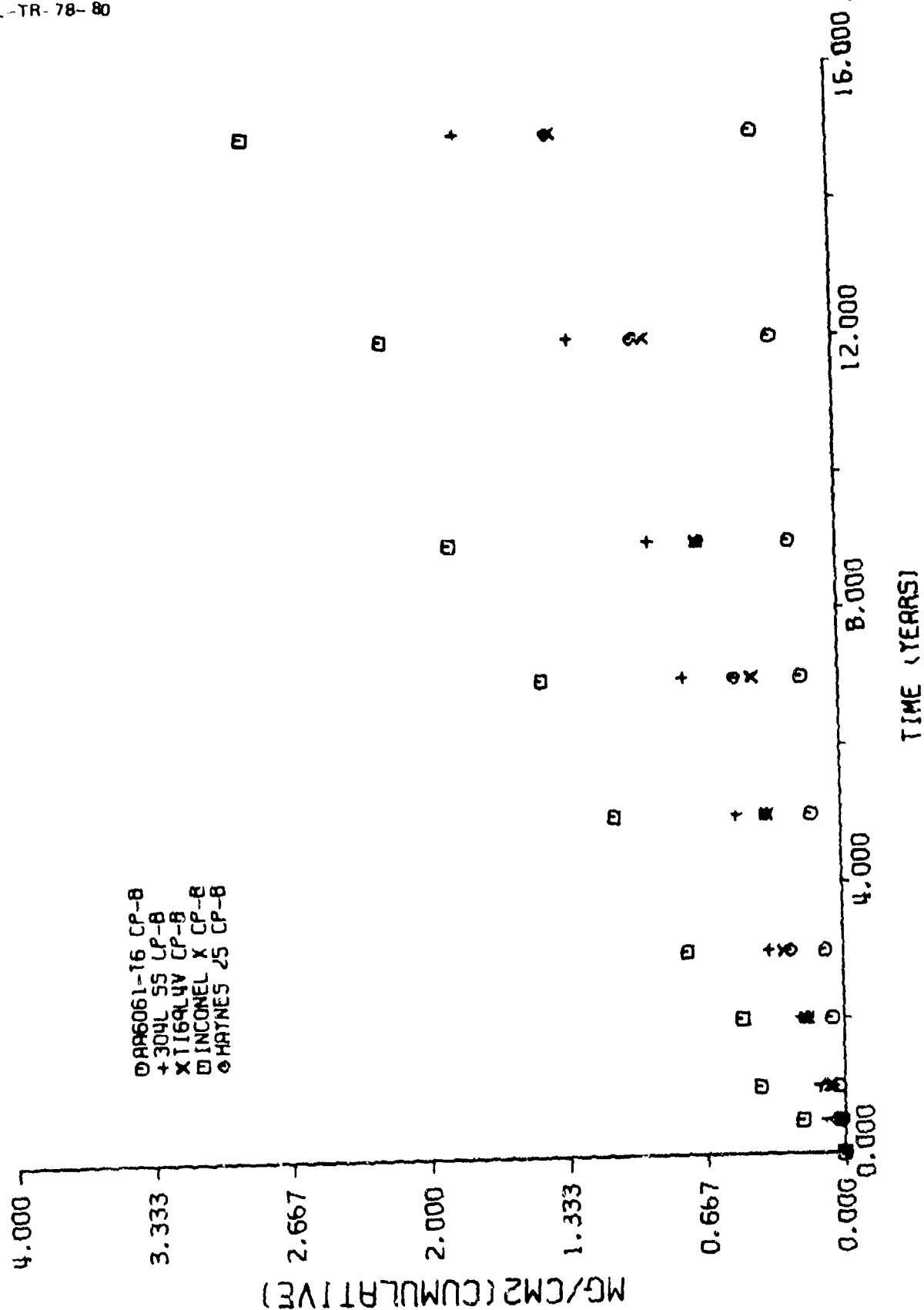
EXTENT OF MONOMETHYLHYDRAZINE DECOMPOSITION (WELD BRAZE EFFECT)



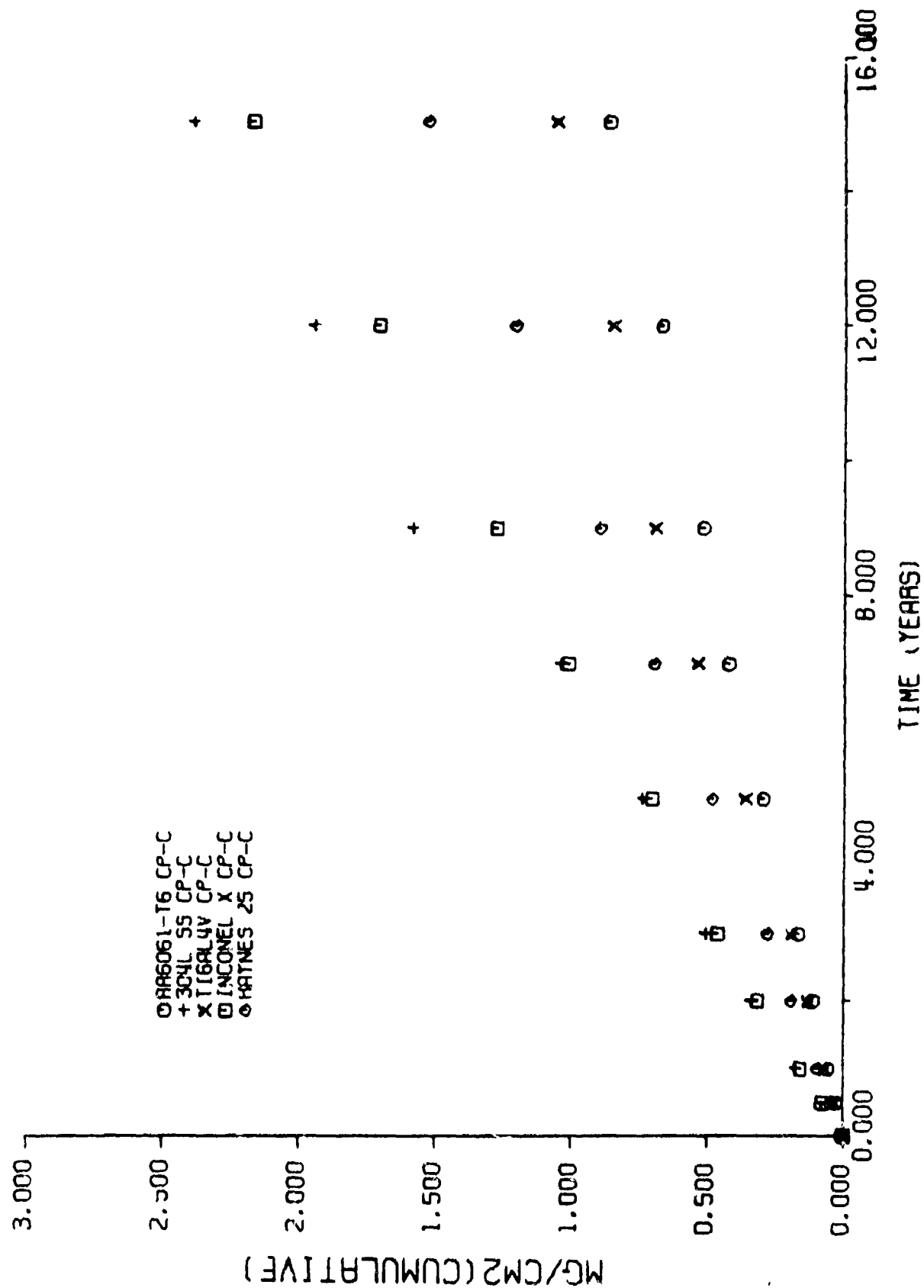
EXTENT OF MONOMETHYLHYDRAZINE DECOMPOSITION (EFFECT OF METAL PRETREATMENT A)

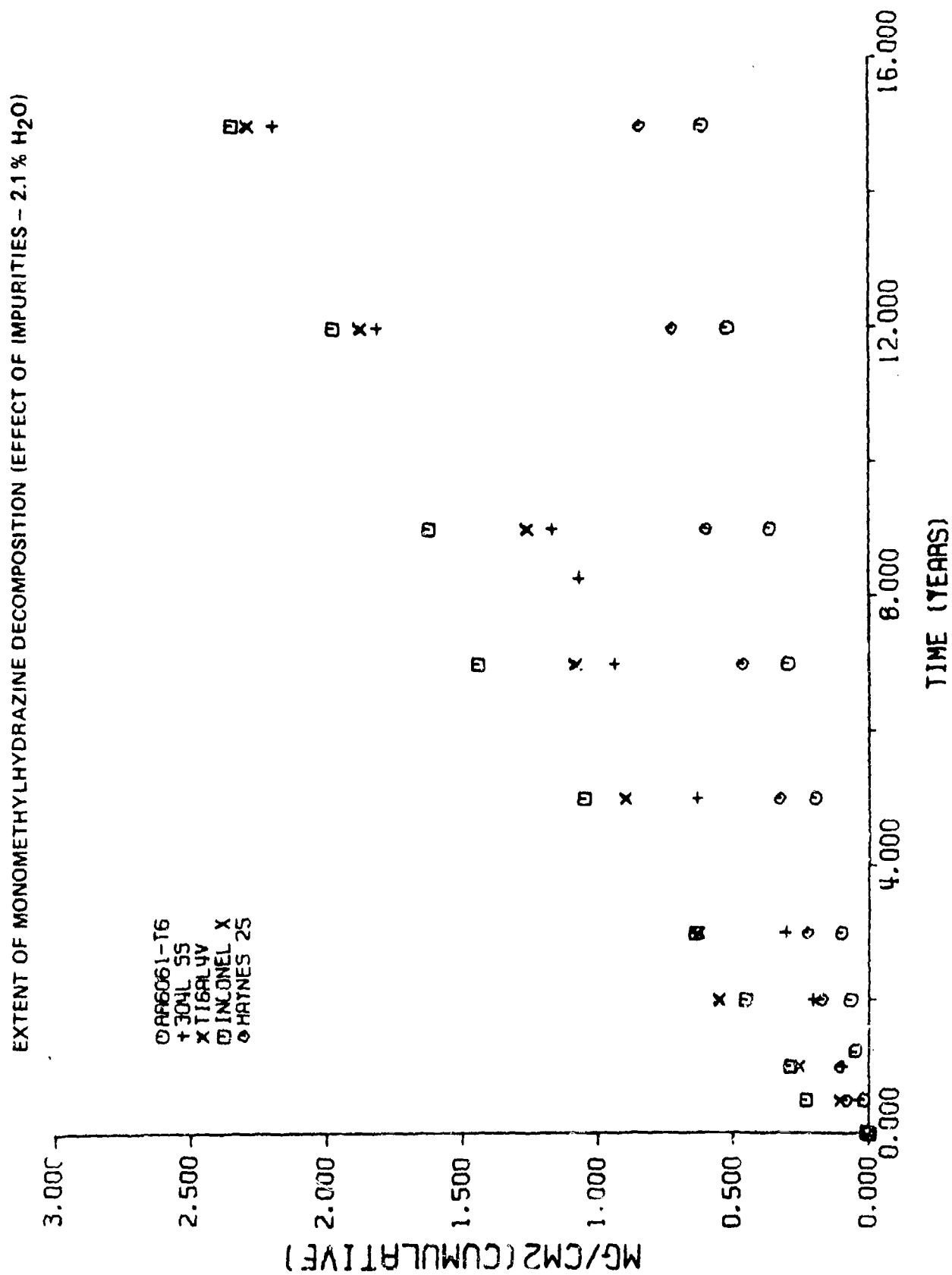


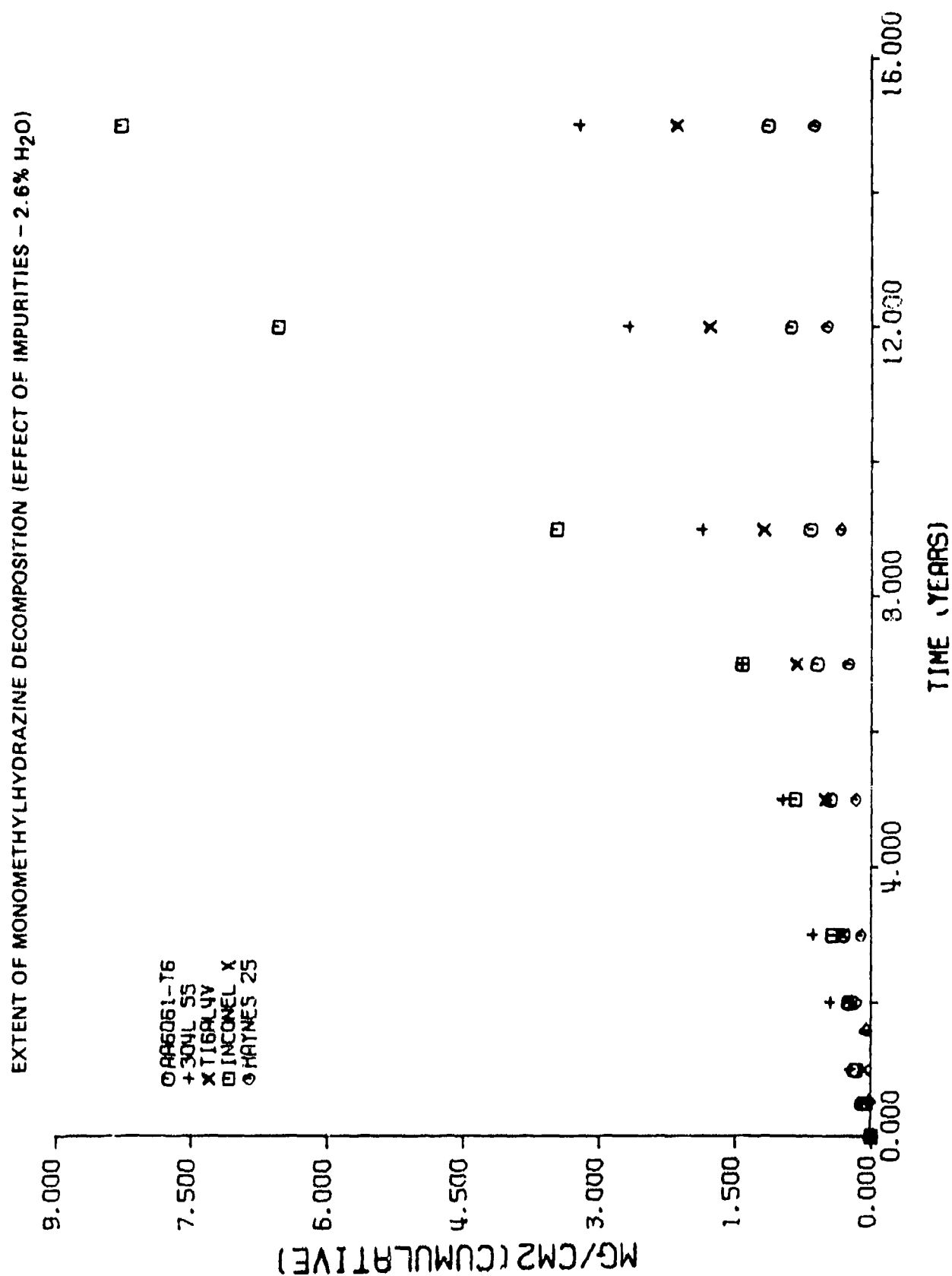
EXTENT OF MONOMETHYLHYDRAZINE DECOMPOSITION (EFFECT OF METAL PRETREATMENT B)

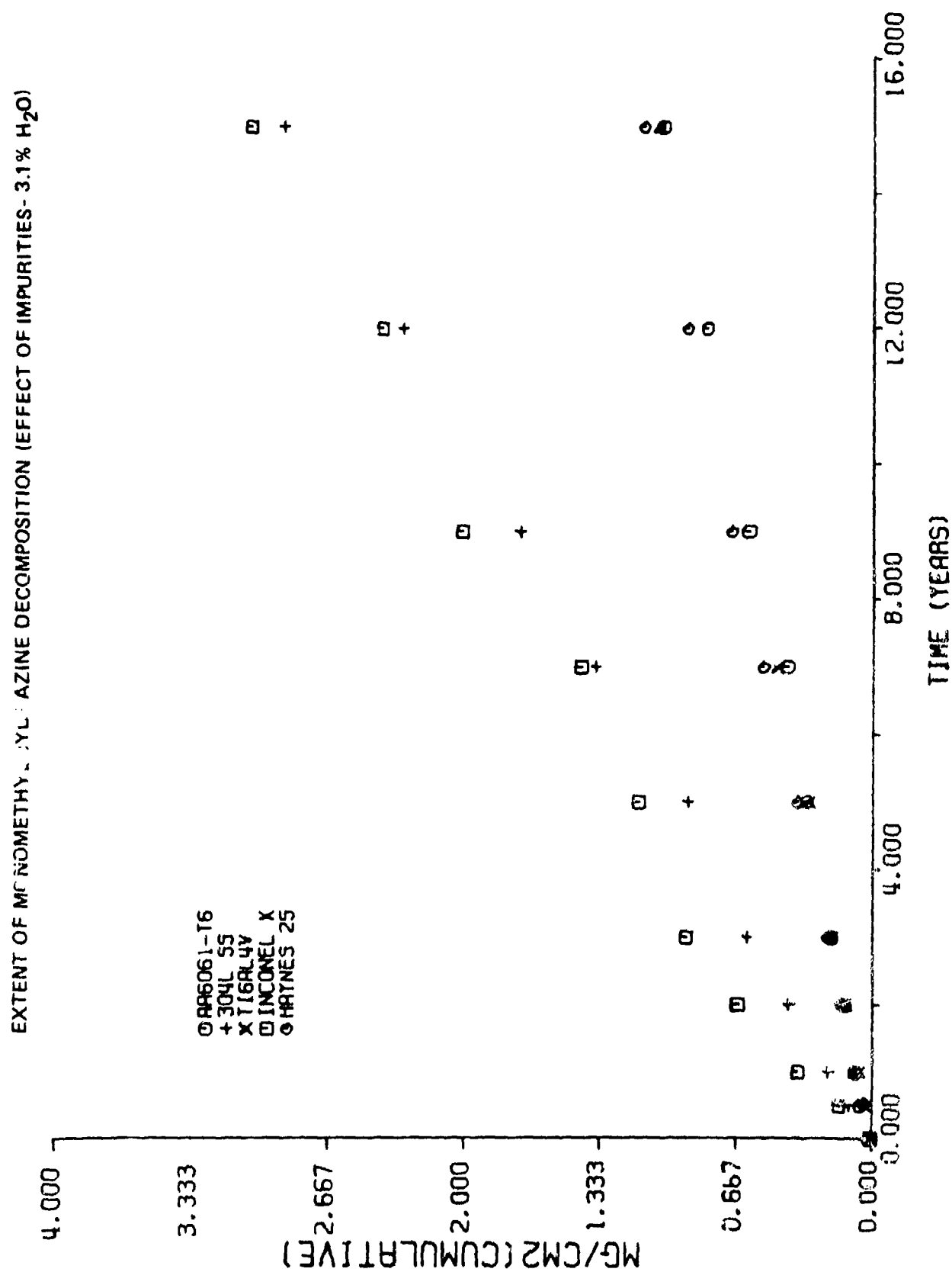


EXTENT OF MONOMETHYLHYDRAZINE DECOMPOSITION (EFFECT OF METAL PRETREATMENT C)









APPENDIX D

METAL PRETREATMENT PROCEDURES

Cleaning Procedure A

Aluminum

Steel

Titanium

Nickel and Cobalt

Cleaning Procedure B

Aluminum

Steel

Titanium

Nickel and Cobalt

Cleaning Procedure C

CLEANING PROCEDURE A

Aluminum

<u>Step</u>	<u>Solution</u>	<u>Temp (°F)</u>	<u>Time (minutes)</u>
1.	Degrease Isopropyl Alcohol (IPA)	Ambient	5-10 Sonic
2.	Rinse - H ₂ O distilled, sonic (performed twice)	Ambient	Until pH within 0.2 of source
3.	Alkaline Oakite, 3% by volume	150 \pm 10	10-15
4.	Repeat Step (2.)		
5.	Detergent clean, 1% solution by volume	70 \pm 20	5-10
6.	Rinse distilled H ₂ O		
7.	Final Rinse - IPA	Ambient	
8.	Dry-Purge N ₂	Ambient	
9.	Dry-vacuum	120 \pm 10	1.0
10.	Dry-vacuum	Ambient	

CLEANING PROCEDURE A

300 Steel

300 Series SS (304L)

<u>Step</u>	<u>Solution</u>	<u>Temp (°F)</u>	<u>Time (minutes)</u>
1.	Degrease Isopropyl Alcohol (IPA)	Ambient	5-10 Sonic
2.	Rinse - H ₂ O, distilled, Sonic (performed twice)	Ambient	Until pH within 0.2 of source
3.	Alkaline Oakite, 3% by volume	170 \pm 10	5-10
4.	Repeat Step (2.)		
5.	Acid HNO ₃ , 10% by volume	75 \pm 10	10-15
6.	Rinse H ₂ O distilled	Ambient	
7.	Repeat Step (2.)		
8.	Detergent Clean, 1% solution by volume	170 \pm 20	5-10
9.	Repeat Step (2.)		
10.	Final Rinse - IPA	Ambient	
11.	Dry-Purge N ₂		
12.	Dry-vacuum	120 \pm 10	1.0
13.	Dry-vacuum	Ambient	

CLEANING PROCEDURE A

400 Steel

Precip. Hard SS + 400 Series SS
(17-7PH, 17-4PH, 430)

<u>Step</u>	<u>Solution</u>	<u>Temp (^oF)</u>	<u>Time (minutes)</u>
1.	Degrease Isopropyl Alcohol (IPA)	Ambient	5-10 Sonic
2.	Rinse - H ₂ O, distilled, Sonic (performed twice)	Ambient	Until pH within 0.2 of source
3.	Alkaline Oakite, 3% by volume	170 \pm 10	5-10
4.	Repeat Step (2.)		
5.	21% HNO ₃ + 22 Grams/liter Sodium Dichromate	75 \pm 15	10-15
6.	Rinse H ₂ O distilled	Ambient	
7.	Repeat Step (2.)		
8.	Detergent Clean, 1% solution by volume	170 \pm 20	5-10
9.	Repeat Step (2.)		
10.	Final Rinse - IPA	Ambient	
11.	Dry-Purge N ₂	Ambient	
12.	Dry-vacuum	120 \pm 10	1.0
13.	Dry-vacuum	Ambient	

CLEANING PROCEDURE A

Titanium

<u>Step</u>	<u>Solution</u>	<u>Temp (°F)</u>	<u>Time (minutes)</u>
1.	Degrease Isopropyl Alcohol (IPA)	Ambient	5-10 Sonic
2.	Rinse - H ₂ O distilled , Sonic (performed twice)	Ambient	Until pH within 0.2 of source
3.	Alkaline Oakite, 3% by volume	170 \pm 10	5-10
4.	Repeat Step (2.)		
5.	Acid HNO ₃ , 45% by volume	75 \pm 10	20-30
6.	Rinse H ₂ O distilled	Ambient	
7.	Repeat Step (2.)		
8.	Detergent Clean, 1% solution by volume	170 \pm 20	5-10
9.	Repeat Step (2.)		
10.	Dry-Purge N ₂	Ambient	
11.	Dry-vacuum	120 \pm 10	1.0
12.	Dry-vacuum	Ambient	

CLEANING PROCEDURE A

Nickel and Cobalt

<u>Step</u>	<u>Solution</u>	<u>Temp (°F)</u>	<u>Time (minutes)</u>
1.	Degrease Isopropyl Alcohol (IPA)	Ambient	5-10 Sonic
2.	Rinse with distilled H ₂ O (Performed twice)	Ambient	Until pH within 0.2 of source
3.	Alkaline Oakite, 3% by volume	170 \pm 10	5-10
4.	Repeat Step (2.)		
5.	HCl, 2% by volume	70 -80	1.0
6.	Rinse with distilled H ₂ O		
7.	Detergent Clean,	170 \pm 20	5-10
8.	Rinse deionized H ₂ O	Ambient	
9.	Dry N ₂ Purge	Ambient	
10.	Dry-vacuum	Ambient	

CLEANING PROCEDURE B

Aluminum

<u>Step</u>	<u>Solution</u>	<u>Temp (°F)</u>	<u>Time (minutes)</u>
1.	Degrease (IPA)	Ambient	5-10 Sonic
2.	Rinse - H ₂ O distilled sonic (performed twice)	Ambient	5-10 Sonic
3.	Alkaline Oakite, 3% by volume	170 \pm 10	5-10
4.	Repeat Step (2.)		
5.	1% HF, 1% HNO ₃ -H ₂ O	Ambient	1
6.	Rinse distilled H ₂ O		
7.	Final Rinse (IPA)	Ambient	
8.	Dry N ₂ Purge	Ambient	
9.	Dry-vacuum	120 \pm 10	1.0
10.	Dry-vacuum	Ambient	

CLEANING PROCEDURE B

Stainless Steel

Series 300 and 400

<u>Step</u>	<u>Solution</u>	<u>Temp (°F)</u>	<u>Time (minutes)</u>
1.	Degrease (IPA)	Ambient	5-10 Sonic
2.	Rinse - Distilled H ₂ O sonic (performed twice)	Ambient	Until pH within 0.2 of source
3.	Alkaline Oakite, 3% by volume	170 ± 10	5-10
4.	Repeat Step (2.)		
5.	Pickling: HCl - 25% HNO ₃ - 5% Inhibitor - 0.5% Balance - H ₂ O	60-70°C	10-20
6.	Rinse distilled H ₂ O	Ambient	Until pH within 0.2 of source
7.	Repeat Step (2.)		
8.	Detergent clean, 1% solution by volume	170 ± 20	5-10
9.	Repeat Step (2.)		
10.	Final Rinse - IPA	Ambient	
11.	Dry N ₂ Purge	Ambient	
12.	Dry-vacuum	120 ± 10	
13.	Dry-vacuum		

CLEANING PROCEDURE B

Titanium

<u>Step</u>	<u>Solution</u>	<u>Temp (°F)</u>	<u>Time (minutes)</u>
1.	Degrease (IPA)	Ambient	5-10 Sonic
2.	Rinse - Distilled H ₂ O sonic (performed twice)	Ambient	Until pH within 0.2 of source
3.	Alkaline Oakite, 3% by volume	170 \pm 10	5-10
4.	Repeat Step (2.)		
5.	Pickling: HNO ₃ - 20% HF - 5% Balance, H ₂ O	Ambient	15-30 seconds
6.	Rinse distilled H ₂ O	Ambient	Until pH within 0.2 of source
7.	Repeat Step (2.)		
8.	Detergent clean, 1% solution by volume	170 \pm 20	5-10
9.	Repeat Step (2.)		
10.	Final Rinse - deionized H ₂ O	Ambient	Until pH within 0.2 of source
11.	Dry Purge N ₂	Ambient	
12.	Dry-vacuum	120 \pm 10	1.0
13.	Dry-vacuum	Ambient	

CLEANING PROCEDURE B

Nickel and Cobalt

<u>Step</u>	<u>Solution</u>	<u>Temp (°F)</u>	<u>Time (minutes)</u>
1.	Degrease with Isopropyl Alcohol (IPA)	Ambient	5-10 Sonic
2.	Rinse with distilled H ₂ O (performed twice)	Ambient	Until pH within 0.2 of source
3.	Alkaline Oakite, 3% by volume	170 \pm 10	5-10
4.	Repeat Step (2.)		
5.	25% HF by volume	70-80	6.0 (seconds)
6.	Rinse with distilled H ₂ O		
7.	Detergent clean, 1% solution by volume	170 \pm 20	5-10
8.	Rinse deionized H ₂ O	Ambient	
9.	Dry N ₂ Purge	Ambient	
10.	Dry-vacuum	Ambient	

CLEANING PROCEDURE C

Isopropyl Alcohol (IPA) and Detergent

<u>Step</u>	<u>Solution</u>	<u>Temp (°F)</u>	<u>Time (minutes)</u>
1.	Detergent solution 3% by volume	Ambient	
2.	Rinse with distilled H ₂ O (performed twice)	Ambient	Until pH within 0.2 of source
3.	IPA rinse	Ambient	5-10 sonic
4.	Rinse with distilled H ₂ O	Ambient	
5.	Dry N ₂ Purge	Ambient	